IMPACTS OF HURRICANE HARVEY ON SEAWATER CARBONATE AND NUTRIENT CHEMISTRY ACROSS THE TEXAS CONTINENTAL SHELF

A Thesis

by

SERENA MERCEDES SMITH

Submitted to the Office of Graduate and Professional Studies of
Texas A&M University
in partial fulfillment of the requirements for the degree of

MASTER OF SCIENCE

Chair of Committee,	Kathryn Shamberger
Committee Members,	Jason Sylvan
	Brendan Roark
Head of Department,	Shari Yvon-Lewis

December 2020

Major Subject: Oceanography

ABSTRACT

The ocean is absorbing an increasing amount of carbon dioxide (CO_2), which is rapidly changing seawater chemistry. As seawater CO_2 increases, ecosystem calcification is hindered by the resulting decline in pH, aragonite saturation state (Ω_{ar}), and carbonate ion concentration. The Flower Garden Banks National Marine Sanctuary (FGB) coral reef ecosystem, which is in the northwestern Gulf of Mexico (GoM) off the Texas coast, is one of the healthiest tropical coral reefs in the Caribbean and GoM with over 50 percent coral coverage. The West Texas continental shelf also hosts a number of different ecologically and economically important calcifying ecosystems, such as oyster reefs, and represents an area that is currently understudied with respect to carbonate chemistry. The GoM is frequented by large tropical storms, including Hurricane Harvey, a category four storm that made landfall on August 25th, 2017, which have been shown to alter the carbonate chemistry of nearshore ecosystems. Although Hurricane Harvey did not hit the FGB directly, there has been concern about indirect but potentially damaging impacts of storm runoff on the FGB coral reefs. Hurricane Harvey produced a record rainfall event that caused extensive flooding and elevated freshwater discharge and terrestrial runoff into the coastal areas off the Texas coast. Hurricane Harvey's strong and prolonged winds may have also enhanced upwelling that brought cold, acidified deep waters toward the surface. This study investigates the effects of the freshwater storm plume and upwelling produced by Hurricane Harvey on the carbonate and nutrient seawater chemistry of the Texas continental shelf. I present water chemistry data from five cruises, two before Harvey (June and August 2017) and three after (September, October, and November 2017). These five cruises were located across the continental shelf of Texas and seawater samples were collected and analyzed for total alkalinity (TA) and dissolved inorganic carbon (DIC), and the remaining carbonate chemistry

parameters (partial pressure of CO_2 (pCO_2), pH, and Ω_{ar}) were calculated. Nutrient concentrations (nitrate (NO^-_3), nitrite (NO^-_2), ammonium (NH^+_4), phosphate (HPO^{2-}_3), and silicate ($HSiO_3^-$) were also analyzed to further characterize how Hurricane Harvey affected seawater chemistry. The floodwaters from Hurricane Harvey delivered a substantial influx of nutrients and rainwater into Galveston Bay and the surrounding coastal region. The rainwater lowered the TA of coastal surface water while the excess nutrients stimulated photosynthesis. The increase in primary production decreased pCO_2 and DIC while increasing pH and Ω_{ar}. The runoff from Hurricane Harvey lowered coastal water pCO_2 to below atmospheric CO_2 levels, even though coastal waters are normally a summertime source of CO_2 to the atmosphere. Further, all carbonate chemistry parameters on the outer continental shelf below ~50 m depth in the September data, collected soon after Hurricane Harvey, have lower temperature, pH, Ω_{ar}, and higher pCO_2 and temperature normalized pCO_2, indicating that the strong prolonged winds from Hurricane Harvey enhanced upwelling that brought deep water to shallower depths. As large tropical storms continue to intensify with global climate change, it is imperative to understand how these storms both aid and hinder the health of calcifying communities and to further understand and characterize how coastal acidification is shaping GoM ecosystems.

CONTRIBUTORS AND FUNDING SOURCES

Contributors

This work was supported by a thesis committee consisting of Professor Kathryn Shamberger and Jason Sylvan of the Department of Oceanography and Professor Brendan Roark of the Department of Geography. All other work conducted for the thesis was completed by the student independently.

Funding Sources

Graduate study was supported by a S-STEM Scholarship and the Texas Sea-Grant Grants-In-Aid

TABLE OF CONTENTS

Page

LIST OF TABLES

1. INTRODUCTION

1.1 Ocean Acidification and Carbonate Chemistry

Global climate change is a fundamental driver in the variation of the oceans chemistry (Feely, Doney, and Cooley 2009). Specifically, the ocean's carbonate chemistry has been altered widely throughout geological time affecting marine geology, ecology and climatology (Boudreau et al. 2019). Presently, modern day oceans are facing an onslaught of after effects caused in part by the increased amounts of carbon dioxide (CO_2) from the burning of fossil fuels, land use changes and cement manufacturing (Le Quere et al. 2018, Caldeira and Wickett 2003). In the Earth's geological past (e.g. the Eocene or 56 to 33.9 million years ago), levels of atmospheric CO_2 have likely been higher than present day levels, however it is the *rate* of CO_2 rise that affects the severity of seawater chemistry changes such as ocean acidification (OA) and is one of the main causes for growing concern (Honisch et al. 2012, Zeebe and Tyrrell 2019, Eyre et al. 2018). The current rapid rates of CO_2 change may rival any other time period, even over a million-year timescale (Zeebe, Ridgwell, and Zachos 2016, Rubino et al. 2013). When CO_2 increases this abruptly, life typically has little chance for evolutionary adaptation and survival (Veron 2008).

As atmospheric CO_2 ($CO_{2(atm)}$) reacts with water, it creates carbonic acid (H_2CO_3) which is chemically indistinguishable from aqueous CO_2 ($CO_{2(aq)}$). H_2CO_3 then further speciates into bicarbonate (HCO_3^-) and carbonate (CO_3^{2-}). During this process bicarbonate increases while carbonate and pH decreases (Caldeira and Wickett 2003, Feely et al. 2004). Fewer CO_3^{2-} ions lower the mineral saturation state (Ω) of calcium carbonate ($CaCO_3$) in seawater (Feely, Doney, and Cooley 2009) (Fig 1) (NOAA National Hurricane Center (NHC) 2018).

$$CO_{2(atm)} \leftrightarrow CO_{2(aq)}$$
$$CO_{2(aq)} + H_2O \leftrightarrow H_2CO_3 \leftrightarrow H^+ + HCO_3^- \leftrightarrow H^+ + CO_3^{2-} \quad \text{(eqn. 1)}$$

Due to the pH of the ocean (~8.1), CO_2 dissociates into a bicarbonate and hydrogen ion. This production of hydrogen ions decreases the overall pH of the oceans, but some of those same hydrogen ions continue to react with carbonate to produce more bicarbonate. Thus, OA lowers the concentration of CO_3^{2-}:

$$CO_{2(aq)} + H_2O \leftrightarrow H_2CO_3$$
$$H_2CO_3 \leftrightarrow HCO_3^- + H^+$$
$$H^+ + CO_3^{2-} \leftrightarrow HCO_3^-$$
$$CO_{2(aq)} + H_2O + CO_3^{2-} \leftrightarrow 2HCO_3^- \quad \text{(eqn. 2)}$$

Calcium Carbonate ($CaCO_3$) saturation state (Ω) is a thermodynamic measurement of the degree to which the surrounding seawater is saturated with respect to $CaCO_3$ to precipitate or dissolve (Jiang et al. 2010).

$$CaCO_3 \leftrightarrow CO_3^{2-} + Ca^{2+} \quad \text{(eqn. 3)}$$

Then expressed as carbonate saturation state:

$$\Omega = \frac{[Ca^{2+}][CO_3^{2-}]}{K_{sp}} \quad \text{(eqn. 4)}$$

Where K_{sp} is the stoichiometric ion concentration product at equilibrium. Ω>1 indicates that precipitation of $CaCO_3$ is favored while Ω<1 indicates dissolution is favored. Because OA causes a decrease in CO_3^{2-}, OA also causes Ω to decrease, making $CaCO_3$ less stable in seawater.

Corals produce a metastable polymorph form of $CaCO_3$ called aragonite ($_{ar}$), which is less stable than $CaCO_3$ mineral calcite (Jiang et al. 2010, Feely, Doney, and Cooley 2009). Aragonite crystals grow in an orthorhombic type structure with needle like forms where calcite crystals present in a trigonal structure with more blocky crystals (Fan et al. 2006). In the ocean, magnesium sticks to calcite, slowing crystal growth. However, magnesium does not interfere with the growth of aragonite, which is part of the reason that modern day hermatypic, or reef building corals, construct their skeletons out of aragonite instead of calcite (Farfan et al. 2018, Nielsen et al. 2016, Wood, Ivantsov, and Zhuravlev 2017). Additionally, warmer waters encourage faster growth of aragonite (Cornelis Klein 2013). Although the surface ocean is super saturated with aragonite there are numerous studies that show dissolution and hindered calcification of aragonite occurs before aragonite saturation state (Ω_{ar}) is below 1 (Kleypas and Yates 2009, Andersson et al. 2009, Shamberger et al. 2011, Manzello et al. 2014, Tribollet et al. 2009). In addition, data suggests that physiological changes and signs of calcification decline occur around a value of 3, but calcification can also decrease at higher Ω_{ar} calcification rates (Eyre et al. 2018, Shamberger et al. 2011), (de Putron et al. 2011). While dissolution is generally expected when $\Omega_{ar} < 1$, coral calcification decreases with decreasing Ω_{ar}, even when Ω_{ar} is well above 1 (de Putron et al. 2011). In addition, different coral species, and even the same species in different locations react differently to ocean acidification (OA). Some corals are considered 'winners' that might flourish in a more acidic environment, while others are 'losers' that disappear altogether in lower pH environments (DeCarlo et al. 2018, Meissner, Lippmann, and Sen Gupta 2012, Mollica et al. 2018). Moreover, some studies have shown that coral reefs can still maintain high coral cover, diversity and calcification rates, despite living in pH and Ω_{ar}

levels that are predicted for the open ocean in 2100 (Shamberger et al. 2014, Barkley et al. 2015).

The seawater carbonate chemistry system is investigated to understand the impacts of OA on ocean chemistry and marine ecosystems. Carbonate chemistry refers to the compounds produced by the dissociation of CO_2 when it reacts with water. There are four measurable carbonate chemistry parameters, pH, the partial pressure of CO_2 (pCO_2), dissolved inorganic carbon (DIC), and total alkalinity (TA). Collectively, the sum of the dissolved forms of CO_2 in seawater are termed dissolved inorganic carbon (DIC) and are expressed as:

$$DIC = [H_2CO_3^*] + [HCO_3^-] + [CO_3^{2-}]$$

$$[H_2CO_3^*] = [CO_{2(aq)}] + [H_2CO_3] \qquad \text{(eqn. 5)}$$

TA is the charge balance in seawater, it keeps track of the charges of the ions of the weak acids in the seawater. Or in other words, the total alkalinity is the number of moles of hydrogen ions that are equivalent to the excess of proton acceptors over proton donors (Wolf-Gladrow 2005). TA is expressed as:

$$TA = -[H^+] + [OH^-] + [HCO_3^-] + 2[CO_3^{2-}] \qquad \text{(eqn. 6)}$$

The carbonate system is the natural buffer for seawater pH. Seawater is an excellent buffer. This is in part due to millions of years of dissolving limestone and other carbonate rocks into the oceanic system. Many processes that effect seawater carbonate chemistry are best described by the changes in DIC and TA. For instance, the input of anthropogenic CO2 into seawater leads to an increase of DIC but does not change TA because the charge balance is not affected.

The extant that OA changes the chemistry of the ocean can be quantified by measuring carbonate chemistry and this can be used to assess the impact of OA on calcifying organisms like coral and oyster reefs that build their shells and skeletons out of calcium. Oyster reefs mitigate coastal erosion while also providing a habitat for numerous fisheries species (Scyphers et al. 2011). Oysters are also important for water filtration. An adult oyster can filter 1.3 gallons of water an hour, or in good conditions, 50 gallons a day (Foundation 2020). Oysters filter water pollutants by either forming small packets that get deposited on the substrate or by consuming them (Lai, Irwin, and Zhang 2020).

Coral reefs are among the most diverse and economically important ecosystems on earth despite only covering approximately 0.1-0.5% of the ocean floor (Connell 1987, Spalding and Grenfell 1997). These dynamic and structurally complex ecosystems are vital for food production, tourism, cultural importance, the mitigation of coastal erosion, materials for pharmaceutical use, and as a protected habitat for aquatic life (Moberg and Folke 1999, Woodhead et al. 2019).

Coral reefs face an array of natural and societal disturbances which include pollution, run-off from sediment and nutrient laden rivers, industrial waste, tropical storms, and habitat degradation (Ennis et al. 2016, Morrison et al. 2013, Hoegh-Guldberg et al. 2017, Carlson, Foo, and Asner 2019). Ocean warming, under the influence of anthropogenic global climate change, causes mass coral bleaching and has been shown to produce more prolonged and intense tropical storms that cause irreparable damage to coral reefs, both near shore and offshore (Cheal et al. 2017, Schleussner et al. 2016). Coral reefs have so far shown a great deal of resiliency and a capacity for restoration; however, a key question is whether that resiliency will be maintained as these and other disturbances are amplified by anthropogenic climate change.

1.2 Coastal Acidification

In addition to taking up anthropogenic CO_2 from the atmosphere, acidification in coastal waters can be caused by several different factors that together can be termed coastal acidification. Coastal acidification can be brought on by natural processes such as river runoff from weathered continental rock as well as be exacerbated by anthropogenic influences.

1.2.1 Natural river and ground water inputs and weathering of continental rock

It has been shown that coastal ecosystems are influenced by interactions from river water plumes which alone or with influence from terrigenous materials are typically acidic relative to the receiving body of water (Salisbury et al. 2008). Rivers tend to have high nutrient and organic matter loads; this causes them to experience greater amounts of respiration than primary production (Cai et al. 2011). The high amount of respiration causes rivers to experience lower pH levels and higher recorded levels of pCO_2 than seawater (Howarth et al. 1992). Ground water, which leaches into estuaries and coastal waters, also has a strong influence on the chemistry of these ecosystems(de Weys, Santos, and Eyre 2011). Ground water's pH is influenced by the infiltration of recharge water, or water that refills or refreshes aquifers, as well as the surrounding geologic composition. Recharge water can vary in pH depending on its residence time to the surrounding bedrock, the longer the time, the higher the chemical influence of the rock is on the composition of the recharge water. If the geology of the aquifer is lacking in carbonate rocks, the groundwater tends to stay acidic(Trust 2003). Ground water can have elevated concentrations of CO_2; This is because groundwater is exposed to decaying (oxidizing) organic matter, a lack of photosynthesizing organisms and the respiration of plant roots and other heterotrophic bacteria. The chemical reaction of free oxygen with reduced iron minerals, like pyrite, is another source of acidity for groundwater systems(Appelo 1993).

1.2.2 Anthropogenic Influences on Coastal Acidification

Coastal processes, along with atmospheric CO_2, influence the complex carbonate chemistry of the coastal ocean ecosystem and are drivers in acidification to some of the most economically important areas of the GoM and globally(Yao et al.). An example of a coastal process that enhances acidification is an excess of nutrients like nitrogen and phosphorus from river runoff. This nutrient laden runoff can create phytoplankton blooms. These blooms stimulate photosynthesis, which draws down CO_2 and increases pH. When the bloom eventually dies, the resultant organic matter falls to the seafloor, where it is remineralized by heterotrophic bacteria that consume oxygen and produce CO_2, creating hypoxia as well as coastal acidification (Gobler and Baumann 2016, Cai et al. 2011). This is especially detrimental in the Gulf of Mexico (GoM), where stratification can enhance the negative effects of hypoxia by preventing the replacement of oxygen from the atmosphere to bottom waters that are depleted of oxygen through respiration processes (Bianchi et al. 2010). Another coastal process affecting acidification is land-based pollution. For example, power plants and agricultural activities increase the amount of sulfur and nitrogen into the atmosphere producing acid rain (Doney et al. 2007). Farming and livestock husbandry in addition to the burning fossil fuels release ammonia, sulfur dioxide, and nitrogen oxides into the atmosphere. There these compounds are converted into nitric acid and sulfuric acid (Doney et al. 2007). A portion of these compounds are moved offshore by winds where they alter seawater chemistry and another portion contributes to acid rain along coast lines. This type of rain is especially damaging to coastal environments because of accumulation downstream and river runoff.

Rivers interact with several different pollutants before unloading into the world's oceans. These can include picking up material through acid mine drainage, which are associated with sulfide minerals like pyrite, that can increase the acidity of the river water (Mattson 1999). During the mining operations, the sulfides are exposed to oxygen and then quickly oxidize to sulfuric acid. Rivers area also in much contact with urban and agricultural runoff, snowmelt, and erosion of sediments from different geological transition zones which all influence the river's water chemistry. Specifically for the GoM, The Mississippi River Basin, which discharges over 16,000 cubic meters of water per second into the Gulf of Mexico, consists of six regions that spread across mostly farmlands in middle America (2020b). These regions are also recorded to have lower alkalinity than more eastern regions(Mattson 1999).

1.3 Hurricanes

1.3.1 Positive Effects of Hurricanes on Coastal Regions

While hurricanes are largely associated with physical damage and other negative effects, it is worth noting that there are positive impacts of large tropical storms. Broadly speaking, hurricanes generate a great deal of rainwater which can break up periods of standing drought (Maxwell et al. 2013). These drought busting storms are especially important in the southwestern United States and have increased in that region during the last 117 years (Maxwell et al. 2013). Hurricanes also balance the global heat budget (Tamarin and Kaspi 2016). Hurricanes have also been shown to replenish barrier islands and salt marshes that in turn help protect shorelines from storm surges created by hurricanes. Marshes that experience shallow burial by hurricanes have shown increased productivity, potentially because of an increase in nutrient levels from deposited sediments such as ammonium and phosphate or increased soil aeration (Baustian and Mendelssohn 2015, Walters and Kirwan 2016). Hurricanes also fertilize mangrove forests which

are important nurseries for many different aquatic and marine species, as well slowing the process of coastline erosion by buffering high impact waves (Castaneda-Moya et al. 2020). Hurricanes also can benefit coral reef ecosystems by cooling surrounding waters. Cooling can take place by the transfer of latent heat or evaporation, mixing of deeper waters, upwelling, or as a result of overcast skies (Manzello et al. 2007). This cooling is especially important during the summer months when average seawater surface temperatures rise and put coral reef ecosystems through thermal stress, and in more extreme conditions, coral bleaching. Coral bleaching happens when the photosynthetic symbiotic zooxanthellae located in the tissue of corals are overloaded with heat and sunlight and start to release reactive oxygen molecules. These molecules are damaging to corals tissues and therefore the coral expels the zooxanthellae from the tissue. The coral loses coloring and energy provided by the symbiont and can eventually die if it does not recover symbionts. Finally, tropical storms aid in coral reproduction via recruitment, dispersal and fragmentation (Foster et al. 2013, Browning et al. 2019, Lugo-Fernandez and Gravois 2010).

1.3.2 Physical Damages to Ecosystems Brought about by Hurricanes

Most studies focus on the physically damaging effects of hurricanes and large tropical storms on environments (Lugo-Fernandez and Gravois 2010, Perry et al. 2014). Hurricanes are among the most devastating natural hazards on earth, affecting the Atlantic Basin including the GoM with just over 5 storms a year on average from 1851 to 2014 (2020a). Hurricanes physically affect reefs by partially or completely burying corals and oysters in sediment deposits from runoff or resuspension which can lead to mortality events (Browning et al. 2019). High winds can cause powerful waves and storm surges that break coral branches and are abrasive to delicate reef structures (Foster et al. 2013, Scott Heron 2005). Large storm induced waves and

currents can also topple over massive coral species (Bries, Debrot, and Meyer 2004). It has been shown that hurricanes may also increase the prevalence of disease among coral reef systems (Foster et al. 2013). Hurricanes have also been shown to increase the likelihood of a harmful algal bloom forming because of increased nutrient import. Hurricanes can lead to an excess of terrestrial runoff and submarine groundwater discharge which is supersaturated with nutrients (Hu, Muller-Karger, and Swarzenski 2006). Hurricanes have also been shown to potentially break apart redtides and other harmful algal blooms and transport them to new locations (Wells et al. 2015).

1.3.3 Hurricane Induced Seawater Chemical Alterations

Hurricanes alter the chemical environment of coastal marine ecosystems, however these changes have not been as well studied as the physical damage caused by hurricanes (Manzello et al. 2013, Lugo-Fernandez and Gravois 2010). Seawater carbonate chemistry can be affected by tropical storms via storm water runoff, upwelling, and turbulent mixing (Lugo-Fernandez and Gravois 2010). Previous work has shown that storm water runoff can cause prolonged (~1 week) acidification in coral reefs, including a drop of 1.0 in Ω_{ar} (Manzello et al. 2014, Kealoha A.K. , Kealoha, Doyle, et al. 2020).

Furthermore, acidification can increase during storm events due to CO_2-rich subsurface waters being entrained and uplifted towards the surface through storm-induced mixing (Lugo-Fernandez and Gravois 2010, Mathis et al. 2012). These storms can also stir up sediment pore waters, which are known to be more acidic and bring them into the calcifying organisms environment (Manzello et al. 2013). Tropical storms have been shown to increase primary production through ventilation of the nitracline (Lin et al. 2003). Increases in nitrogen can cause phytoplankton blooms, which cloud surface waters, inhibiting coral reef photosynthesis, causing

a decrease in dissolved oxygen through enhancement of heterotrophic respiration during remineralization of organic matter (Walker, Leben, and Balasubramanian 2005, Lin et al. 2003).

Upwelling can also be enhanced during large tropical storms which can take up to 10 days to settle back into a neutral state (Walker, Leben, and Balasubramanian 2005, Rao, Babu, and Dube 2004). Although cooling from storms can prevent coral bleaching, upwelling events have also been shown to have devastating effects on reef systems, including mass mortality events, by bringing up deeper, cooler, and more acidic waters (Laboy-Nieves et al. 2001, Mathis et al. 2012, Bond et al. 2011). Additionally, the nepheloid layer, a deep section of water composed of suspended terrigenous silts and inorganic detritus, can be brought up from depth (Lugo-Fernandez and Gravois 2010). The resuspension of these materials may, in turn, affect parameters of the carbonate chemistry surrounding the reef due to the high pCO_2 in sediment pore waters (Lugo-Fernandez and Gravois 2010, Diercks et al. 2018). The impact of hurricanes can be both advantageous and damaging. Small hurricanes can provide relief from thermal stress and help populate new regions, whereas large storms can bring on rapid chemical changes and devastating physical damage. Coral reefs have experienced effects from hurricanes and have continued to flourish for millions of years. However, compounding effects from increases thermal stress, oceans acidification, and habitat destructions could lead to the destruction of these environmentally and economically valuable ecosystems.

1.4 Site description: The Gulf of Mexico

1.4.1 Importance and general environmental threats to the GoM

The Northern GoM ecosystems support a wide range of valuable economic resources. The U.S. territorial waters of the GoM support a large American based fishing industry in which 23.7 billion in sales was made in 2016, and which supplied 137,000 jobs (2018). Despite being

such an important economic source for the surrounding GoM states, the GoM is subject to an onslaught of anthropogenic attacks that include eutrophication, hypoxia, oil spills, warming, and ocean acidification, which is still not well understood in the GoM (Scavia et al. 2002). Moreover, acidification of subsurface coastal waters on the Texas shelf is enhanced by eutrophication; the upscaled eutrophication that occurs in the GoM is in part because of the Mississippi-Atchafalaya River Basin (MARB).The MARB watershed contains 31 states in addition to two Canadian provinces, making it the third largest river basin in the world (Hypoxia Task Force 2017). Much of the MARB river basin runs through farming regions in the central USA, and any farmland waste is drained into the system, creating a highly nutrient rich waterway. This nutrient laden water is eventually dumped into the Northern GoM where the excess nutrients create eutrophication leading to phytoplankton blooms and eventually hypoxia (Laurent et al. 2017). When the bloom starts to die off, the increased abundance of heterotrophic organisms shifts the balance of O_2 production/consumption and the production of CO_2. Eutrophication-induced hypoxia is further exacerbated by water column stratification that prohibits mixing of the oxygenated surface water and oxygen deplete bottom water; without this stratification, oxygen rich surface waters would be able to mix with deeper oxygen depleted waters (Turner, Rabalais, and Justic 2008, Diaz and Rosenberg 2008). The increase of CO_2 leads to acidification in coastal waters (Laurent et al. 2017, Hypoxia Task Force 2017, Diaz and Rosenberg 2008). In addition to experiencing acidification associated with hypoxia in bottom waters, ocean acidification driven changes in surface water are expected to be significantly greater in the GoM than other U.S. coastal waters by the end of this century ; this might be due to the influences of the hydrological cycle and well as enhanced upwelling (Keul et al. 2010, Salisbury et al. 2008). Long term CO_2 trends in the GoM, show that the coastal ocean exhibits more variability than the open ocean

(Kealoha, Shamberger, et al. 2020). The variability in both the open ocean and coastal ocean in the GoM is influenced by biological components linked to the Mississippi-Atchafalaya River discharge and seasonal changes in temperature. The open ocean element of the GoM show comparable acidification trends as global open ocean acidification trends (Kealoha, Shamberger, et al. 2020). Through the fall into spring, coastal currents move low CO_2 and low salinity water from the Louisiana shelf over the West Texas shelf. In the summer, a shift in prevailing winds cause eastward movement of the coastal currents which can cause upwelling conditions as well as pooling of the inner shelf waters (Kealoha, Shamberger, et al. 2020, Zavala-Hidalgo et al. 2014).

1.4.2 Hydrology and Nutrients of the GoM

The waters of the GoM enter through the Yucatan Channel and exit the GoM through the Florida Straits (Hypoxia Task Force 2017). On the continental shelf, seawater is diluted by the large amounts of river water. The main circulation pattern of ocean water in this area moves along the northern GoM coastline, and the flow of ocean water over the Texas-Louisiana shelf moves primarily to the west (cyclonic); however, during July and August wind patterns change which causes the westward flow to decrease and reverse (Department, of Commerce, and Office of National Marine Sanctuaries 2008, Hypoxia Task Force 2017). The Northern Gulf of Mexico's nutrient composition is highly influenced by the Mississippi River and its distributary, the Atchafalaya River. The Mississippi drains 40% of the continental United States fresh water into the northern GoM (Sylvan and Ammerman 2014, 2013). Since the 1950 through to the 1980's the Mississippi has tripled its nitrate load due to increased agricultural activities, however the silicate concentration has been reduced by nearly 50% (Rabalais et al. 2002, Cai et al. 2011, Cai et al. 2013). Shelf circulation, which is modulated by alongshore winds that vary seasonally,

influences nutrient distribution in this region. From fall to spring (September - May), wind direction is downcoast or a southwest direction. This directionality creates currents that push the Mississippi river plume along the coast more towards the Texas continental shelf (Angles et al. 2019). During this time, discharge from the Mississippi begins to ramp up (beginning in the fall) and peaks with maximum freshwater discharge in the spring. During the summer months (June - August) the prevailing winds shift to a north-northeastward direction which drives up coast circulation and creates favorable conditions for upwelling (Angles et al. 2019).

Over the Louisiana shelf, there is a spring and early summer phosphorus (P)-limitation just as the freshwater discharge from the Mississippi river reaches its peak and starts to taper off (Sylvan and Ammerman 2013). This is followed by a nitrogen (N) limiting conditions in the late summer and through the fall when freshwater discharge is at a minimum (Sylvan and Ammerman 2013). Because the Mississippi has a strong influence on waters over the west Texas shelf, especially in the fall through spring, I would imagine that the similar nutrient limitations apply in the waters over the Texas shelf.

1.4.3 Important environmental and economic ecosystems in the GoM

The GoM also hosts important ecosystems such as estuaries and marsh lands that are susceptible to coastal acidification because they host a number of species that go through biomineralization (Hu et al. 2015). Estuaries help filter runoff from rivers and are therefore important habitats for maintaining the health of waterways. After Hurricane Harvey, the changes in the seawater carbonate systems surrounding different estuaries in the northern GoM varied (Hu et al. 2020). Some estuaries were impacted more than others, highlighting the variability in seawater chemistry ecosystem reaction and recovery (Hu et al. 2020). The GoM is home to a variety of environmentally and economically important calcifying organisms. For instance, the

Texas continental shelf is home to oysters, clams, mussels and echinoderms that are sensitive to seawater chemistry changes, especially alterations to pH (Meng et al. 2019, Johnson et al. 2020). Echinoderms are not as well studied, but they do construct their shell-like structures from high magnesium calcite, which dissolves faster than aragonite, creating a serious concern for these animals in their ability to protect themselves (Johnson et al. 2020). Oyster larvae, if subjected to low enough pH, can fail to begin growing their shells (Meng et al. 2019). There is typically a huge growth spurt in the first 2 days of an oyster's life so that the oysters can begin to feed. However, lower pH environments destroy those early stages of growth and can cause mass die-offs (Clark and Gobler 2016).

1.4.4 The Flower Garden Banks National Marine Sanctuary

The Gulf of Mexico basin began to form after the supercontinent of Pangea started to break apart during the Triassic (~200 million years ago). A rift valley formed and eventually in the early Jurassic, an ancestral GoM was created. Throughout this hot and dry period, the gulf was intermittently covered by a shallow sea. However, with restrictions to the open ocean, this type of environment caused intense evaporation and formed a thick layer of salt or evaporite deposits in the gulf called the 'Louann formation' (Zingula 2008b).

As time progressed and the continents continued to spread, the gulf deepened and the waters within the gulf became less saline while clastic sediments were deposited by rivers from the terrestrial environment that covered the thick layer of salt (Austin 2014). Because the overlaying sediments became denser than the underlying layer of salt, the salt began to migrate towards areas of weakness, a process known as structural uplift; this resulted in the formation of salt domes or diapirs in the region (Zingula 2008a). These salt domes create an environment

which allows for the formation of coral reef habitats unusually far offshore, including the Flower Garden Banks National Marine Sanctuary (FGB).

The FGB are located in the subtropical oligotrophic waters of the northwestern area of the GoM, approximately 190 km off the coast of the Texas/Louisiana boarder (Johnston et al. 2019). The ecosystems that make up the FGB are unique in that the coral reefs are located on the edge of the continental shelf break, which would normally be too deep to allow for tropical Scleractinian corals. However, due to the uplifting of the salt domes, the East/West and Stetson banks reach depth shallow enough (~20 m) for coral ecosystems to form so far from the coast. It is estimated that the East and West bank's coral reefs began to develop on top of the salt domes between 10,000 to 15,000 years ago (Zingula 2008b). The FGB was established in 1992 as a federally managed ecosystem. The FGB is considered to be of national significance under the National Marine Sanctuaries Act, and it is currently the only sanctuary site located in the GoM (Johnston MA 2017). The FGB has 3 distinct areas under protection: The East Bank and the older West Bank, as well as the more northerly Stetson Bank. The East and West Banks are about 21 km apart, each with a depth ranging from 16-140 m, and the Stetson Bank sits 48 km to the northwest of the West Bank (Johnston MA 2017, Department, of Commerce, and Office of National Marine Sanctuaries 2008). East bank is roughly 8 km in length and 5 km wide while West bank is 11 km in length and 5 km wide (Kealoha, Doyle, et al. 2020). The West bank has gradual slopes while the East has steep drop offs on both the east and south slops. Surface currents at both the West and East banks are influenced by westward-propagating eddies that are derived from the Loop Current. Mixed layer depths are generally located between about 20 and 40 m for the majority of the year (Teague et al. 2013).

It is postulated that the FGB corals originated from Mexican reefs (Zingula 2008b). The FGB is considered a high latitude marginal coral reef, representing the northern most tropical species around the contiguous United States (Johnston et al. 2019). Here, distribution of coral is constrained by temperature and light availability; nevertheless, the mean living coral coverage has remained near or above 50 percent, making them some of the healthiest reefs remaining in the Caribbean and GoM (DeBose et al. 2013). Although the FGB are considered a near pristine habitat, they have a relatively low diversity of species within them: only 22 of over 60 western Atlantic and Caribbean region hermatypic coral species occur in this area (Johnston MA 2017).

1.5 Main focus of this Study

This work specifically investigates how Hurricane Harvey impacted the carbonate and dissolved inorganic nutrient chemistry on the Texas continental shelf, including the FGB. Hurricane Harvey, considered a 1000-year precipitation event, was initially a poorly organized depression after working its way into the GoM. However, Harvey intensified rapidly late on the 23rd of August 2017 in an environment of light wind shear, warm water, and high moisture. The storm intensified into a category 4 hurricane before making landfall on August 25th, 2017 (Fig 2). Hurricane Harvey stalled over the Houston area for approximately four days and is estimated to have dropped more than 60 inches of rainwater, this amount of rainwater surpasses pervious records of 52 inches in Hawaii making it the most significant tropical cyclone rainfall event in United States history. Out of the 19 rain gauges in Harris County, Texas, 9 of them recorded all-time high flood stages (Eric S. Blake 2018). Not only are the peak rainfall records extraordinary, but the area affect by Harvey is truly overwhelming. It is estimated that 11.1×10^9 m^3 of freshwater flowed into Galveston Bay, which is 3 times the entire bay's volume (Du et al. 2020,

Du and Park 2019, Du et al. 2019). This intense flooding created a freshwater plume that pushed out of Galveston Bay picking up pollutants along the way (Du and Park 2019).

1.6 Research Questions

What was the impact of Hurricane Harvey runoff on the seawater chemistry of the Texas Continental Shelf?

This study investigates depth profiles from 2017 cruises before and after Hurricane Harvey to investigate how Harvey runoff impacted the seawater chemistry of the Texas continental shelf and to determine if fresh water from Harvey runoff reached the FGB. Fresh water can be very detrimental to reef ecosystems (Johnston et al. 2019). In 2016 there was a mass die off event in the FGB that was partially attributed to the presence of a freshwater surface layer caused from unusually high river discharge (Johnston et al. 2019, Kealoha, Doyle, et al. 2020). If a freshwater plume did reach the FGB following Harvey it could have altered the carbonate chemistry of surface waters and potentially had negative impacts on the reef ecosystem. In a previous study, it was found that flooding in Texas leads to freshwater runoff that has low concentrations of both TA and DIC. Therefore this same outcome is expected after the intense flooding brought about by Hurricane Harvey (Kealoha, Doyle, et al. 2020). Intense flooding events typically are loaded with excess nutrients that can fuel phytoplankton blooms (Steichen et al. 2020). Increased photosynthesis drives down pCO_2 and DIC while raising pH and Ω_{ar}.

Did Hurricane Harvey cause upwelling along the Texas Continental Shelf?

It has been shown that hurricanes can induce upwelling and that coral reefs subjected to these upwelled waters can either benefit or be damaged by the changes induced by the upwelling event (Walker, Leben, and Balasubramanian 2005, Mathis et al. 2012, Lugo-Fernandez and

Gravois 2010). Carbonate chemistry parameters, nutrient data, and dissolved oxygen data from the 2017 FGB and 2017 west Texas cruises (Table 1) were analyzed to determine shifts in these parameters that could indicate upwelling. It is hypothesized that Hurricane Harvey induced upwelling of deep water towards the surface which caused a decrease in TA, temperature, pH and Ω_{ar}, as well as an increase in DIC and pCO_2.

2. METHODS

Discrete seawater samples were collected for TA, DIC, dissolved oxygen (DO), and nutrient analyses on five research cruises in 2017, before and after Hurricane Harvey (Table 1, Fig 3). Four of the five cruises (June, August, September, and November) come from a set of data referred to as the West Texas or WTX cruises. The goal of the WTX cruises was to gain a better understanding of the mechanisms and controls of hypoxia in the northern GoM. The WTX cruises consist of five main transects on the Texas coast that extend from near shore to the edge of the continental shelf, approximately 80 km offshore, and each transect includes five stations. The most southern transect was located near the Baffin Bay (27.05^{o}N, -96.40^{o}W) while the most northern transect begins just north of East Matagorda Bay (29.39 ^{o}N -94.13 ^{o}W). The June and August WTX cruises (pre-Harvey) include these five Texas shelf transects, while the September and November WTX cruises following hurricane Harvey also included two additional five site lines, one each across the West and East Bank with in the FGB, and an additional cross-shelf transect that stretches from Galveston Bay out towards the FGB (Fig 3). The October Rapid Response cruise following Hurricane Harvey (FGB1017) includes a five by five site FGB grid and the transect from Galveston Bay to the FGB (Fig 3). The FGB grid stations are centered over the East and West Banks, with each station located roughly 8 km apart longitudinally and 5 km latitudinally (Fig 3). Data were not collected in the FGB during the June or August pre-Harvey cruises.

Table 1. *Names, dates general locations, and ship for each cruise*

Cruise Name	Date	Location	Vessel
WTX1	June 12-15, 2017	West Texas Shelf	R/V Manta
WXT2	August 8-11, 2017	West Texas Shelf	R/V Manta
WTX3	September 23 – October 12017	West Texas Shelf/ Galveston Transect/FGB Grid	R/V Manta
WTX4	November 15- 20, 2017	West Texas Shelf/ Galveston Transect/FGB Grid	R/V Manta
FGB1017	October 20-24, 2017	Galveston Transect/FGB Grid	R/V Point Sur

Seawater samples for all analyses were collected using a Niskin bottle rosette on a Seabird Electronic (SBE25) CTD profiler. Water to be used for analysis of carbonate chemistry was collected from the Niskin bottles using borosilicate 250 ml glass bottles which were then immediately poisoned with 100 µl of saturated mercuric chloride and sealed with Apiezon grease(Dickson, Sabine, and Christian 2007) and samples were analyzed for TA and DIC at Texas A&M University (TAMU) in Dr. Katie Shamberger's lab using a **V**ersatile **IN**strument for the **D**etermination of **T**otal inorganic carbon and titration **A**lkalinity (VINDTA) produced by Marianda Marine Analytics and Data. pCO_2, Ω_{ar}, and all remaining carbonate chemistry parameters were calculated using CO2SYS(Pierrot 2006) and the equilibrium constants of Lueker et al (2000)(Lueker, Dickson, and Keeling 2000). For TA and DIC analyses, Certified Reference Materials (CRMs) were provided by A. Dickson at the Scripps Institute of Oceanography and were used to calibrate for TA and DIC(Dickson, Sabine, and Christian 2007). The averages of the precisions for DIC ranged from 1.92 to 2.57 and 1.43 to 1.96 for TA.

Water samples collected for analysis of nutrient chemistry (nitrate (NO^-_3), nitrite (NO^-_2), ammonium (NH^+_4), phosphate (HPO^{2-}_3), and silicate ($HSiO_3^-$)) were collected into polycarbonate flasks after filtration through GF/C 0.2 μm filters, then frozen and analyzed post cruise by Geochemical and Environmental Research Group (GERG). Samples were analyzed to standard World Ocean Circulation Experiment (WOCE) segmented flow methodology using an Astoria Analyzer (Astoria-Pacific)(WHPO 1994). DO was measured using Winkler titrations. After collecting the water from the Niskin bottles into flasks, aliquots of manganese chloride and sodium hydroxide-sodium iodide were added. Winkler titrations were performed using sodium thiosulfate with an amperometric dead-stop endpoint determination with a double platinum electrode within 12 hours of collection(Gordon et al. 1994).

Normalization of pCO_2 to a constant temperature ($npCO_2$) removes the effects of temperature changes on pCO_2. The variability observed in $npCO_2$ is therefore due to a combination of biological, air-sea gas exchange, and upwelling/mixing effects. The effects of temperature on isochemical water conditions is given by the equation:

$$npCO_2 = pCO_{2insitu} * EXP\left(0.0423 * (SST_{mean} - SST_{insitu})\right) \qquad \text{(eqn. 7)}$$

Where $pCO_{2insitu}$ and SST_{insitu} are the measured values and SST_{mean} is the annual mean SST (Sea Surface Temperature) of the entire data set (25 °C)(Takahashi et al. 2002).

3. RESULTS

Surface samples refer to the shallowest sample collected at each site and were collected between 0.5 – 5.3 m. All surface vales are grouped into categories that include north, south, onshore, and offshore. The north and south designations are based on the 28^{o} latitudinal line with samples falling north or south of this line. The inshore samples are from the two sites closest to shore from each of the five west Texas transects as well as the transect leading from Galveston Bay while the offshore samples are from the two sites furthest offshore in each transect, as well as the entire FGB grid. Sites falling outside of the transects or grid are designated as whatever the site closest to them is designated as.

For depth trends, categories include bottom and deep samples. Bottom samples refer to the deepest sample at each site, therefore sites inshore have a bottom sample that is much shallower than the bottom samples offshore on the FGB grid. Deep samples include all samples that are ≥ 50 m. 50 m was chosen because visual trends started to change at approximately this depth and the surface mixed layer is typically around this depth in the GoM (Prasad and Hogan 2007). The nutrient data is right skewed, or positively skewed, meaning that compared to a normally distributed graph with a bell shape, most of the data falls on the right side of the graph. On right skewed data, the standard deviation can be larger than the average because the data is distributed unevenly. In cases like this, the median, or the middle number, may be a better representation of the data.

3.1 June 2017

Surface trends: The June samples were taken exclusively off the west Texas shelf and do not include the FGB grid or the transect from Galveston. June surface samples range from 1- 4.5 m. Salinity on the west Texas shelf increases southwards and offshore, with a minimum of 20.76 and a maximum of 35.55 on the surface (Figs 3-5). However, salinity ranges located closer to the

mouths of Matagorda Bay and Corpus Christi Bay in the southern region of samples, are more restricted and have higher salinity with a minimum of 29.32 (Fig 4-5). The average surface salinity for June was 29.30 ± 3.93. There is a smaller range in temperature changes than in salinity changes showing a slight trend moving from offshore, with a minimum temperature of 26.0°C to a maximum of 28.9°C and an average of 28.2 ± 0.6°C for all surface samples (Figs 6-7). The pH is higher in the more northern samples, closer to Galveston bay with the highest pH of 8.30 compared with the average pH of all June surface samples at 8.08 ± 0.08 (Figs 8-9, Table 2). pCO_2 portrays inverse trends of pH, with a lower surface average in the north at 343.52 ± 81.73 µatm and offshore average of 410.83 ± 65.92 µatm (Figs 10-11, Table 2). The Ω_{ar} tends to be highest nearer to shore and generally in the more northern samples, with onshore sites averaging 3.79 ± 0.26 and offshore sites averaging 3.79 ± 0.32, but with a northern average of 3.93 ± 0.53 and the highest surface value of 5.03 (Figs 12-13, Table 2). TA and DIC both had higher average values for offshore and southern sites (Figs 14-17, Table 2). For DO, the northern set of samples is approximately 0.26 mL/L higher than the southern samples (Figs 18-19, Table 2). NO_3^- was below detection limits on average in surface waters in June (Figs 20-21, Table 2). HPO_4^{2-}, NH_4^+, DIN, and NO_2^- all had higher median inshore values compared to their offshore values, and higher median values in the northern sites compared to the southern sites (Figs 22-23, and 26-31, Table 2). $HSiO_3^-$ had higher median values offshore and in the southern sites (Figs 24-25, Table 2). Urea had a higher inshore median than then offshore median and similar medians between the northern and southern samples (Figs 32-33, Table 2).

Depth trends: The surface values for June range from 1 to 4.5 m while the bottom samples range from 11.9 to 102.5 m. Salinity increases with depth ranging from 20.76 at the surface to 36.44 at a depth of 80.70 m. Salinity had an overall average of 31.89 ± 4.15 (Figs 4-5). Temperatures at

the surface averaged 28.2 ± 0.6 °C and decrease with depth, reaching 19°C at 102 m (Figs 6-7). pH decreases and pCO_2 increases with depth. pCO_2 has a minimum value of 206.4 µatm at 1.4 m and a maximum of 741.32 µatm (Figs 8-11, Table 2). The Ω_{ar} decreases with depth with a minimum and maximum of 2.27 and 5.03, respectively (Figs 12-13, Table 2). TA and DIC both increase slightly with depth (Figs 14-17, Table 2). The overall average DO is 4.22 ± 0.96 mL/L, surface average is 4.83 ± 0.42 mL/L, bottom sample (11.9 – 102.5 m) average is 3.50 ± 1.06 mL/L, and deep sample (>50 m) average is 3.00 ± 0.79 mL/L (Figs 18-19, Table 3). NO_3^- increased with depth from a median of 0.00 µmol/L as the surface to 2.62 µmol/L in the bottom samples and 6.32 µmol/L in the deep samples (Figs 20-21, Table 2). $HSiO_3^-$ and NO_2^- also increased with depth from 3.93 µmol/L and 0.09 µmol/L to 11.03 µmol/L and 0.16 µmol/L, respectively (Figs 24-25 and 28-29-32, Table 3). In contrast HPO_4^{2-}, NH_4^+, and Urea had the highest median samples at the surface, 1.01 µmol/L, 1.56 µmol/L, and 1.02 µmol/L, respectively (Figs 22-23, and 26-27, and 32-33, Table 3)

Table 2. *Carbonate Chemistry parameters at different locations at the surface and at depth from June 12-15, 2017*

June 2017	**TA µmol/kg**	**DIC µmol/kg**	**pH**	**pCO_2 µatm**	**Ω_{ar}**
All Data					
Average	2360.39 ± 61.81	2073.00 ± 79.34	8.03 ± 0.08	445.07 ± 101.3	3.45 ± 0.55
Median	2385.65	2079.28	8.04	430.92	3.62
Range	2154.78 - 2423.64	1844.42 - 2202.90	7.84 - 8.3	206.43 - 741.32	2.27 - 5.03
Surface					
Average	2329.85 ± 71.99	2022.64 ± 77.80	8.08 ± 0.08	390.45 ± 73.14	3.79 ± 0.37
Median	2355.21	2061.38	8.05	419.24	3.7
Range	2154.78 - 2409.74	1844.42 - 2124.18	7.98 - 8.3	206.43 - 494.89	3.34 - 5.03
Bottom					
Average	2384.40 ± 37.50	2124.97 ± 59.00	7.98 ± 0.08	512.87 ± 108.50	3.06 ± 0.59
Median	2398.25	2141.83	7.97	550.99	2.93
Average >50 m	2396.30 ± 7.20	2170.73 ± 9.84	7.94 ± 0.02	547.35 ± 24.76	2.55 ± 0.18
Median >50 m	2398.25	2171.71	7.94	548.12	2.63
Range	2262 - 2423.64	1941.68 - 2202.90	7.84 - 8.18	301.74 - 741.32	2.27 - 4.07
North					
Average	2281.61 ± 83.31	1968 ± 87.11	8.14 ± 0.09	343.52 ± 81.73	3.93 ± 0.53
Median	2269.62	1941.97	8.16	325.5	3.76
Range	2154.78 - 2387.30	1844.42 - 2076.55	8.02 - 8.30	206.43 - 452.00	3.37 - 5.03
South					
Average	2366.55 ± 18.02	2064.54 ± 20.81	8.04 ± 0.031	429.23 ± 33.06	3.69 ± 0.13
Median	2368.66	2071.09	8.05	428.37	3.69
Range	2335.23 - 2385.27	2028.15 - 2085.87	7.98 - 8.09	374.86 - 494.89	3.45 - 3.90
Onshore					
Average	2287.08 ± 84.44	1987.96 ± 74.00	8.11 ± 0.06	362.93 ± 58.9	3.79 ± 0.26
Median	2294.92	1983.19	8.12	359.42	3.78
Range	2154.78 - 237527	1891.14 - 2077.66	8.03 - 8.18	295.52 - 445.26	3.40 - 4.16
Offshore					
Average	2361.59 ± 39.64	2048.03 ± 57.35	8.06 ± 0.07	410.83 ± 65.92	3.79 ± 0.32
Median	2375.28	2073	8.05	419.24	3.71
Range	2268.37 - 2400.78	1905.59 - 2088.15	7.98 - 8.22	262.33 - 494.89	3.45 - 4.55

Table 3. *Nutrient and dissolved oxygen concentrations at different locations at the surface and at depth from June 12-15, 2017*

June 2017	NO_3^- µmol/L	HPO^{2-}_4 µmol/L	$HSIO_3^-$ µmol/L	NH_4^+ µmol/L	NO_2^- µmol/L	Urea µmol/L	DIN µmol/L	Dissolved Oxygen mL/L
All Data								
Average	1.69 ± 2.83	1.06 ± 0.85	7.73 ± 6.31	2.39 ± 4.51	0.46 ± 0.85	0.79 ± 0.52	4.49 ± 5.76	4.24 ± 0.97
Median	0.02	0.76	5.55	1.56	0.16	0.68	2.75	4.64
Range	0 - 12.55	0.19 - 6.07	1.33 - 33.77	0 -36.76	0 -4.72	2.22 - 0.68	0.06 - 40.03	1.77 - 6.06
Surface								
Average	0.42 ± 1.03	1.38 ± 1.27	5.22 ± 3.74	1.80 ± 1.29	0.267 ± 0.40	0.90 ± 0.51	2.49 ± 2.07	4.83 ± 0.42
Median	0	1.01	3.93	1.56	0.09	1.02	1.72	4.8
Range	0 - 3.9	0.28 – 6.07	16.46 - 1.33	0.27 - 5.09	0 – 1.37	0.18 - 2.02	0.29 - 8.56	3.88 - 6.06
Bottom								
Average	3.41 ± 3.75	0.94 ± 0.51	11.14 ± 7.85	1.70 ± 1.17	0.69 ± 1.14	0.78 ± 0.56	5.74 ± 4.38	3.50 ± 1.06
Median	2.62	0.77	10.48	1.28	0.21	0.66	4.1	3.48
Average >50 m	8.04 ± 2.82	0.87 ± 0.30	11.37 ± 2.95	1.05 ± 0.80	0.12 ± 0.08	0.01 ± 0.01	9.21 ± 3.60	3.00 ± 0.79
Median >50 m	6.32	0.81	11.03	0.75	0.16	0.01	7.09	2.79
Range	0 - 12.55	0.27 - 2.16	1.80 - 33.77	0.12 - 4.03	0 - 4.72	0.07 - 2.22	0.67 - 15.15	1.77 - 5.09
North								
Average	1.05 ± 1.47	1.42 ± 0.91	5.74 ± 5.55	2.12 ± 1.16	0.53 ± 0.52	0.92 ± 0.60	3.71 ± 2.44	4.76± 0.52
Median	0.00	1.25	3.41	1.82	0.45	1.02	4.1	4.7
Range	0 - 3.9	0.28 - 2.85	1.33 - 16.46	0.75 - 3.50	0.04 - 1.37	0.27 - 2.02	0.81 - 8.57	3.94 - 6.06
South								
Average	0.00 ± 0.01	1.35 ± 1.72	4.93 ± 1.77	1.75 ± 1.28	0.04 ± 0.07	0.99 ± 0.43	1.80 ± 1.31	5.02 ± 0.18
Median	0	0.7	5.19	1.47	0	1.09	1.47	5
Range	0 - 0.03	0.35 - 6.07	2.42 - 7.33	0.45 - 5.09	0 -0.19	0.20 - 1.51	0.45 - 5.21	4.78 - 5.38
Onshore								
Average	1.16 ± 1.95	1.59 ± 0.81	5.60 ± 5.00	3.50 ± 3.75	0.48 ± 0.52	1.27 ± 0.48	5.14 ± 5.37	4.84 ± 0.20
Median	0	1.34	3.68	2.46	0.42	1.23	3.82	4.77
Range	0 - 5.12	0.68 - 2.85	1.69 - 16.46	0.45 - 13.24	0 - 1.37	0.35 - 2.02	0.45 - 18.88	4.6 - 5.28
Offshore								
Average	0.25 ± 0.74	1.14 ± 1.87	4.77 ± 2.21	1.27 ± 0.83	0.06 ± 0.07	0.55 ± 0.36	1.58 ± 1.45	4.85 ± 0.25
Median	0	0.57	4.31	1.31	0.04	0.39	1.34	4.79

Table 3. *Continued*

June 2017	NO_3^- µmol/L	HPO^{2-}_4 µmol/L	$HSIO_3^-$ µmol/L	NH_4^+ µmol/L	NO_2^- µmol/L	Urea µmol/L	DIN µmol/L	Dissolved Oxygen mL/L
Range	0 - 2.22	0.28 - 6.07	1.33 - 8.02	0 - 2.79	0 - 0.22	0.20 - 1.13	0.06 - 5.05	4.56 - 5.38

3.2 August 2017

Surface trends: Surface values include all samples taken from 0.5 – 3.1 m. Surface salinity increases southwards with a distinct trend, from an average of 34.19 ± 1.30 in the northern sites to 36.26 ± 0.53 in the south (Figs 4-5). Salinity is the lowest coming out of Galveston Bay at 32.04, at the sample site closest to the opening of the bay (Figs 4-5). August has the highest recorded temperatures with a max of 31.10 °C at the surface (Figs 6-7). Cooler temperatures were offshore in the southern sites, averaging 29.64 ± 0.77°C and the more northern samples averaging 30.30 ± 0.45 °C (Figs 6-7). pH generally increases with distance from the shore with inshore averages at 8.00 ± 0.01 and offshore averages 8.02 ± 0.01 pH (Figs 8-9, Table 4). The pCO_2 trends are less pronounced but are still inverse of pH, with inshore average of 467.78 ± 36.79 µatm and offshore 435.07 ± 6.64 µatm (Figs 10-11, Table 4). Ω_{ar} also increases with distance from shore with inshore sites averaging 3.87 ± 0.22 and offshore averaging 4.01 ± 0.03 (Figs 12-13, Table 4). TA and DIC have similar surface averages across all designations (Figs 14-15, Table 4). DO had similar averages between inshore and offshore values and a higher southern average of 5.02 ± 0.18 mL/L compared to the northern average of 4.76 ± 0.52 mL/L (Fig 18-19 Table 5). NO_3^- was below detection limits on average in surface waters in August (Figs 20-21, Table 5). HPO_4^{2-}, NH_4^+ and Urea have higher median values for offshore sites

compared to inshore sites (Figs 22-23, and 26-27, Table 5). $HSiO_3^-$ and NO_2^- have a higher median inshore than offshore sites (Figs 24-25, and 28-29, Table 5). All surface locations had higher medians in the northern sites (Table 5).

Depth trends: Bottom samples range from 10.9 – 102.6 m. Salinity is very homogenous in August, with surface salinity averages at 35.10 ± 1.46 and bottom salinities averaging 35.85 ± 0.99 (Fig 5). Temperatures at the surface averaged 30.01 ± 0.69 °C and decreased with depth with a minimum temperature of 18.76 °C at 102 m and a maximum temperature at 31.10°C taken from a surface bucket sample (Fig 7). pH decreases with depth while pCO_2 increases with the average bottom samples being 7.98 ± 0.04 and 495.02 ± 54.11 µatm respectively and the average surface samples at 8.02 ± 0.02 and 446.03 ± 18.96 µatm, respectively (Figs 8 and 10, Table 4). Ω_{ar} decreases with depth with a surface and deep average of 3.97 ± 0.11 and 2.79 ± 0.36, respectively (Fig 13, Table 4). TA and DIC increase with depth with surface and deep averages of 2407.59 ± 11.60 µmol/kg, 2067.70 ± 11.80 µmol/kg, and 2398.65 ± 7.88 µmol/kg, 2149.39 ± 27.45 µmol/kg, respectively (Figs 15 and 17, Table 4). DO decreases with depth with a surface average of 4.83 ± 0.42 mL/L and a range of 3.88 – 6.06 mL/L, bottom average of 3.50 ± 1.06 mL/L, and a deep average of 3.00 ± 0.79 µmol/L (Fig 19, Table 5). NO_3^- and NO_2^- both increase with depth with surface medians of NO_3^- being below detectable levels NO_2^- at 0.14 µmol/L and deep medians at 3.33 µmol/L and 0.24 µmol/L respectively (Figs 20 and 28, Table 5). HPO_4^{2-} and NH_4^+, had the highest median at the surface 0.7 µmol/L and 3.81 µmol/L respectively and the lowest median in the bottom samples, 0.56 µmol/L and 3.76 µmol/L, respectively (Figs 23 and 26 Table 5). $HSiO_3^-$ had the highest median in the bottom samples with an intermediate median in the surface values and lowest median at the surface (Fig 24 and Table 5). Urea concentrations decreased with depth (Fig 33 and Table 5).

Table 4. *Carbonate Chemistry parameters at different locations at the surface and at depth from August 08-11, 2017*

August 2017	**TA µmol/kg**	**DIC µmol/kg**	**pH**	**pCO_2 µatm**	**Ω_{ar}**
All Data					
Average	2408.9 ± 10.89	2090.80 ± 33.42	8.00 ± 0.04	465.03 ± 49.00	3.68 ± 0.42
Median	2408.5	2081.6	8.01	455.53	3.86
Range	2371.06 - 2436.59	2035.08 - 2192.15	7.88 - 8.08	375.56 - 658.40	2.34 - 4.32
Surface					
Average	2407.59 ± 11.60	2067.70 ± 11.80	8.02 ± 0.02	446.03 ± 18.96	3.97 ± 0.11
Median	2406.92	2067.97	8.02	447.97	4
Range	2371.06 - 2428.75	2041.44 - 2087.81	7.99 - 8.07	392.12 - 478.63	3.67 - 4.16
Bottom					
Average	2409.84 ± 11.89	2120.05 ± 32.83	7.98 ± 0.04	495.02 ± 54.11	3.34 ± 0.47
Median	2411.1	2112.09	7.99	485.57	3.41
Average >50 m	2398.65 ± 7.88	2149.33 ± 27.45	7.98 ± 0.04	494.51 ± 48.01	2.79 ± 0.36
Median >50 m	2399.02	2152.51	7.97	504.86	2.76
Range	2379.31 - 2436.59	2070.39 - 2192.15	7.88 - 8.05	410.61 - 658.40	2.34 - 3.96
North					
Average	2405.25 ± 13.93	2068.85 ± 10.77	8.02 ± 0.02	446.12 ± 21.07	3.99 ± 0.10
Median	2405.6	2068.47	8.02	448.4	4.01
Range	2371.06 - 2428.75	2041.44 - 2087.67	7.99 - 8.07	392.1 - 478.60	3.7 - 4.16
South					
Average	2411.10 ± 8.31	2068.32 ± 13.44	8.01 ± 0.01	448.27 ± 17.55	3.94 ± 0.13
Median	2408.82	2072.56	8.01	451.4	3.96
Range	2400.28 - 2428.20	2049.97 - 2087.81	7.99 - 8.04	414.7 - 474.2	3.67 - 4.07
Onshore					
Average	2408.211 ± 14.12	2079.66 ± 20.94	8.00 ± 0.02	467.78 ± 36.79	3.87 ± 0.22
Median	2410.18	2072.56	8.01	461.4	3.95
Range	2371.06 - 2428.20	2062.25 - 2137.19	7.94 - 8.04	429.2 - 571.6	3.35 - 4.06
Offshore					
Average	2404.45 ± 6.09	2059.02 ± 8.19	8.02 ± 0.01	435.07 ± 6.64	4.01 ± 0.03
Median	2405.42	2059.46	8.02	433	4.01
Range	2396.61 - 2417.81	2049.97 - 2077.22	8.01 - 8.03	427.6 - 445.4	3.95 - 4.06

Table 5. *Nutrient and dissolved oxygen concentrations at different locations at the surface and at depth from August 08-11, 2017*

August 2017	**NO_3^-** µmol/L	**HPO^{2-}_4** µmol/L	**$HSIO_3^-$** µmol/L	**NH_4^+** µmol/L	**NO_2^-** µmol/L	**Urea** µmol/L	**DIN** µmol/L	**Dissolved Oxygen** mL/L
All Data								
Surface								
Average	0.19 ± 0.62	0.78 ± 0.86	4.56 ± 3.66	4.05 ± 1.90	0.15 ± 0.08	0.44 ± 0.45	4.41 ± 1.99	4.53 ± 0.26
Median	0	0.7	3.62	3.81	0.14	0.34	4.27	4.47
Range	0 - 3.48	0 - 3.55	0 - 14.05	0.06 - 8.97	0 - 0.38	0 - 1.78	0 - 9.04	4.28 - 5.87
Depth								
Average	1.31 ± 2.85	0.69 ± 0.77	6.91 ± 5.10	3.87 ± 1.90	0.28 ± 0.24	0.31 ± 0.37	5.45 ± 3.62	3.73 ± 0.65
Median	0	0.44	5.65	3.61	0.21	0.19	4.41	3.91
Average >50 m	4.96 ± 4.46	0.80 ± 0.83	3.50 ± 4.56	5.03 ± 3.25	0.23 ± 0.08	0.36 ± 0.63	10.22 ± 4.91	3.24 ± 0.62
Median >50 m	3.33	0.56	2.39	3.76	0.24	0.05	12.59	3.21
Range	0 - 11.8	0 - 2.85	0 - 18.71	1.30 - 11.52	0.06 - 1.04	0 - 1.73	1.40 - 15.07	2.12 - 4.64
North								
Average	0.15 ± 0.23	1.04 ± 0.96	5.36 ± 3.70	4.45 ± 2.05	0.16 ± 0.09	0.61 ± 0.49	4.76 ± 2.13	4.48 ± 0.11
Median	0.00	0.75	5.43	4.22	0.15	0.48	4.4	4.46
Range	0 - 0.65	0 - 3.55	0 - 14.05	1.36 - 8.97	0 -0.38	0 - 1.78	1.45 - 9.04	4.28 - 4.78
South								
Average	0.25 ± 0.93	0.49 ± 0.60	3.76 ± 3.56	3.80 ± 1.38	0.14 ± 0.07	0.26 ± 0.30	4.22 ± 1.26	4.50 ± 0.08
Median	0	0.23	2.33	3.57	0.12	0.15	4.01	4.5
Range	0 - 3.48	0 - 1.82	0 - 10.09	1.89 - 6.43	0.05 - 0.25	0 - 0.97	2.59 - 6.64	4.41 - 4.66
Onshore								
Average	0.06 ± 0.14	0.74 ± 0.90	6.667 ± 3.33	3.97 ± 2.24	0.16 ± 0.10	0.35 ± 0.34	4.70 ± 2.03	4.66 ± 0.38
Median	0	0.45	6.38	3.37	0.15	0.34	3.85	4.53
Range	0 - 0.51	0 - 2.9	2.23 - 17.49	2.36 - 8.97	0.05 - 0.47	0 - 1.18	2.56 - 9.04	4.1 - 4.78
Offshore								
Average	0.38 ± 1.04	0.63 ± 0.60	3.16 ± 4.10	3.91 ± 1.73	0.16 ± 0.06	0.57 ± 0.62	4.45 ± 1.72	4.45 ± 0.03
Median	0	0.74	1.11	3.81	0.14	0.44	4.3	4.45
Range	0 - 3.48	0 - 1.82	0 - 12.26	1.89 - 7.26	0.07 - 0.25	0 - 1.78	1.98 - 7.77	4.41 - 4.51

3.3 September 2017

Surface trends: Surface depths range from 2.3 – 5.3 m and deep samples range from 11.4 – 208.0 m. September data was collected following Hurricane Harvey and included the FGB as well as the transect from Galveston. Salinity in September is highly reduced from previous cruises and surface values increase moving away from shore with inshore averages at 26.46 ± 2.91 and offshore averages at 34.75 ± 1.87 (Fig 4, Table 6). Surface temperatures do not exhibit any strong spatial trends, with a minimum surface temperature of 27.63°C and a maximum surface value of 29.43°C (Fig 6, Table 6). pH surface averages decrease with distance from shore, while pCO_2 surface averages increase with distance, inshore surface averages of 8.05 ± 0.00 and 408.81 ± 8.97 µatm and offshore averages of 8.04 ± 0.01 and 411.87 ± 16.84 µatm, respectively (Figs 8 and 10, Table 6). Ω_{ar} increases with distance from shore, with the highest surface value at 4.16 µmol/kg located over the FGB grid, along with TA and DIC with inshore averages at 3.96 ± 0.23, 2390.63 ± 29.22 µmol/kg, and 2050.99 ± 4.95 µmol/kg, and offshore averages of 4.01 ± 0.18, 2400.81 ± 19.24 µmol/kg, and 2053.07 ± 7.89 µmol/kg, respectively (Fig 12, 14, and 16 Table 6). For both TA and DIC, the southern offshore values had higher averages than the inshore northern values. DO had general homogeneity throughout all surface areas for September. The largest average was in the southern sites with an average of 4.75 ± 0.56 mL/L (Figs 14, 16 and 18, Table 6). All Nutrients except for NO_3^- exhibited the same strong surface spatial medians (Fig 20, Table 7). All Nutrients had the highest medians inshore and in the northern sites (Figs 20-33, Table 7). NO_3^- had a higher median in the northern site, however there was a slightly higher median in the offshore sites than then inshore sites, being 0.19 µmol/kg to 0.18 µmol/kg (Fig 20, Table 7).

Depth trends: Fresher water induced from Hurricane Harvey reaches further out into The Gulf of Mexico than all other cruises with the lowest salinity of all five cruises being 22.04 °C at the surface on a station just south of Galveston bay (Fig 5, Table 6). The average surface salinity was 30.59 ±4.46 while the average bottom salinity was 34.03 ± 2.99 (Fig 5, Table 6). Temperatures decrease with depth with a minimum and maximum temperature of 14.34°C at 208 m and 34.74°C at the surface near the mouth of Galveston Bay (Fig 7, Table 6). pH decreases with depth with the surface, bottom, and deep averaging 8.06 ± 0.03, 7.95 ± 0.05 and 7.71 ± 1.45 (Fig 9, Table 6). Contrastingly pCO_2 had an average surface value of 393.33 ± 28.93 µatm and a bottom average of 519.34 ± 64.29 µatm (Fig 11, Table 6). The overall average Ω_{ar} was 3.53 ± 0.66 µmol/kg and decreases with depth with a surface average of 3.78 ± 0.36 and a bottom average of 2.62 ± 0.58 (Fig 13, Table 6). The minimum overall value for Ω_{ar} was located at a depth of 208 m and had a value of 1.83 (Fig 13, Table 6). TA and DIC both had their lowest averages in the surface samples (2311.97 ± 135.72 µmol/kg and 1991.65 ±96.75 µmol/kg), but the highest averages were in the bottom samples, not the deep samples (Figs 15 and 17, Table 6). DO in the surface has an average of 4.68 ± 0.59 mL/L and a range of 3.93 – 8.00, which is higher than the averages of the bottom samples and the deep samples with respective averages of 3.55 ± 0.64 and 3.49 ± 2.93 mL/L and a bottom range of 2.58 – 6.21 mL/L (Fig 19, Table 7). All nutrients except for NO_3^- and urea had the highest medians in the bottom samples, then the deep samples and the lowest medians in the surface samples (Fig 20, Table 7). NO_3^- increased with depth with the highest median in the bottom samples and the lowest at the surface with, 4.24 µmol/L and 0.13 µmol/L, respectively (Fig 20, Table 7). Urea decreased with depth with the highest median at the surface and the lowest median in the deep samples, 0.57 µmol/L and 0.45 µmol/L, respectively (Fig 33, Table 7).

Table 6. *Carbonate Chemistry parameters at different locations at the surface and at depth from September 23- October 1, 2017*

September 2017	**TA µmol/kg**	**DIC µmol/kg**	**pH**	**pCO_2 µatm**	**Ω_{ar} µmol/kg**
All Data					
Average	2369.09 ± 88.94	2062.30 ± 85.80	8.02 ± 0.05	436.08 ± 63.82	3.52 ± 0.66
Median	2404.16	2054.72	8.04	410.05	3.83
Range	1985.43 - 2414.05	1754.59 - 2191.17	7.91 - 8.11	343.08 - 576.46	1.83 - 4.16
Surface					
Average	2311.97 ± 135.72	1991.65 ± 96.75	8.06 ± 0.03	393.33 ± 28.93	3.78 ± 0.36
Median	2401.95	2049.71	8.05	401.11	3.86
Range	1985.43 - 2414.05	1754.60 - 2070.35	8.02 - 8.11	343.08 - 444.10	3.02 - 4.16
Bottom					
Average	2387.89 ± 17.46	2154.53 ± 37.15	7.96 ± 0.05	519.34 ± 64.29	2.62 ± 0.58
Median	2390.73	2172.01	7.93	549.33	2.46
Average >50 m	2313.44 ± 434.43	2063.63 ± 383.48	7.71 ± 1.45	477.03 ± 101.81	2.82 ± 0.77
Median >50 m	2397.44	2131.84	7.97	494.96	2.86
Range	2353.86 - 2407.72	2072.83 - 2191.17	7.91 - 8.04	412.01 - 576.46	1.83 - 3.70
North					
Average	2344.60 ± 88.42	2021.66 ± 69.26	8.05 ± 0.03	407.93 ± 35.51	3.77 ± 0.22
Median	2385.02	2051.87	8.05	412.97	3.73
Range	2156.67 - 2408.52	1880.81 - 2070.35	8.02 - 8.11	343.08 - 444.10	3.49 - 4.07
South					
Average	2408.25 ± 1.21	2050.03 ± 2.83	8.05 ± 0.01	402.87 ± 6.85	4.10 ± 0.04
Median	2408.55	2050.45	8.04	401.86	4.11
Range	2406.47 - 2409.93	2045.69 - 2054.23	8.04 - 8.06	391.4 - 411.93	4.05 - 4.16
Inshore					
Average	2390.63 ± 29.22	2050.99 ± 4.95	8.05 ± 0.00	408.81 ± 8.97	3.96 ± 0.23
Median	2406.27	2051.77	8.05	406.04	4.07
Range	2356.91 - 2408.52	2045.69 - 2055.51	8.046-8.049	401.56 - 418.84	3.70 - 4.11
Offshore					
Average	2400.81 ± 19.24	2053.07 ± 7.89	8.04 ± 0.01	411.87 ± 16.84	4.01 ± 0.18
Median	2407.6	2051.18	8.05	407.02	4.07
Range	2337.64 - 2409.93	2045.69 - 2070.35	8.02 - 8.06	391.4 - 444.10	3.55 - 4.16

Table 7. *Nutrient and dissolved oxygen concentrations at different locations at the surface and at depth from September 23- October 1, 2017*

September 2017	**NO_3^-** µmol/L	**HPO^{2-}_4** µmol/L	**$HSIO_3^-$** µmol/L	**NH_4^+** µmol/L	**NO_2^-** µmol/L	**Urea** µmol/L	**DIN** µmol/L	**Dissolved Oxygen** mL/L
All Data								
Average	1.18 ± 2.51	1.46 ± 1.49	6.16 ± 7.24	2.56 ± 1.22	0.39 ± 0.53	0.69 ± 0.77	4.03 ± 3.07	4.25 ± 0.88
Median	0.27	1.1	3.64	2.39	0.22	0.55	3.23	4.47
Range	0 - 16.90	0 -12.71	0 - 46.29	0.08 - 13.12	0.02 - 4.76	0 - 10.78	0 - 19.58	1.73 - 7.96
Surface								
Average	0.24 ± 0.29	1.60 ± 1.78	4.08 ± 3.94	2.38 ± 0.86	0.19 ± 0.13	0.66 ± 0.52	2.78 ± 0.94	4.68 ± 0.59
Median	0.1355	1.116	2.61	2.312	0.157	0.5655	2.82	4.55
Range	0 - 1.2	0 - 9.10	0 - 14.99	0.69 - 4.22	0.05 - 0.562	0 - 2.47	1.09 - 4.49	3.93 - 8.00
Bottom								
Average	3.41 ± 4.13	1.75 ± 2.08	10.69 ± 10.14	2.51 ± 0.81	0.72 ± 0.88	0.70 ± 0.64	6.63 ± 4.18	3.55 ± 0.64
Median	1.46	1.25	5.98	2.49	0.38	0.54	5.46	3.39
Average >50 m	5.56 ± 5.21	1.60 ± 1.45	3.88 ± 4.30	2.37 ± 0.85	0.24 ± 0.13	0.73 ± 0.79	6.82 ± 4.85	3.49 ± 2.93
Median >50 m	4.2415	1.2215	2.798	2.3345	0.2265	0.448	4.87	2.926449
Range	0.1 - 16.90	0 - 5.80	0 - 20.11	1.08 - 4.02	0.05 - 0.50	0 - 3.22	1.82 - 15.11	2.58 - 6.21
North								
Average	0.35 ± 0.65	1.60 ± 1.42	7.65 ± 8.47	2.60 ± 0.94	0.29 ± 0.29	0.84 ± 0.59	3.34 ± 1.56	4.62 ± 0.63
Median	0.19	1.41	4.82	2.62	0.26	0.86	3.17	4.53
	0 - 3.85	0 - 6.65	0 - 35.15	0.69 - 4.45	0.05 - 1.68	0 - 2.47	1.09 - 5	3.62 - 7.96
South								
Average	0.26 ± 0.33	1.75 ± 1.82	5.41 ± 4.56	2.60 ± 0.80	0.21 ± 0.13	0.68 ± 0.43	3.06 ± 0.86	4.75 ± 0.56
Median	0.14	1.29	2.68	2.49	0.17	0.62	2.98	4.67
	0 -1.1	0.25 - 9.1	0.85 - 20.74	1.41 - 4.11	0.05 - 0.56	0.12 - 1.86	1.6 - 4.22	4.44 - 7.15
Onshore								
Average	0.39 ± 0.86	2.09 ± 1.51	10.92 ± 9.91	3.11 ± 0.91	0.36 ± 0.36	0.99 ± 0.55	3.86 ± 1.76	4.58 ± 0.35
Median	0.18	1.73	9.8	3.18	0.28	0.96	3.83	4.68
	0 - 3.85	0 - 6.65	0 - 35.15	1.45 - 4.45	0.05 - 1.68	0.15 - 2.47	1.75 - 9.98	3.62 - 5.04
Offshore								
Average	0.29 ± 0.32	0.94 ± 0.77	2.55 ± 2.66	2.13 ± 0.73	0.13 ± 0.08	0.54 ± 0.49	2.31 ± 0.82	4.52 ± 0.12
Median	0.19	0.8	2.16	2.2	0.12	0.41	2.06	4.51

Table 7. *Continued*

September 2017	**NO_3^-** µmol/L	**HPO^{2-}_4** µmol/L	**$HSIO_3^-$** µmol/L	**NH_4^+** µmol/L	**NO_2^-** µmol/L	**Urea** µmol/L	**DIN** µmol/L	**Dissolved Oxygen** mL/L
Range	0 - 1.1	0 - 3.46	0 - 11.76	0.69 - 3.65	0.05 - 0.36	0 - 2.47	1.09 - 3.88	4.11 - 4.51

3.4 October 2017

Surface trends: Surface samples range from 2.69 – 5.22 m and bottom samples range from 14.79 – 292.42 m. October data is restricted to a line leading out to the FGB and the grid of the FGB. Salinity increase with distance from shore with the surface station closest to the mouth of Galveston Bay showing the freshest sample at 26.24 (Fig 4). Surface salinity progressively increases along the Galveston transect leading out to the FGB grid with the highest surface salinity value at the most south-western grid point with a value of 36.33 (Fig 4). Temperatures increase with distance from shore with the Galveston transect, going from 25.28 °C at the mouth of Galveston bay to 28.04 °C beginning at the FGB grid (Fig 4). The pH trends stay relatively homogenous at the surface as do trends in pCO_2 (Figs 8 and 10, Table 8). The surface minimum value of pH is 8.04, nearer to the mouth of Galveston Bay and the maximum surface value is 8.12, located on the most eastern side of the FGB grid (Figs 8 and 10, Table 8). pCO_2 has a surface range of 329.95 to 430.20 µatm, located at the same samples of the maximum and minimum of pH (Figs 8 and 10, Table 8). Surface Ω_{ar} also increases with distance from shore with the lowest value at 2.95 again at the station closest to the mouth of Galveston Bay (Fig 12, Table 8). The highest surface Ω_{ar} value at 4.28 is located on the most eastern side of the FGB grid (Fig 9 Table 8). DO does not show average trends in any of the surface values (Fig 18,

Table 9). Because October only had the FGB grid, no north/south or inshore/offshore trends are being reported.

Depth trends: The average surface and bottom salinity were similar with averages of 35.69 and 35.74 respectively (Fig 5). The overall average salinity was 36.07 ± 1.05 with a minimum of 26.24 located at the mouth of Galveston Bay and a maximum of 36.47 located in deeper waters (125.55 m) in the middle of the FGB grid (Fig 5). Over all temperatures range from 12.92 °C at a depth of 292.42 m to 28.14 °C at a depth of 51.26 m on the FGB grid with an overall average of 25.78 ± 3.51 °C (Fig 7). pH has the highest average at the surface and decreases with depth (Fig 9, Table 8). However, the bottom and deep samples were similar, with an average surface and bottom of 8.06 ± 0.01 and 7.98 ± 0.05 (Fig 9 Table 8). The maximum and minimum value of pH is 8.12 and 7.89 (Fig 9 Table 8). pCO_2 increases with depth with an overall minimum and maximum of 329.95 and 586.75 µatm and overall average of 426.95 ± 54.09 µatm (Fig 11 Table 8). The average pCO_2 values of the surface, bottom and deep samples are 392.63 ± 15.31 µatm, 488.91 ± 61.74 µatm and 497.22 ± 59.33 µatm (Fig 11 Table 8). Ω_{ar} decreases with depth with surface, bottom and deep samples averaging 3.97 ± 0.22, 2.92 ± 0.71 and 2.83 ± 0.69, respectively (Fig 13 Table 8). DO had higher surface averages than the bottom samples, at 4.49 ± 0.28 and 3.60 ± 0.85 mL/L respectively (Fig 19 Table 9). NO_3^-, HPO_4^{2-}, and urea all increased with depth having high medians in the deep samples, 2.19 µmol/L, 0.71 µmol/L, and 0.19 µmol/L, respectively, and low medians at the surface 1.11 µmol/L, 0.63 µmol/L and 0.14 µmol/L, respectively (Figs 20, 22 and 33, Table 9). $HSiO_3^-$, NO_2^-, and NH_4^+ all had intermediate means in the deep samples while $HSiO_3^-$ and NO_2^- both had low medians in the surface samples, 2.02 µmol/L and 0.04 µmol/L, respectively and NH_4^+ had a high median at the surface, 2.45 µmol/L (Figs 24, 26, and 28, Table 9).

Table 8. *Carbonate Chemistry parameters at different locations at the surface and at depth from October 20-24, 2017*

October 2017	**TA** µmol/kg	**DIC** µmol/kg	**pH**	**pCO_2** µatm	**Ω_{ar}**
All Data					
Average	2397.86 ± 17.03	2079.60 ± 45.96	8.03 ± 0.04	428.06 ± 54.86	3.60 ± 0.62
Median	2401.62	2055.25	8.05	399.56	3.93
Range	2259.90 - 2417.13	2008.21 - 2194.10	7.89 - 8.12	329.95 - 586.75	1.65 - 4.38
Surface					
Average	2397.32 ± 26.54	2048.12 ± 12.59	8.06 ± 0.01	392.63 ± 15.31	3.97 ± 0.22
Median	2402.45	2047.55	8.06	390.94	4.01
Range	2259.90 - 2417.13	2008.21 - 2077.27	8.04 - 8.12	329.95 - 430.20	2.95 - 4.28
Bottom					
Average	2391.48 ± 17.48	2130.99 ± 48.82	7.98 ± 0.05	488.91 ± 61.74	2.92 ± 0.71
Median	2400.37	2135.05	7.98	489.4	2.97
Average >50 m	2390.0 ± 17.80	2137.19 ± 47.50	7.97 ± 0.05	497.22 ± 59.33	2.83 ± 0.69
Median >50 m	24000.38	2137.47	7.98	491.56	2.92
Range	2341.21 - 2411.66	2043.90 - 2194.10	7.89 - 8.07	390.70 - 586.75	1.65 - 4.03

Table 9. *Nutrient and dissolved oxygen concentrations at different locations at the surface and at depth from October 20-24, 2017*

October 2017	**NO_3^-** µmol/L	**HPO^{2-}_4** µmol/L	**$HSIO_3^-$** µmol/L	**NH_4^+** µmol/L	**NO_2^-** µmol/L	**Urea** µmol/L	**DIN** µmol/L	**Dissolved Oxygen** mL/L
All Data								
Average	2.51 ± 4.43	0.70 ± 0.33	3.93 ± 3.28	2.41 ± 2.12	0.12 ± 0.13	0.20 ± 0.18	5.00 ± 5.20	4.46 ± 0.78
Median	1.11	0.66	2.96	2.34	0.08	0.18	3.57	4.68
Range	0.04 - 21.23	0.07 - 2.51	0.83 - 23.20	0.11 - 20.94	0 - 0.84	0.01 - 1.66	0 - 35.5	2.41 - 5.54
Surface								
Average	1.07 ± 0.29	0.65 ± 0.30	4.81 ± 5.94	2.24 ± 1.40	0.09 ± 0.16	0.21 ± 0.30	3.40 ± 1.34	4.89 ± 0.28
Median	1.11	0.625	2.019	2.45	0.038	0.144	3.61	4.91
Range	0.11 - 1.39	0.26 - 1.73	0.83 - 23.2	0.27 - 5.38	0.00 - 0.84	0.01 - 1.66	1.54 - 6.43	4.49 - 5.54

Table 9. *Continued*

October 2017	**NO_3^-** µmol/L	**HPO^{2-}_4** µmol/L	**$HSIO_3^-$** µmol/L	**NH_4^+** µmol/L	**NO_2^-** µmol/L	**Urea** µmol/L	**DIN** µmol/L	**Dissolved Oxygen** mL/L
Bottom								
Average	6.20 ± 7.23	0.71 ± 0.42	5.21 ± 1.99	2.05 ± 1.19	0.13 ± 0.14	0.18 ± 0.09	8.38 ± 7.47	3.6 ± 0.85
Median	1.8965	0.6955	5.0255	1.9755	0.095	0.175	4.59	3.57
Average >50 m	6.81 ± 7.37	0.73 ± 0.43	5.08 ± 2.0	2.06 ± 1.22	0.13 ± 0.15	0.19 ± 0.09	9.00 ± 7.62	3.50 ± 0.83
Median >50 m	2.193	0.706	4.996	2	0.095	0.186	4.81	3.52
Range	0.11 - 21.23	0.07 - 2.51	1.21 - 9.84	0.39 - 5.00	0.01 - 0.79	0.05 - 0.45	0.79 - 24.61	2.41 - 5.08

3.5 November 2017

Surface trends: Surface samples range from 1.9 – 3.6 m, while bottom samples range from 11.7 – 204.7 m. Salinity shows a slight increase with distance from shore with surface inshore and offshore averages at 31.73 ± 2.21 and 34.93 ± 2.12, respectively (Fig 4). Surface temperatures show almost no trend with inshore and offshore averages at 23.08 ± 1.02 and 24.61 ± 5.43 °C, respectively (Fig 5). The coolest surface temperatures are collected in the northern sites around the mouth of Galveston Bay (Fig 5). pH and pCO_2 stay relatively homogenous at the surface with a range of 8.06 - 8.13 and 330.60 - 434.96 µatm (Figs 8 and 10, Table 10). Ω_{ar} slightly increases with distance from shore with inshore and offshore averages of 3.34 ± 0.23 and 4.03 ± 0.32 (Fig 12, Table 10). The surface range for Ω_{ar} is 3.12 - 4.75, with the highest recorded surface value located on the western side of the FGB grid (Fig 12, Table 10). TA has the highest surface average in the southern region and offshore, 2422.82 ± 8.53 µmol/kg and 2419.79 ± 9.31µmol/kg, respectively, while DIC has the highest averages inshore and in the northern sites, 2091.90 ±11.60 and 2086.98 ± 10.55, respectively (Figs 14 and 16, Table 10). DO had generally

homogenous surface values across all regions (Fig 18, Table 11). All nutrients had higher medians inshore than offshore (Table 11). HPO_4^{2-} and NH_4^+ had higher medians in the southern sites while all other nutrients had higher medians in the northern sites (Figs 22 and 26, Table 11). *Depth trends:* The surface samples range in a depth from 1.9 -3.6 m and the bottom samples range in a depth from 11.7 -204.7 m. Salinity has an overall range of 25.59 to 36.47 and an average of 34.41 ± 2.45 (Fig 5). The average of the surface and bottom salinities is 33.59 ± 2.66 and 34.79 ± 2.00, respectively, (Fig 5). Temperatures decrease with depth with an overall range and average of 15.43 – 36.20 °C and 24.11± 2.08 °C, with the lowest temperature at a depth of 193.8 m and the warmest temperature at 3 m in the FGB grid (Fig 7). pH decreases with depth with overall range of pH values being 7.95 at 172 m to 8.13 at 2.1 m (Fig 7 Table 10). pCO_2 increases with depth with an overall range of 330.63 – 524.88 µatm and a surface, bottom and deep average of 367.33 ± 22.89 µatm, 453.12 ± 56.79 µatm, and 473.87 ± 45.14 µatm, respectively (Fig 11 Table 10). Ω_{ar} decreases with depth with an overall range of 2.16 – 4.75 µmol/kg with the lowest value at a depth of 204.7 m (Fig 13 Table 10). DO overall surface, bottom and deep averages are 4.68 ± 0.87 mL/L, 4.50 ± 0.78 mL/L, and 4.58 ± 0.79 mL/L, respectively (Fig 19, Table 11). All Nutrients except for urea have high medians in their bottom samples, and out of those nutrients, HPO_4^{2-}, $HSiO_3^-$, and NH_4^+ have the lowest medians in the deep samples (Figs 23, 24, 26, and 33, Table 11). NO_3^- and NO_2^- have the lowest medians in the surface samples (Figs 20 and 28, Table 11). Urea decreased with decreasing depth, with medians of 0.46 µmol/L, 0.43 µmol/L and 0.37 µmol/L, respectively (Fig 33, Table 11).

Table 10. *Carbonate Chemistry parameters at different locations at the surface and at depth from November 15-20, 2017*

November 2017	**TA** µmol/kg	**DIC** µmol/kg	**pH**	**pCO2** µatm	**Ω_{ar}**
All Data					
Average	2412.04 ± 20.36	2092.28 ± 34.12	8.07 ± 0.05	391.57 ± 50.75	3.62 ± 0.53
Median	2418.51	2075.03	8.09	371.61	3.85
Range	2347.27 - 2438.76	2061.60 - 2185.35	7.95 - 8.13	330.63 - 533.46	2.16 - 4.75
Surface					
Average	2395.62 ± 26.21	2081.83 ± 12.42	8.10 ± 0.02	367.33 ± 22.89	3.71 ± 0.42
Median	2404.24	2081.47	8.1	364.36	3.68
Range	2347.27 - 2424.49	2061.60 - 2108.99	8.06 - 8.13	330.63 - 434.96	3.12 - 4.75
Bottom					
Average	2409.49 ± 18.31	2138.56 ± 40.45	8.01 ± 0.05	453.12 ± 56.79	3.01 ± 0.62
Median	2414.01	2151.04	8.01	459.9	2.98
Average >50 m	2406.68 ± 19.90	2153.34 ± 30.57	7.99 ± 0.04	473.87 ± 45.14	2.80 ± 0.53
Median >50 m	2408.6	2159.38	7.99	476.22	2.85
Range	2380.37 - 2428.74	2069.48 - 2185.35	7.95 - 8.08	377.76 - 524.88	2.16 - 3.85
North					
Average	2388.73 ± 26.22	2086.98 ± 10.55	8.11 ± 0.02	366.90 ± 27.32	3.62 ± 0.47
Median	2387.17	2086.51	8.1	364.08	3.54
Range	2347.27 - 2424.49	2073.69 - 2108.99	8.06 - 8.13	330.63 - 434.96	3.12 - 4.75
South					
Average	2422.82 ± 8.53	2068.40 ± 4.56	8.09 ± 0.01	363.51 ± 11.90	3.98 ± 0.11
Median	2419.04	2069.86	8.09	367.55	3.93
Range	2417.63 - 2435.56	2061.60 - 2072.78	8.08 - 8.11	343.85 - 373.22	3.88 - 4.14
Onshore					
Average	2373.15 ± 24.94	2091.90 ± 11.60	8.11 ± 0.01	360.37 ± 17.67	3.34 ± 0.23
Median	2363.51	2087.95	8.11	364.77	3.25
Range	2347.27 - 2413.10	2078.66 - 2108.99	8.10 - 8.13	330.63 - 376.03	3.12 - 3.69
Offshore					
Average	2419.79 ± 9.31	2071.88 ±6.66	8.09 ± 0.01	372.24 ± 26.91	4.03 ± 0.32
Median	2418.53	2072.21	8.09	365.95	3.93

Table 10. *Continued*

November 2017	**TA** µmol/kg	**DIC** µmol/kg	**pH**	**pCO2** µatm	**Ω_{ar}**
Range	2404.24 - 2435.56	2061.60 - 2084.28	8/06 - 8.11	343.85 - 434.96	3.68 - 4.75

Table 11. *Nutrient and dissolved oxygen concentrations at different locations at the surface and at depth from November 15-20, 2017*

November 2017	**NO_3^-** µmol/L	**HPO_4^{2-}** µmol/L	**$HSIO_3^-$** µmol/L	**NH_4^+** µmol/L	**NO_2^-** µmol/L	**Urea** µmol/L	**DIN** µmol/L	**Dissolved Oxygen** mL/L
All Data								
Average	1.1 ± 2.37	0.86 ± 0.62	6.33 ± 6.44	3.1 ± 2.15	0.29 ± 0.31	0.49 ± 00.38	4.50 ± 3.20	4.75 ± 0.82
Median	0.45	0.72	3.97	2.92	0.18	0.43	3.83	4.69
Range	0 - 15.75	0 - 3.53	0 - 60.15	0 - 26.97	0 - 1.34	0 - 2.32	0 - 28.43	2.60 - 8.79
Surface								
Average	0.42 ± 0.52	0.90 ±0.69	7.93 ± 9.74	3.32 ± 3.85	0.26 ± 0.29	0.50 ± 0.37	4.01 ± 4.11	4.82 ± 0.27
Median	0.213	0.775	4.883	2.865	0.146	0.458	3.42	4.76
Range	0 - 1.94	0 - 2.24	0.72 - 60.15	0 - 26.97	0 - 1.13	0 - 1.70	0 - 28.44	3.79 - 5.21
Bottom								
Average	2.33 ± 4.04	0.88 ± 0.54	6.69 ± 4.57	3.09 ± 1.37	0.38 ± 0.37	0.50 ± 0.36	5.8 ± 3.82	4.50 ± 0.78
Median	0.6765	0.8805	5.198	2.9235	0.213	0.428	4.49	4.5
Average >50 m	5.10 ± 5.27	0.64 ± 0.43	3.78 ± 1.76	2.54 ± 0.82	0.20 ± 0.15	0.39 ± 0.41	7.85 ± 5.13	4.58 ± 0.79
Median >50 m	2.664	0.533	3.301	2.564	0.161	0.366	5.33	3.909134042
Range	0 - 15.75	0.1 - 2.41	0.21 - 18.11	0.62 - 9.88	0.01 - 1.34	0 - 1.80	2.24 - 17.64	2.60 - 6.67
North								
Average	0.46 ± 0.44	0.94 ± 0.70	9.02 ± 6.08	3.80 ± 5.27	0.30 ± 0.31	0.48 ± 0.28	4.56 ± 5.47	4.86 ± 0.33
Median	0.42	0.755	7.5365	2.7555	0.1715	0.4625	3.48	4.91
Range	0 - 1.45	0 - 2.21	1.41 - 20.52	1.06 - 26.97	0 - 1.13	0.04 - 1.01	1.06 - 28.44	3.79 - 5.21
South								
Average	0.38 ± 0.60	0.86 ± 0.69	6.79 ± 12.55	2.82 ± 1.23	0.23 ± 0.27	0.53 ± 0.45	3.28 ± 1.94	4.78 ± 0.18
Median	0.077	0.788	3.345	2.995	0.136	0.43	3.32	4.69
Range	0 - 1.94	0.05 - 2.24	0.72 - 60.15	0 - 6.09	0 - 0.94	0 - 1.70	0 - 8.97	4.56 - 5.21
Onshore								

Table 11. *Continued*

November 2017	**NO_3^-** µmol/L	**HPO_4^{2-}** µmol/L	**$HSIO_3^-$** µmol/L	**NH_4^+** µmol/L	**NO_2^-** µmol/L	**Urea** µmol/L	**DIN** µmol/L	**Dissolved Oxygen** mL/L
Average	0.61 ± 0.56	1.42 ± 0.62	15.03 ± 14.23	4.99 ± 6.42	0.53 ± 0.35	0.71 ± 0.38	6.13 ± 6.60	4.93 ± 0.24
Median	0.5315	1.3885	13.274	3.2605	0.5875	0.6775	4.3	4.98
Range	0 - 1.94	0.57 - 2.21	1.70 - 60.15	2.01 - 26.97	0.03 - 1.13	0.09 - 1.70	2.30 - 28.44	4.65 - 5.21
Offshore								
Average	0.28 ± 0.45	0.54 ± 0.54	3.51 ± 1.99	2.32 ± 0.94	0.08 ± 0.08	0.30 ± 0.26	2.57 ± 1.23	4.69 ± 0.27
Median	0.0685	0.3585	3.1705	2.466	0.0685	0.304	3.09	4.69
Range	0 - 1.56	0 - 2.24	0.72 - 8.01	0 - 3.81	0 - 0.32	0 - 1.01	0 - 4.43	3.79 -5.08

4. DISCUSSION

4.1 Seasonal Trends

Seasonal trends in temperature, salinity, and carbonate chemistry parameters are evident in surface waters. Surface waters warm through the summer from June to August and then cool down heading into the fall from August to November, where November temperatures are cooler than October ones (Fig 34). August has the warmest surface waters and November has the coolest. Seasonal temperature trends are also evident at depth with in the upper 50 m of the water column, with cooling occurring from August to November (Fig 34). Salinity reflects seasonal changes in freshwater runoff from land, with June being fresher compared to August, October, and November (Fig 35). Eastern Texas is considered a subtropical zone where April, May, and June are typically the rainiest (Smith and Chang 2020).

Rainfall increases flow of the Mississippi and Trinity rivers during the spring and early summer. The Trinity river is the longest river in Texas with its entire watershed located within the states borders. The Trinity empties into Galveston Bay with a peak median daily 44 year flow for the Trinity river of ~ 368.12 m^3/sec in mid-May, and slowing during the late summer through the winter with a minimum median 44 year flow of around ~31.15 m^3/sec in the later part of October. (Sylvan and Ammerman 2013, USGS). September, which on a typical year falls into low flow months with a median 44 year flow of approximately 39.64 m^3/sec and a 2014 average of 33 ± 1 m^3/sec had an exceptionally high flow rate of 153.67 ± 315.58 m^3/sec due to the effects of Hurricane Harvey, and will be excluded from the remainder of the discussion of seasonal trends. Impacts of Hurricane Harvey are discussed in detail in the following two sections.

Seasonal trends in pH and pCO_2 are also evident that follow the seasonal trends in temperature (Figs 36-37). Colder water is capable of holding higher amounts of dissolved gas, causing pCO_2 to go down, because the potential of the water to hold the gas went up. As the pCO_2 goes down, the pH increases, especially seen in August with the highest surface overall average pCO_2 at 446.03 ± 18.96 µatm and the lowest overall surface average 8.02 ± 0.02 (Figs 36-37, Table 4). As temperatures start to cool, pCO_2 begins to decreases while pH increases with the lowest surface pCO_2 overall average in November at a value of 367.33 ± 22.89 µatm and the highest average surface and overall pH values at 8.10 ± 0.02 and 8.07 ± 0.05, respectively (Fig 36-37, Table 10). June is a somewhat intermediate with the highest range for surface pH (7.98 – 8.30), followed by November and October (Tables 2, 10, and 8). All surface values from each cruise have similar normalized surface pCO_2, or in other words, when the effects of seasonal temperature changes are removed, the surface values of pCO_2 become grouped together. Any variation from that grouping is therefore a result of influences outside of, indicating that variability in surface pCO_2 is dominated by seasonal temperature changes (Fig 37).

Since Ω_{ar} is tightly coupled with pCO_2, one might expect to see a seasonal trend in the surface Ω_{ar} data. However, Ω_{ar} does not show a clear surface seasonal trend, which is likely due to the opposing influences of temperature and CO_2 (Fig 38, Tables 2,4,6,8,10). Since decreasing temperature decreases pCO_2, and thus the amount of acidification, Ω_{ar} should increase with a decrease in temperature. However, temperature affects Ω_{ar} directly since temperature is used to calculate K_{sp}, therefore, lower temperatures lower the Ω_{ar}. For example, when calculating Ω_{ar} for August and November, if everything between those two months is held constant (i.e. the average surface TA, DIC, salinity and zero nutrients are assumed for simplification), except for

temperature, the difference between August and November Ω_{ar} due only to changes in temperature is approximately 0.14. Then, if Ω_{ar} is calculated with constant average surface temperature, TA, salinity, and zero nutrients, but average surface values for August and November pCO_2 are used, the difference between August and November Ω_{ar} is 0.47, which is larger than the change in Ω_{ar} caused by temperature changes alone. This demonstrates that seasonal changes in temperature partially offset changes in Ω_{ar} caused by pCO_2. The remaining difference between August and November Ω_{ar} may be offset by summertime photosynthesis drawing down pCO_2, therefore preventing a seasonal surface trend from appearing in the Ω_{ar} data (Kealoha, Shamberger, et al. 2020).

There are no clear seasonal trends in surface DO or nutrients, likely because of variability associated with runoff from land, coastal biological productivity, and physical water circulation (Figs 18-33).

4.2 Terrestrial runoff

Hurricane Harvey produced over 60 inches of rainwater over the Houston area. This rainwater rapidly drained into Galveston Bay causing a drastic decrease in bay-wide salinity. A freshwater plume then extended out from the mouth of Galveston Bay into the GoM and can be tracked using water properties including, salinity and surface temperature, recorded by the Texas Automated Buoy System (TABS). TABS is a coastal network of moored near real time observation buoys which are scattered around the continental shelf of Texas and take seawater measurements at approximately 2 m depth. The TABS show that the majority of the freshwater from Harvey flowed from Galveston bay out into the GOM and then was moved southward along the Texas coast (Fig 39-40). The freshwater plume created by Harvey is first observed by buoy B which is located just outside of the mouth of Galveston Bay (Fig 39). The drop in salinity

was first observed on the date of the storm event due to increased rain. Salinity measurements at buoy B were further decreased by stormwater runoff in the preceding days and weeks (Fig 40). Next, a change in salinity was recorded by buoy F, with the lowest recorded salinity of 27.33 at 14:30 on September 1, 2017, indicating that the freshwater was pushed offshore as buoy F is just southeast of buoy B. Later, in early September, a decrease in salinity at buoy D is measured, the most southwestern buoy in this study, located just north of Corpus Christi (Fig 40). Buoy V, which is locates roughly 3 km from the East FGB and 25 km form the West FGB, though it was not in operation until the 30th of August, also recorded a slight decrease in salinity in mid-September (Fig 40). Although only a small amount of stormwater runoff made it out to the FBG, as seen starting around September 7th and lasting approximately 10 days, until the 17th. The majority of the freshwater plume was transported southwards along the coast, as indicated by the much more dramatic declines in salinity at buoys B,F, and D, than at buoy V. The southern transport of the freshwater plume spared the FGB coral reef ecosystem from serious storm runoff induced damage.

The freshwater plume produced by Hurricane Harvey made it out to the FGB, but the resulting decline in ocean water salinity was not as prolonged, as deep, or severe as the decline in salinity experienced during the 2016 FGB mortality event (Johnston et al. 2019, Kealoha, Doyle, et al. 2020). The post-Harvey freshwater event was recorded by buoy V to be short lived and confined to the surface layer, meaning that the freshwater failed to reach a depth of 20 m (Figs 4-5). The salinity data collected by the September cruise did not indicate any declines in salinity, further supporting that the freshing of the surface waters surrounding the FGB was short. Salinity and TA are closely related, typically with a linear relationship (Fine, Willey, and Millero 2017). Data from the September 2017 cruise show that salinity, pH, and Ω_{ar} increase moving offshore

and lower salinity indicate that Hurricane Harvey runoff extended ~100 km offshore at that time (Figs 4, 6, and 12). At the depth (~20 m) and location of the FGB reefs, pH and Ω_{ar} were at levels that are supportive for coral reef calcification for the September, October, and November cruises with averages at the depth of ~20 m for pH and Ω_{ar} being 8.06 ± 0.02 and 4.00 ± 0.08, respectively. A recent study suggests that despite having a smaller change in salinity than the 2016 mortality event, some coral species still showed signs of stress following Hurricane Harvey. This stress was attributed to poor water quality caused by stormwater runoff following Hurricane Harvey (Wright et al. 2019). Gene ontology enrichment for coral genes on the FGB were differentially expressed following Hurricane Harvey. The study suggests that this indicates an increase in cellular oxidative stress responses. The study reports that no tissue loss was observed on FGB reefs, however, the results suggest poor water quality following the hurricane caused FGB corals to undergo sub-lethal stress. Despite this, the September data do not show that freshwater reached the depth of the coral crest at ~20 m (Fig 5). It is important to note that the freshwater plume observed in September over the Texas continental shelf only extends down to around 25 m, indicating that there is a possibility that the freshwater plume created by hurricane Harvey did extend down deep enough to interact with the FGB coral community, but had dissipated by the time of the September cruise (Fig 5).

In a typical year, surface water samples of TA along the Texas shelf would be comparable for August and September, however, due to increased stormwater runoff produced by Hurricane Harvey, September exhibits lower concentrations of TA with the overall lowest TA value of 1985.43 µmol/kg (Fig 41, Tables 4 and 6). TA has an apparent relationship with salinity, which is supported by Kealoha et. al (2020) when excesses flood water with low TA reached the FGB and contributed to the mortality event. Hicks et al. (in prep) also measured the

storm water runoff produced by hurricane Harvey and determined it had lower values of TA than river runoff in the region during non-flooding periods. Therefore, TA can be used as a tracer for Harvey storm water and its flow across the Texas continental shelf. Surface waters over the shelf have low TA following Hurricane Harvey indicating that these waters were highly influenced by storm water runoff (Fig 14 and 41). TA as well as DIC lose this relationship with salinity and become more determined by depth as TA decreases and DIC increases in the deep waters near the FGB (Figs 41 and 42).

All five cruises showed that DO decreased with depth, but no hypoxia was detected. Typically, a hypoxic region forms in mid-summer in the northern GoM due to stratification and an increase in nutrients. There was no strong trend of DO correlating with salinity (Fig 25 and 26). Solubility of oxygen is dependent on salinity, where freshwater will have a higher absolute concentration of DO than seawater, however the freshwater plume created by Harvey did not increase the nearshore DO (Fig 44-45).

NO_3^- concentration were low in surface waters during all cruises and increased with depth (Fig 46-47). This is because the NO_3^- is taken up rapidly by opportunistic diatoms and other phytoplankton, especially during blooms that ramped up after freshwater input that occurred following hurricane Harvey (Figs46-47). September, made extraordinarily wet due to the occurrence of Hurricane Harvey, has higher NO_3^- and HPO_4^{2-} concentrations in the upper 50 m than October and November. This is especially striking taking into account that October and November are periods when there are increasing amounts of nutrients due to wind driven input from the Mississippi River. This also suggests that increased nutrients are being transported to the GoM from land during higher periods of terrestrial runoff and river input due to large storm events like Hurricane Harvey (Figs 46-47 and 48-49).

There were several phytoplankton blooms recorded in Galveston Bay following hurricane Harvey. These blooms occurred because of increased nutrients brought into the normally N limited bay (Steichen et al. 2020). The increase in nutrient export into Galveston Bay, and the surrounding coastal ecosystems, was recorded to be short lived (Patrick et al. 2020). Galveston Bay was reported to have started to recover back to a marine environment, as opposed to a freshwater environment immediately following the storm, approximately four weeks after hurricane Harvey, which corresponds with the beginning of the September cruise (~September 22nd) (Steichen et al. 2020).

On continental shelf waters, the influx of NO_3^- would have been consumed rapidly, as evidenced by low surface NO_3 concentrations during the September cruise, potentially resulting in an excess of HPO_4^{2-}. In addition, light limitation might also interfere with the ability of phytoplankton to take up HPO_4^{2-} in slightly deeper waters. Nutrient rich and turbid waters keep light from penetrating into the water column preventing photosynthesis and nutrient uptake. Subsurface maxes for HPO_4^{2-} are seen in both June and September indicating that terrestrial runoff creates situations of enhanced HPO_4^{2-} in shelf water (Figs 48 and 49). As salinity decreases in September, there is an increase in HPO_4^{2-}. However, the increased concentrations in HPO_4^{2-} go deeper in the water column than the freshwater plume was recorded (~ 25 m) (Fig 48). When further analyzing the depth profiles and salinity profiles of phosphate, it has higher concentrations spanning along all samples taken across the Texas shelf following Hurricane Harvey (Fig 47 and 48). This indicates that there might have been mixing of bottom sediments along the shelf caused by the hurricane and that resuspension may have caused increased HPO_4^{2-} concentrations beyond what was brought into the Gulf by stormwater runoff.

NO_2^- and $HSiO_3^-$ also show higher concentrations in surface and subsurface waters (0 – 50 m) in June and September when there is more freshwater runoff from land, than in the other months sampled, (Figs 50-51 and 53-54). The discharge of rainwater was immense after hurricane Harvey which mobilized terrestrial sediments and nutrients. It is also likely that the increased storm water created a rise in the area's water tables which caused organic matter to leech from the sediments and drain into streams and river systems (Patrick et al. 2020). An increase in nutrients can be produced because of enhanced heterotrophic microbial respiration that can be seen weeks after the storm event (Patrick et al. 2020). NO_2^- and NH_4^+ both increase with salinity, which may indicate that NO_2 is derived from ammonia oxidation. HPO_4^{2-}, $HSiO_3^-$, NH_4^+, NO_2^-, and urea all increase with decreasing salinity, indicating that terrestrial runoff is an important controlling factor for these nutrient concentrations (Figs 49, 51, 53, 55 and 57).

Increased nutrients caused phytoplankton blooms and increased primary production that altered the carbonate chemistry of surface waters along the Texas coast following Hurricane Harvey. Enhanced photosynthesis after Hurricane Harvey may have decreased DIC as seen in the depth profiles and salinity graphs in September (Fig 42 and 58). The process of photosynthesis consumes CO_2 thus lowering the amount of available CO_2, which is a component of DIC. DIC, like TA, is also noted as having lower values in Harvey stormwater (Fig 59). The reduction of pCO_2 reduces acidity and increases pH (Fig 59). It appears that as salinity decreases so does Ω_{ar}, (Figs 60 and 61). Those pCO2 values with lower salinities (<28) do have the same pattern in relation to Ω_{ar} (Fig 62). The enhanced photosynthesis and decreased pCO_2 exacerbates the depletion of DIC in the surface waters that were already being flushed with low DIC from stormwater runoff (Fig 61). DIC had the lowest recorded values in September with the lowest recorded value of 1754.59 µmol/kg (Table 6).

Generally, coastal waters in the GoM are a sink for atmospheric CO_2 during the spring and fall due to enhanced biological productivity and cooler temperatures. In contrast, coastal waters are an atmospheric source during the summer and winter because of higher temperatures and increased respiration (Kealoha, Shamberger, et al. 2020). However, due to the increased terrestrial runoff created by Hurricane Harvey and subsequent stimulation of increased primary production, the shelf waters had lower pCO_2 than atmospheric levels. This low pCO_2 suggests that areas affected by Harvey storm water runoff may have switched from a summertime source to a sink for atmospheric CO_2 (Fig 63). The average surface pCO_2 and $npCO_2$ for September was 393.33 ± 28.93 µatm and 428.86 ± 151.18 µatm, respectively, compared to an average atmospheric pCO_2 for September 2017 of 406 µatm (Table 6, https://www.co2.earth/monthly-co2). However, at salinities of ≤ 30, average surface pCO_2 and $npCO_2$ for September were 365.49 ± 17.78 and 313.41 ± 14.79 µatm demonstrating that enhanced primary productivity and CO_2 drawdown were associated with freshwater runoff.

4.3 Upwelling

In the northern GoM, from fall to spring (September to May), the prevailing wind direction is downcoast or in a southwest direction. This pushes the Mississippi river plume, and the excess nutrients within, towards the Texas continental shelf. During this time, the circulation over the outer shelf and the shelf break is largely clockwise, most likely due to the impingement of deteriorating anticyclonic eddies on the shelf edge (Zavala-Hidalgo et al. 2014). However, during the summer months (June to August), the prevailing winds shift to a north-northeastward direction. This alteration in wind direction drives up coast circulation and creates favorable conditions for upwelling along the continental shelf of Texas (Angles et al. 2019). These periods of upwelling are also influenced by the Loop Current and the Loop Current Eddies that interact

with the slope, however there is still much ambiguity in how these systems work (Zavala-Hidalgo et al. 2014). Hurricane Harvey occurred in a transitional period between conditions that favor upwelling and conditions that typically carry the Mississippi river plume from the Louisiana shelf towards the Texas coast. Therefore, Hurricane Harvey may have either created new upwelling or may have enhanced upwelling already occurring near the shelf break prior to the storm during this transitional period.

Deep waters typically have high nutrient concentrations and are more acidic. Nutrients at the surface are taken up by phytoplankton to fuel primary production. After phytoplankton are no longer active in surface waters, they form aggregates that sink and are remineralized. This process concentrates nutrients in deep waters that can be brought up in upwelling events (Susumu et al. 2014). Another important process dictating deep water chemistry is respiration. Phytoplankton are limited by sunlight availability; deeper waters have little to no sunlight which drives down photosynthesis and increases respiration. Once a critical depth is reached, respiration overtakes photosynthesis and pCO_2 starts to build. This creates deep waters that are higher in pCO_2 and more acidic (Mathis et al. 2012). Upwelling events therefore bring deep, cold, nutrient rich, acidified water up the continental slope, along the edge of the shelf and towards shallower depths. Upwelling events can be identified by measuring water that has elevated nutrient concentrations and is acidified, with low pH, Ω_a, and TA, at shallower depths than is usually found.

June, August, and September show subtle shifts in temperature, carbonate chemistry, DO, and nutrient changes in their respective depth profiles that may indicate upwelling. In all September data, the carbonate chemistry parameters, between 50 -75 m, the September data have lower temperatures, pH, and Ω_{ar} and higher pCO_2 and $npCO_2$ than October and November (Figs

36, 38 and 37 and 43). DO is lower in September than in October and November from ~50 – 100 m, while nitrate, phosphate, and urea are all higher down to ~ 200 m (Figs 44, 46, 48, 56). In addition, nitrate and nitrite are elevated in August samples at approximately -95^0 longitude and 50-75 m, upwelling system that contributed to nutrient concentrations on the Texas continental shelf prior to Hurricane Harvey. (Figs 21 and 29).

Temperature data show that water samples taken between 50 -75 m during the September cruise are cooler than those taken during October and November, even though surface temperatures are lower in October and November (Fig 7). The $npCO_2$ data especially exemplify these upwelling driven shifts at depth because the effect of temperature has been removed (Fig 63). The surface $npCO_2$ values across cruises overlap while deeper waters still exhibit separation. Strong disconnection begins around 50 m where September samples are shifted to the right indicating higher $npCO_2$, potentially suggesting more acidic waters upwelling towards the surface. June and August data do not extend as deep as the latter cruises but are also shifted to the right of the October and November data below 50 m, again, possibly indicating upwelling.

The consequences of upwelling events can be damaging to coral reef ecosystems because upwelled waters typically have higher acidity and pCO_2 and are undersaturated in terms of aragonite content (Mathis et al. 2012, Walker, Leben, and Balasubramanian 2005). The lower values of pH have been shown to decrease net calcification respiration and prey capture rates (Keul et al. 2010, Georgian et al. 2016). Because the FGB are marginal reefs located at high latitudes, broader seasonal variations in temperature add additional stress to the reef communities (Guinotte, Buddemeier, and Kleypas 2003, van Hooidonk et al. 2014). Furthermore, future reef calcification could be increasingly challenged with the precent changes in Ω_{ar} predicted to be greater at high-latitude reefs (Camp et al. 2018). In addition, the relatively deep location of the

FGB may expose the reef systems to open ocean physical processes that may stress the reef ecosystem, such as persistent upwelling off the shelf break and spin off eddies from the Loop Current. This study suggests that while the GoM naturally experiences upwelling events during the summer months due to shifts in wind direction without the influence of Hurricanes, large storm events, in addition to high wave energy and low light conditions, can still enhance existing upwelling systems and induce excess stress onto calcifying ecosystems (Angles et al. 2019, Wright et al. 2019). Importantly, Hurricane Harvey appears to have induced upwelling beyond the usual seasonal upwelling period, thereby extending the time period over which these coral reefs may usually be exposed to deep, acidified water from summer months into early fall.

A study conducted by Wright et al 2019 suggested that sub-lethal stress observed in gene expressions of the FGB coral reefs were due to freshwater runoff from Hurricane Harvey reaching the FGB. I propose that this stress may also be attributed, in part, to the enhancement of upwelling waters that were either created by, or exacerbated by, Hurricane Harvey.

5. CONCLUSIONS

Hurricane Harvey produced record breaking amount of rainfall. The nutrient laden stormwater runoff from Harvey temporarily changed the coastal carbonate and nutrient chemistry. The rainwater lowered the coastal TA and DIC, while the nutrient rich terrestrial runoff increased primary productivity, lowering pCO_2 and increasing pH. This likely shifted the northern GoM from a CO_2 source in the summer to a CO_2 sink. Further, Hurricane Harvey's strong and prolonged winds enhanced an upwelling system near the edge of the Texas continental shelf. TA, DIC, and pCO_2 all increased ~50 -75 m depth in September compared to other months, while pH and Ω_{ar} both decreased at the same depth. During the summertime, upwelling conditions exist, and Hurricane Harvey enhanced and extended these upwelling conditions into the fall (late September) that brought up colder acidified waters closer to surface waters and the FGB coral reefs. The impact of hurricanes on coastal carbonate chemistry is poorly understood and as hurricanes intensifying due to global climate change, the need to understand the carbonate and nutrient chemistry of the GoM becomes more urgent. This study represents an important advance in understanding impacts of both storm-induced upwelling and terrestrial storm runoff on coastal carbonate chemistry dynamics.

REFERENCES

2018. "Fisheries Economics of the United States, 2016." National Oceanic and Atmospheric Administration, accessed 10/2019. https://www.fisheries.noaa.gov/content/fisheries-economics-united-states-2016.

2020a. "National Hurricane Center and Central Pacific Hurricane Center ". National Oceanic and Atmospheric Administration. https://www.nhc.noaa.gov/climo/.

2020b. "U.S. Department of the Interior: Mississippi River ". National Park Services accessed 6/15/2020. https://www.nps.gov/miss/riverfacts.htm.

Andersson, A. J., I. B. Kuffner, F. T. Mackenzie, P. L. Jokiel, K. S. Rodgers, and A. Tan. 2009. "Net Loss of CaCO3 from a subtropical calcifying community due to seawater acidification: mesocosm-scale experimental evidence." *Biogeosciences* 6 (8):1811-1823. doi: 10.5194/bg-6-1811-2009.

Angles, S., A. Jordi, D. W. Henrichs, and L. Campbell. 2019. "Influence of coastal upwelling and river discharge on the phytoplankton community composition in the northwestern Gulf of Mexico." *Progress in Oceanography* 173:26-36. doi: 10.1016/j.pocean.2019.02.001.

Appelo, C.A.J. and Postma, D. . 1993. "Geochemistry, groundwater and pollution " In, 536 Rotterdam.

Austin, James. 2014. "Geologic History of Gulf Of Mexico 2014 Expedition Operating Areas." Office of Ocean Exploration and Research

National Oceanic and Atmospheric Administration

U.S. Department of Commerce. https://oceanexplorer.noaa.gov/okeanos/explorations/ex1402/background/geology/welcome.html.

Barkley, H. C., A. L. Cohen, Y. Golbuu, V. R. Starczak, T. M. DeCarlo, and K. E. F. Shamberger. 2015. "Changes in coral reef communities across a natural gradient in seawater pH." *Science Advances* 1 (5):7. doi: 10.1126/sciadv.1500328.

Baustian, Joseph J., and Irving A. Mendelssohn. 2015. "Hurricane-Induced Sedimentation Improves Marsh Resilience and Vegetation Vigor under High Rates of Relative Sea Level Rise." *Wetlands* 35 (4):795-802. doi: 10.1007/s13157-015-0670-2.

Bianchi, T. S., S. F. DiMarco, J. H. Cowan, R. D. Hetland, P. Chapman, J. W. Day, and M. A. Allison. 2010. "The science of hypoxia in the Northern Gulf of Mexico: A review." *Science of the Total Environment* 408 (7):1471-1484. doi: 10.1016/j.scitotenv.2009.11.047.

Bond, N. A., M. F. Cronin, C. Sabine, Y. Kawai, H. Ichikawa, P. Freitag, and K. Ronnholm. 2011. "Upper ocean response to Typhoon Choi-Wan as measured by the Kuroshio Extension Observatory mooring." *Journal of Geophysical Research-Oceans* 116:8. doi: 10.1029/2010jc006548.

Boudreau, B. P., J. J. Middelburg, A. Sluijs, and R. van der Ploeg. 2019. "Secular variations in the carbonate chemistry of the oceans over the Cenozoic." *Earth and Planetary Science Letters* 512:194-206. doi: 10.1016/j.epsl.2019.02.004.

Bries, J. M., A. O. Debrot, and D. L. Meyer. 2004. "Damage to the leeward reefs of Curacao and Bonaire, Netherlands Antilles from a rare storm event: Hurricane Lenny, November 1999." *Coral Reefs* 23 (2):297-307. doi: 10.1007/s00338-004-0379-9.

Browning, T. N., D. E. Sawyer, G. R. Brooks, R. A. Larson, C. E. Ramos-Scharron, and M. Canals-Silander. 2019. "Widespread Deposition in a Coastal Bay Following Three Major 2017 Hurricanes (Irma, Jose, and Maria)." *Scientific Reports* 9:13. doi: 10.1038/s41598-019-43062-4.

Cai, W. J., X. P. Hu, W. J. Huang, M. C. Murrell, J. C. Lehrter, S. E. Lohrenz, W. C. Chou, W. D. Zhai, J. T. Hollibaugh, Y. C. Wang, P. S. Zhao, X. H. Guo, K. Gundersen, M. H. Dai, and G. C. Gong. 2011. "Acidification of subsurface coastal waters enhanced by eutrophication." *Nature Geoscience* 4 (11):766-770. doi: 10.1038/ngeo1297.

Cai, Y. H., L. D. Guo, X. R. Wang, S. E. Lohrenz, and A. K. Mojzis. 2013. "Effects of tropical cyclones on river chemistry: A case study of the lower Pearl River during Hurricanes Gustav and Ike." *Estuarine Coastal and Shelf Science* 129:180-188. doi: 10.1016/j.ecss.2013.05.019.

Caldeira, K., and M. E. Wickett. 2003. "Anthropogenic carbon and ocean pH." *Nature* 425 (6956):365-365. doi: 10.1038/425365a.

Camp, Emma F., Verena Schoepf, Peter J. Mumby, Leonardo A. Hardtke, Riccardo Rodolfo-Metalpa, David J. Smith, and David J. Suggett. 2018. "The Future of Coral Reefs Subject to Rapid Climate Change: Lessons from Natural Extreme Environments." *Frontiers in Marine Science* 5 (4). doi: 10.3389/fmars.2018.00004.

Carlson, R. R., S. A. Foo, and G. P. Asner. 2019. "Land Use Impacts on Coral Reef Health: A Ridge-to-Reef Perspective." *Frontiers in Marine Science* 6:19. doi: 10.3389/fmars.2019.00562.

Castaneda-Moya, E., V. H. Rivera-Monroy, R. M. Chambers, X. C. Zhao, L. Lamb-Wotton, A. Gorsky, E. E. Gaiser, T. G. Troxler, J. S. Kominoski, and M. Hiatt. 2020. "Hurricanes fertilize mangrove forests in the Gulf of Mexico (Florida Everglades, USA)." *Proceedings of the National Academy of Sciences of the United States of America* 117 (9):4831-4841. doi: 10.1073/pnas.1908597117.

Cheal, A. J., M. A. Macneil, M. J. Emslie, and H. Sweatman. 2017. "The threat to coral reefs from more intense cyclones under climate change." *Global Change Biology* 23 (4):1511-1524. doi: 10.1111/gcb.13593.

Clark, H. R., and C. J. Gobler. 2016. "Diurnal fluctuations in CO2 and dissolved oxygen concentrations do not provide a refuge from hypoxia and acidification for early-life-stage bivalves." *Marine Ecology Progress Series* 558:1-14. doi: 10.3354/meps11852.

Connell, J. H. 1987. "Citation-Classic - Diversity in Tropical Rain-Forests and Coral Reefs." *Current Contents/Agriculture Biology & Environmental Sciences* (46):16-16.

Cornelis Klein, Anthony Philpotts. 2013. *Earth Materials Introduction to Mineralogy and Petrology*. 32 Avenue of the Americas, New York, NY Cambridge University Press.

de Putron, S. J., D. C. McCorkle, A. L. Cohen, and A. B. Dillon. 2011. "The impact of seawater saturation state and bicarbonate ion concentration on calcification by new recruits of two Atlantic corals." *Coral Reefs* 30 (2):321-328. doi: 10.1007/s00338-010-0697-z.

de Weys, J., I. R. Santos, and B. D. Eyre. 2011. "Linking Groundwater Discharge to Severe Estuarine Acidification during a Flood in a Modified Wetland." *Environmental Science & Technology* 45 (8):3310-3316. doi: 10.1021/es104071r.

DeBose, J. L., M. F. Nuttall, E. L. Hickerson, and G. P. Schmahl. 2013. "A high-latitude coral community with an uncertain future: Stetson Bank, northwestern Gulf of Mexico." *Coral Reefs* 32 (1):255-267. doi: 10.1007/s00338-012-0971-3.

DeCarlo, T. M., S. Comeau, C. E. Cornwall, and M. T. McCulloch. 2018. "Coral resistance to ocean acidification linked to increased calcium at the site of calcification." *Proceedings of the Royal Society B-Biological Sciences* 285 (1878):7. doi: 10.1098/rspb.2018.0564.

Department, U.S., National Oceanic and Atmospheric Administration of Commerce, and Office of National Marine Sanctuaries. 2008. Flower Garden Banks National Marine Sanctuary Condition Report 2008. Silver Spring, MD.

Diaz, R. J., and R. Rosenberg. 2008. "Spreading dead zones and consequences for marine ecosystems." *Science* 321 (5891):926-929. doi: 10.1126/science.1156401.

Dickson, A G, C L Sabine, and J R Christian. 2007. *Guide to Best Practices for Ocean CO2 Measurements.*, *PICES Special Publication;3*

IOCCP Report; 8. Sidney, British Columbia: North Pacific Marine Science Organization.

Diercks, A. R., C. Dike, V. L. Asper, S. F. DiMarco, J. P. Chanton, and U. Passow. 2018. "Scales of seafloor sediment resuspension in the northern Gulf of Mexico." *Elementa-Science of the Anthropocene* 6:28. doi: 10.1525/elementa.285.

Doney, Scott C., Natalie Mahowald, Ivan Lima, Richard A. Feely, Fred T. Mackenzie, Jean-Francois Lamarque, and Phil J. Rasch. 2007. "Impact of anthropogenic atmospheric

nitrogen and sulfur deposition on ocean acidification and the inorganic carbon system." *Proceedings of the National Academy of Sciences* 104 (37):14580-14585. doi: 10.1073/pnas.0702218104.

Du, J. B., K. Park, X. Yu, Y. L. J. Zhang, and F. Ye. 2020. "Massive pollutants released to Galveston Bay during Hurricane Harvey: Understanding their retention and pathway using Lagrangian numerical simulations." *Science of the Total Environment* 704:10. doi: 10.1016/j.scitotenv.2019.135364.

Du, Jiabi, and Kyeong Park. 2019. "Estuarine salinity recovery from an extreme precipitation event: Hurricane Harvey in Galveston Bay." *Science of The Total Environment* 670:1049-1059. doi: https://doi.org/10.1016/j.scitotenv.2019.03.265.

Du, Jiabi, Kyeong Park, Timothy M. Dellapenna, and Jacinta M. Clay. 2019. "Dramatic hydrodynamic and sedimentary responses in Galveston Bay and adjacent inner shelf to Hurricane Harvey." *Science of The Total Environment* 653:554-564. doi: https://doi.org/10.1016/j.scitotenv.2018.10.403.

Ennis, R. S., M. E. Brandt, K. R. W. Grimes, and T. B. Smith. 2016. "Coral reef health response to chronic and acute changes in water quality in St. Thomas, United States Virgin Islands." *Marine Pollution Bulletin* 111 (1-2):418-427. doi: 10.1016/j.marpolbul.2016.07.033.

Eric S. Blake, David A. Zelinsky. 2018. National Hurricane Center Tropical Cyclone Report: Hurricane Harvey. edited by National Oceanic and Atmospheric Admisnistration and the National Weather Service.

Eyre, B. D., T. Cyronak, P. Drupp, E. H. De Carlo, J. P. Sachs, and A. J. Andersson. 2018. "Coral reefs will transition to net dissolving before end of century." *Science* 359 (6378):908-911. doi: 10.1126/science.aao1118.

Fan, C. F., J. Chen, Y. Chen, J. F. Ji, and H. H. Teng. 2006. "Relationship between solubility and solubility product: The roles of crystal sizes and crystallographic directions." *Geochimica Et Cosmochimica Acta* 70 (15):3820-3829. doi: 10.1016/j.gca.2006.06.011.

Farfan, G. A., E. E. Cordes, R. G. Waller, T. M. DeCarlo, and C. M. Hansel. 2018. "Mineralogy of Deep-Sea Coral Aragonites as a Function of Aragonite Saturation State." *Frontiers in Marine Science* 5:15. doi: 10.3389/fmars.2018.00473.

Feely, R. A., S. C. Doney, and S. R. Cooley. 2009. "Ocean Acidification: Present Conditions and Future Changes in a High-CO2 World." *Oceanography* 22 (4):36-47. doi: 10.5670/oceanog.2009.95.

Feely, R. A., C. L. Sabine, K. Lee, W. Berelson, J. Kleypas, V. J. Fabry, and F. J. Millero. 2004. "Impact of anthropogenic CO2 on the CaCO3 system in the oceans." *Science* 305 (5682):362-366. doi: 10.1126/science.1097329.

Fine, R. A., D. A. Willey, and F. J. Millero. 2017. "Global variability and changes in ocean total alkalinity from Aquarius satellite data." *Geophysical Research Letters* 44 (1):261-267. doi: 10.1002/2016gl071712.

Foster, Nicola L., Iliana B. Baums, Juan A. Sanchez, Claire B. Paris, Iliana Chollett, Claudia L. Agudelo, Mark J. A. Vermeij, and Peter J. Mumby. 2013. "Hurricane-driven patterns of clonality in an ecosystem engineer: the Caribbean coral Montastraea annularis." *PloS one* 8 (1):e53283-e53283. doi: 10.1371/journal.pone.0053283.

Foundation, Chesapeake Bay. 2020. Oyster Fact Sheet.

Georgian, S. E., D. DeLeo, A. Durkin, C. E. Gomez, M. Kurman, J. J. Lunden, and E. E. Cordes. 2016. "Oceanographic patterns and carbonate chemistry in the vicinity of cold-water coral reefs in the Gulf of Mexico: Implications for resilience in a changing ocean." *Limnology and Oceanography* 61 (2):648-665. doi: 10.1002/lno.10242.

Gobler, Christopher J., and Hannes Baumann. 2016. "Hypoxia and acidification in ocean ecosystems: coupled dynamics and effects on marine life." *Biology letters* 12 (5):20150976. doi: 10.1098/rsbl.2015.0976.

Gordon, L. I., J. C. Jennings, A. A. Ross, and J. M. Krest. 1994. "World ocean circulation experiment. WOCE operations manual. Volume 3. The observational programme. Section 3.1. WOCE hydrographic programme. Part 3.1.3. WHP operations and methods. (revision 1)."

Guinotte, J. M., R. W. Buddemeier, and J. A. Kleypas. 2003. "Future coral reef habitat marginality: temporal and spatial effects of climate change in the Pacific basin." *Coral Reefs* 22 (4):551-558. doi: 10.1007/s00338-003-0331-4.

Hoegh-Guldberg, O., E. S. Poloczanska, W. Skirving, and S. Dove. 2017. "Coral Reef Ecosystems under Climate Change and Ocean Acidification." *Frontiers in Marine Science* 4:20. doi: 10.3389/fmars.2017.00158.

Honisch, B., A. Ridgwell, D. N. Schmidt, E. Thomas, S. J. Gibbs, A. Sluijs, R. Zeebe, L. Kump, R. C. Martindale, S. E. Greene, W. Kiessling, J. Ries, J. C. Zachos, D. L. Royer, S. Barker, T. M. Marchitto, R. Moyer, C. Pelejero, P. Ziveri, G. L. Foster, and B. Williams. 2012. "The Geological Record of Ocean Acidification." *Science* 335 (6072):1058-1063. doi: 10.1126/science.1208277.

Howarth, R. W., R. Marino, R. Garritt, and D. Sherman. 1992. "ECOSYSTEM RESPIRATION AND ORGANIC-CARBON PROCESSING IN A LARGE, TIDALLY INFLUENCED RIVER - THE HUDSON RIVER." *Biogeochemistry* 16 (2):83-102.

Hu, C. M., F. E. Muller-Karger, and P. W. Swarzenski. 2006. "Hurricanes, submarine groundwater discharge, and Florida's red tides." *Geophysical Research Letters* 33 (11):5. doi: 10.1029/2005gl025449.

Hu, X. P., J. B. Pollack, M. R. McCutcheon, P. A. Montagna, and Z. X. Ouyang. 2015. "Long-Term Alkalinity Decrease and Acidification of Estuaries in Northwestern Gulf of Mexico." *Environmental Science & Technology* 49 (6):3401-3409. doi: 10.1021/es505945p.

Hu, X. P., H. M. Yao, C. J. Staryk, M. R. McCutcheon, M. Wetz, and L. Walker. 2020. "Disparate Responses of Carbonate System in Two Adjacent Subtropical Estuaries to the Influence of Hurricane Harvey - A Case Study." *Frontiers in Marine Science* 7:13. doi: 10.3389/fmars.2020.00026.

Hypoxia Task Force , EPA. 2017. Mississippi River/Gulf of Mexico Watershed Nutrient Task Force 2017 Report to Congress.

Jiang, L. Q., W. J. Cai, R. A. Feely, Y. C. Wang, X. H. Guo, D. K. Gledhill, X. P. Hu, F. Arzayus, F. Z. Chen, J. Hartmann, and L. J. Zhang. 2010. "Carbonate mineral saturation states along the US East Coast." *Limnology and Oceanography* 55 (6):2424-2432. doi: 10.4319/lo.2010.55.6.2424.

Johnson, R., J. Harianto, M. Thomson, and M. Byrne. 2020. "The effects of long-term exposure to low pH on the skeletal microstructure of the sea urchin Heliocidaris erythrogramma." *Journal of Experimental Marine Biology and Ecology* 523:7. doi: 10.1016/j.jembe.2019.151250.

Johnston, M. A., E. L. Hickerson, M. F. Nuttall, R. D. Blakeway, T. K. Sterne, R. J. Eckert, and G. P. Schmahl. 2019. "Coral bleaching and recovery from 2016 to 2017 at East and West Flower Garden Banks, Gulf of Mexico." *Coral Reefs* 38 (4):787-799. doi: 10.1007/s00338-019-01788-7.

Johnston MA, Eckert RJ, Nuttall MF, Sterne TK, Embesi JA, Manzello DP, Hickerson EL, Schmahl GP 2017. Long-term monitoring at the East and West Flower Garden Banks National Marine Sanctuary, 2013–2015,. In *US Dept of Interior, Bureau of Ocean Energy Management, Gulf of Mexico OCS Study BOEM 2017-058*. New Orleans, Louisiana.

Kealoha, A. K., S. M. Doyle, K. E. F. Shamberger, J. B. Sylvan, R. D. Hetland, and S. F. DiMarco. 2020. "Localized hypoxia may have caused coral reef mortality at the Flower Garden Banks." *Coral Reefs* 39 (1):119-132. doi: 10.1007/s00338-019-01883-9.

Kealoha A.K., S.M. Doyle, K.E.F. Shamberger, J.B. Sylvan, R.D. Hetland, S.F. DiMarco. . "Localized hypoxia drives coral reef mortality at the Flower Garden Banks." *Coral Reefs*.

Kealoha, Andrea K., Kathryn E. F. Shamberger, Steven F. DiMarco, Kristen M. Thyng, Robert D. Hetland, Derek P. Manzello, Niall C. Slowey, and Ian C. Enochs. 2020. "Surface Water CO2 variability in the Gulf of Mexico (1996–2017)." *Scientific Reports* 10 (1):12279. doi: 10.1038/s41598-020-68924-0.

Keul, N., J. W. Morse, R. Wanninkhof, D. K. Gledhill, and T. S. Bianchi. 2010. "Carbonate Chemistry Dynamics of Surface Waters in the Northern Gulf of Mexico." *Aquatic Geochemistry* 16 (3):337-351. doi: 10.1007/s10498-010-9091-2.

Kleypas, J. A., and K. K. Yates. 2009. "Coral Reefs and Ocean Acidification." *Oceanography* 22 (4):108-117. doi: 10.5670/oceanog.2009.101.

Laboy-Nieves, E. N., E. Klein, J. E. Conde, F. Losada, J. J. Cruz, and D. Bone. 2001. "Mass mortality of tropical marine communities in Morrocoy, Venezuela." *Bulletin of Marine Science* 68 (2):163-179.

Lai, Q. T., E. R. Irwin, and Y. Q. Zhang. 2020. "Estimating nitrogen removal services of eastern oyster (Crassostrea virginica) in Mobile Bay, Alabama." *Ecological Indicators* 117:9. doi: 10.1016/j.ecolind.2020.106541.

Laurent, A., K. Fennel, W. J. Cai, W. J. Huang, L. Barbero, and R. Wanninkhof. 2017. "Eutrophication-induced acidification of coastal waters in the northern Gulf of Mexico: Insights into origin and processes from a coupled physical-biogeochemical model." *Geophysical Research Letters* 44 (2):946-956. doi: 10.1002/2016gl071881.

Le Quere, C., R. M. Andrew, P. Friedlingstein, S. Sitch, J. Pongratz, A. C. Manning, J. I. Korsbakken, G. P. Peters, J. G. Canadell, R. B. Jackson, T. A. Boden, P. P. Tans, O. D. Andrews, V. K. Arora, D. C. E. Bakker, L. Barbero, M. Becker, R. A. Betts, L. Bopp, F. Chevallier, L. P. Chini, P. Ciais, C. E. Cosca, J. Cross, K. Currie, T. Gasser, I. Harris, J. Hauck, V. Haverd, R. A. Houghton, C. W. Hunt, G. Hurtt, T. Ilyina, A. K. Jain, E. Kato, M. Kautz, R. F. Keeling, K. K. Goldewijk, A. Kortzinger, P. Landschutzer, N. Lefevre, A. Lenton, S. Lienert, I. Lima, D. Lombardozzi, N. Metzl, F. Millero, P. M. S. Monteiro, D. R. Munro, Jems Nabel, S. Nakaoka, Y. Nojiri, X. A. Padin, A. Peregon, B. Pfeil, D. Pierrot, B. Poulter, G. Rehder, J. Reimer, C. Rodenbeck, J. Schwinger, R. Seferian, I. Skjelvan, B. D. Stocker, H. Q. Tian, B. Tilbrook, F. N. Tubiello, I. T. van der Laan-Luijkx, G. R. van der Werf, S. van Heuven, N. Viovy, N. Vuichard, A. P. Walker, A. J. Watson, A. J. Wiltshire, S. Zaehle, and D. Zhu. 2018. "Global Carbon Budget 2017." *Earth System Science Data* 10 (1):405-448. doi: 10.5194/essd-10-405-2018.

Lin, I., W. T. Liu, C. C. Wu, G. T. F. Wong, C. M. Hu, Z. Q. Chen, W. D. Liang, Y. Yang, and K. K. Liu. 2003. "New evidence for enhanced ocean primary production triggered by tropical cyclone." *Geophysical Research Letters* 30 (13):4. doi: 10.1029/2003gl017141.

Lueker, T. J., A. G. Dickson, and C. D. Keeling. 2000. "Ocean pCO(2) calculated from dissolved inorganic carbon, alkalinity, and equations for K-1 and K-2: validation based on laboratory measurements of CO2 in gas and seawater at equilibrium." *Marine Chemistry* 70 (1-3):105-119. doi: 10.1016/s0304-4203(00)00022-0.

Lugo-Fernandez, A., and M. Gravois. 2010. "Understanding impacts of tropical storms and hurricanes on submerged bank reefs and coral communities in the northwestern Gulf of

Mexico." *Continental Shelf Research* 30 (10-11):1226-1240. doi: 10.1016/j.csr.2010.03.014.

Manzello, D., I. Enochs, S. Musielewicz, R. Carlton, and D. Gledhill. 2013. "Tropical cyclones cause CaCO3 undersaturation of coral reef seawater in a high-CO2 world." *Journal of Geophysical Research-Oceans* 118 (10):5312-5321. doi: 10.1002/jgrc.20378.

Manzello, D. P., M. Brandt, T. B. Smith, D. Lirman, J. C. Hendee, and R. S. Nemeth. 2007. "Hurricanes benefit bleached corals." *Proceedings of the National Academy of Sciences of the United States of America* 104 (29):12035-12039. doi: 10.1073/pnas.0701194104.

Manzello, D. P., I. C. Enochs, A. Bruckner, P. G. Renaud, G. Kolodziej, D. A. Budd, R. Carlton, and P. W. Glynn. 2014. "Galapagos coral reef persistence after ENSO warming across an acidification gradient." *Geophysical Research Letters* 41 (24):9001-9008. doi: 10.1002/2014gl062501.

Mathis, J. T., R. S. Pickart, R. H. Byrne, C. L. McNeil, G. W. K. Moore, L. W. Juranek, X. W. Liu, J. Ma, R. A. Easley, M. M. Elliot, J. N. Cross, S. C. Reisdorph, F. Bahr, J. Morison, T. Lichendorf, and R. A. Feely. 2012. "Storm-induced upwelling of high pCO(2) waters onto the continental shelf of the western Arctic Ocean and implications for carbonate mineral saturation states." *Geophysical Research Letters* 39:6. doi: 10.1029/2012gl051574.

Mattson, Mark D. 1999. "Acid lakes and rivers." In *Environmental Geology*, 6-9. Dordrecht: Springer Netherlands.

Maxwell, Justin T., Jason T. Ortegren, Paul A. Knapp, and Peter T. Soulé. 2013. "Tropical Cyclones and Drought Amelioration in the Gulf and Southeastern Coastal United States." *Journal of Climate* 26 (21):8440-8452. doi: 10.1175/jcli-d-12-00824.1.

Meissner, K. J., T. Lippmann, and A. Sen Gupta. 2012. "Large-scale stress factors affecting coral reefs: open ocean sea surface temperature and surface seawater aragonite saturation over the next 400 years." *Coral Reefs* 31 (2):309-319. doi: 10.1007/s00338-011-0866-8.

Meng, Y., Z. B. Guo, H. M. Yao, K. W. K. Yeung, and V. Thiyagarajan. 2019. "Calcium carbonate unit realignment under acidification: A potential compensatory mechanism in an edible estuarine oyster." *Marine Pollution Bulletin* 139:141-149. doi: 10.1016/j.marpolbul.2018.12.030.

Moberg, F., and C. Folke. 1999. "Ecological goods and services of coral reef ecosystems." *Ecological Economics* 29 (2):215-233. doi: 10.1016/s0921-8009(99)00009-9.

Mollica, N. R., W. F. Guo, A. L. Cohen, K. F. Huang, G. L. Foster, H. K. Donald, and A. R. Solow. 2018. "Ocean acidification affects coral growth by reducing skeletal density." *Proceedings of the National Academy of Sciences of the United States of America* 115 (8):1754-1759. doi: 10.1073/pnas.1712806115.

Morrison, R. J., G. R. W. Denton, U. B. Tamata, and J. Grignon. 2013. "Anthropogenic biogeochemical impacts on coral reefs in the Pacific Islands-An overview." *Deep-Sea Research Part Ii-Topical Studies in Oceanography* 96:5-12. doi: 10.1016/j.dsr2.2013.02.014.

Nielsen, M. R., K. K. Sand, J. D. Rodriguez-Blanco, N. Bovet, J. Generosi, K. N. Dalby, and S. L. S. Stipp. 2016. "Inhibition of Calcite Growth: Combined Effects of Mg2+ and SO42–." *Crystal Growth & Design* 16 (11):6199-6207. doi: 10.1021/acs.cgd.6b00536.

NOAA National Hurricane Center (NHC), D. Arctur, E. Boghici. 2018. "NOAA NHC - Harvey 2017 Storm Track." https://doi.org/10.4211/hs.6168b9969c984b658952a896710b65ef.

Patrick, C. J., L. Yeager, A. R. Armitage, F. Carvallo, V. M. Congdon, K. H. Dunton, M. Fisher, A. K. Hardison, J. D. Hogan, J. Hosen, X. Hu, B. K. Reese, S. Kinard, J. S. Kominoski, X. Lin, Z. Liu, P. A. Montagna, S. C. Pennings, L. Walker, C. A. Weaver, and M. Wetz. 2020. "A System Level Analysis of Coastal Ecosystem Responses to Hurricane Impacts." *Estuaries and Coasts* 43 (5):943-959. doi: 10.1007/s12237-019-00690-3.

Perry, C. T., S. G. Smithers, P. S. Kench, and B. Pears. 2014. "Impacts of Cyclone Yasi on nearshore, terrigenous sediment-dominated reefs of the central Great Barrier Reef, Australia." *Geomorphology* 222:92-105. doi: https://doi.org/10.1016/j.geomorph.2014.03.012.

Pierrot, D. E. Lewis, and D. W. R. Wallace. 2006. MS Excel Program Developed for CO2 System Calculations. ORNL/CDIAC-105a. Carbon Dioxide Information Analysis Center,

Oak Ridge National Laboratory, U.S. Department of Energy. Oak Ridge, Tennessee. .

Prasad, T. G., and P. J. Hogan. 2007. "Upper-ocean response to Hurricane Ivan in a 1/25 degrees nested Gulf of Mexico HYCOM." *Journal of Geophysical Research-Oceans* 112 (C4):18. doi: 10.1029/2006jc003695.

Rabalais, N. N., R. E. Turner, Q. Dortch, D. Justic, V. J. Bierman, and W. J. Wiseman. 2002. "Nutrient-enhanced productivity in the northern Gulf of Mexico: past, present and future." *Hydrobiologia* 475 (1):39-63. doi: 10.1023/a:1020388503274.

Rao, A. D., S. V. Babu, and S. K. Dube. 2004. "Impact of a tropical cyclone on coastal upwelling processes." *Natural Hazards* 31 (2):415-435. doi: 10.1023/B:NHAZ.0000023360.37260.5b.

Rubino, M., D. M. Etheridge, C. M. Trudinger, C. E. Allison, M. O. Battle, R. L. Langenfelds, L. P. Steele, M. Curran, M. Bender, J. W. C. White, T. M. Jenk, T. Blunier, and R. J. Francey. 2013. "A revised 1000 year atmospheric δ13C-CO2 record from Law Dome and South Pole, Antarctica." *Journal of Geophysical Research: Atmospheres* 118 (15):8482-8499. doi: 10.1002/jgrd.50668.

Salisbury, Joseph, Mark Green, Chris Hunt, and Janet Campbell. 2008. "Coastal Acidification by Rivers:A Threat to Shellfish?" *Eos, Transactions American Geophysical Union* 89 (50):513-513. doi: 10.1029/2008eo500001.

Scavia, D., J. C. Field, D. F. Boesch, R. W. Buddemeier, V. Burkett, D. R. Cayan, M. Fogarty, M. A. Harwell, R. W. Howarth, C. Mason, D. J. Reed, T. C. Royer, A. H. Sallenger, and J. G. Titus. 2002. "Climate change impacts on US coastal and marine ecosystems." *Estuaries* 25 (2):149-164. doi: 10.1007/bf02691304.

Schleussner, C. F., T. K. Lissner, E. M. Fischer, J. Wohland, M. Perrette, A. Golly, J. Rogelj, K. Childers, J. Schewe, K. Frieler, M. Mengel, W. Hare, and M. Schaeffer. 2016. "Differential climate impacts for policy-relevant limits to global warming: the case of 1.5 degrees C and 2 degrees C." *Earth System Dynamics* 7 (2):327-351. doi: 10.5194/esd-7-327-2016.

Scott Heron, Jessica Morgan, Mark Eakin, William Skirving 2005. "Hurricanes and their effects on coral reefs " *Status of Caribbean Coral Reefs after Bleaching and Hurricanes in 2005*.

Scyphers, S. B., S. P. Powers, K. L. Heck, and D. Byron. 2011. "Oyster Reefs as Natural Breakwaters Mitigate Shoreline Loss and Facilitate Fisheries." *Plos One* 6 (8):12. doi: 10.1371/journal.pone.0022396.

Shamberger, K. E. F., A. L. Cohen, Y. Golbuu, D. C. McCorkle, S. J. Lentz, and H. C. Barkley. 2014. "Diverse coral communities in naturally acidified waters of a Western Pacific reef." *Geophysical Research Letters* 41 (2):499-504. doi: 10.1002/2013gl058489.

Shamberger, K. E. F., R. A. Feely, C. L. Sabine, M. J. Atkinson, E. H. DeCarlo, F. T. Mackenzie, P. S. Drupp, and D. A. Butterfield. 2011. "Calcification and organic production on a Hawaiian coral reef." *Marine Chemistry* 127 (1-4):64-75. doi: 10.1016/j.marchem.2011.08.003.

Smith, Robert Kennedy, and Der-Chen Chang. 2020. "Utilizing Recent Climate Data in Eastern Texas to Calculate Trends in Measures of Aridity and Estimate Changes in Watering Demand for Landscape Preservation." *Journal of Applied Meteorology and Climatology* 59 (1):143-152. doi: 10.1175/jamc-d-19-0193.1.

Spalding, M. D., and A. M. Grenfell. 1997. "New estimates of global and regional coral reef areas." *Coral Reefs* 16 (4):225-230. doi: 10.1007/s003380050078.

Steichen, J. L., J. M. Labonte, R. Windham, D. Hala, K. Kaiser, S. Setta, P. C. Faulkner, H. Bacosa, G. Yan, M. Kamalanathan, and A. Quigg. 2020. "Microbial, Physical, and Chemical Changes in Galveston Bay Following an Extreme Flooding Event, Hurricane Harvey." *Frontiers in Marine Science* 7:21. doi: 10.3389/fmars.2020.00186.

Susumu, Honjo, Woods Hole M. A. U. S. A. Woods Hole Oceanographic Institution, I. Eglinton Timothy, Zurich Switzerland Eidgenössische Technische Hochschule, Woods Hole M. A. U. S. A. Woods Hole Oceanographic Institution, D. Taylor Craig, Woods Hole M. A. U. S. A. Woods Hole Oceanographic Institution, M. Ulmer Kevin, Inc East Sandwich M. A. Seaquester, Woods Hole M. A. U. S. A. Whoi, M. Sievert Stefan, Woods Hole M. A. U. S. A. Woods Hole Oceanographic Institution, Bracher Astrid, Polar Alfred Wegener Institute for, Bremerhaven Germany Marine Research, R. German Christopher, Woods Hole M. A. U. S. A. Woods Hole Oceanographic Institution, Edgcomb Virginia, Woods Hole M. A. U. S. A. Woods Hole Oceanographic Institution, Francois Roger, Vancouver Canada University of British Columbia, M. Debora Iglesias-Rodriguez, Santa Barbara C. A. U. S. A. University of California, Mooy Benjamin Van, Woods Hole M. A. U. S. A. Woods Hole Oceanographic Institution, J. Repeta Daniel, and Woods Hole M. A. U. S. A. Woods Hole Oceanographic Institution. 2014. "Understanding the Role of the Biological Pump in the Global Carbon Cycle: An Imperative for Ocean Science." *Oceanography* 27.

Sylvan, J. B., and J. W. Ammerman. 2013. "Seasonal distributions of organic nutrients on the Louisiana continental shelf and their implications for nutrient limitation and hypoxia formation." *Marine Chemistry* 154:113-123. doi: 10.1016/j.marchem.2013.05.008.

Sylvan, J. B., and J. W. Ammerman. 2014. "Seasonal distributions of organic nutrients on the Louisiana continental shelf and their implications for nutrient limitation and hypoxia formation (vol 154, pg 113, 2013)." *Marine Chemistry* 164:130-130. doi: 10.1016/j.marchem.2014.06.008.

Takahashi, Taro, Stewart C. Sutherland, Colm Sweeney, Alain Poisson, Nicolas Metzl, Bronte Tilbrook, Nicolas Bates, Rik Wanninkhof, Richard A. Feely, Christopher Sabine, Jon Olafsson, and Yukihiro Nojiri. 2002. "Global sea–air CO2 flux based on climatological surface ocean pCO2, and seasonal biological and temperature effects." *Deep Sea Research Part II: Topical Studies in Oceanography* 49 (9):1601-1622. doi: https://doi.org/10.1016/S0967-0645(02)00003-6.

Tamarin, Talia, and Yohai Kaspi. 2016. "The Poleward Motion of Extratropical Cyclones from a Potential Vorticity Tendency Analysis." *Journal of the Atmospheric Sciences* 73 (4):1687-1707. doi: 10.1175/jas-d-15-0168.1.

Teague, W. J., H. W. Wijesekera, E. Jarosz, D. B. Fribance, A. Lugo-Fernandez, and Z. R. Hallock. 2013. "Current and hydrographic conditions at the East Flower Garden Bank in 2011." *Continental Shelf Research* 63:43-58. doi: 10.1016/j.csr.2013.04.039.

Tribollet, A., C. Godinot, M. Atkinson, and C. Langdon. 2009. "Effects of elevated pCO(2) on dissolution of coral carbonates by microbial euendoliths." *Global Biogeochemical Cycles* 23:7. doi: 10.1029/2008gb003286.

Trust, American Ground Water. 2003. "Acid Rain and Ground water pH ". American Ground Water Trust

Turner, R. E., N. N. Rabalais, and D. Justic. 2008. "Gulf of Mexico hypoxia: Alternate states and a legacy." *Environmental Science & Technology* 42 (7):2323-2327. doi: 10.1021/es071617k.

USGS. "USGS 08066250 Trinity Rv nr Goodrich, TX ". USGS. https://nwis.waterdata.usgs.gov/nwis/uv?cb_00060=on&cb_00065=on&format=gif&site_no=08066250&period=&begin_date=2017-09-01&end_date=2017-09-29.

van Hooidonk, R., J. A. Maynard, D. Manzello, and S. Planes. 2014. "Opposite latitudinal gradients in projected ocean acidification and bleaching impacts on coral reefs." *Global Change Biology* 20 (1):103-112. doi: 10.1111/gcb.12394.

Veron, J. E. N. 2008. "Mass extinctions and ocean acidification: biological constraints on geological dilemmas." *Coral Reefs* 27 (3):459-472. doi: 10.1007/s00338-008-0381-8.

Walker, N. D., R. R. Leben, and S. Balasubramanian. 2005. "Hurricane-forced upwelling and chlorophyll a enhancement within cold-core cyclones in the Gulf of Mexico." *Geophysical Research Letters* 32 (18):5. doi: 10.1029/2005gl023716.

Walters, David C., and Matthew L. Kirwan. 2016. "Optimal hurricane overwash thickness for maximizing marsh resilience to sea level rise." *Ecology and evolution* 6 (9):2948-2956. doi: 10.1002/ece3.2024.

Wells, Mark L., Vera L. Trainer, Theodore J. Smayda, Bengt S. O. Karlson, Charles G. Trick, Raphael M. Kudela, Akira Ishikawa, Stewart Bernard, Angela Wulff, Donald M. Anderson, and William P. Cochlan. 2015. "Harmful algal blooms and climate change: Learning from the past and present to forecast the future." *Harmful algae* 49:68-93. doi: 10.1016/j.hal.2015.07.009.

WHPO. 1994. WHPO Operations and Methods. In *WOCE Hydrographic Office Report 91/1, as revised*. WOCE Hydrographic Program Office, Woods Hole, MA.

Wolf-Gladrow, Richard E. Zeebe and Dieter. 2005. *CO2 in Seawater Equilibrium, Kinetics, Isotopes*. Edited by David Halpern. Vol. 65, *Elsevier Oceanography Series* San Diego: Elsevier.

Wood, R., A. Y. Ivantsov, and A. Y. Zhuravlev. 2017. "First macrobiota biomineralization was environmentally triggered." *Proceedings of the Royal Society B-Biological Sciences* 284 (1851):7. doi: 10.1098/rspb.2017.0059.

Woodhead, A. J., C. C. Hicks, A. V. Norstrom, G. J. Williams, and N. A. J. Graham. 2019. "Coral reef ecosystem services in the Anthropocene." *Functional Ecology* 33 (6):1023-1034. doi: 10.1111/1365-2435.13331.

Wright, R. M., A. M. S. Correa, L. A. Quigley, L. Z. Santiago-Vazquez, K. E. F. Shamberger, and S. W. Davies. 2019. "Gene Expression of Endangered Coral (Orbicella spp.) in

Flower Garden Banks National Marine Sanctuary After Hurricane Harvey." *Frontiers in Marine Science* 6:11. doi: 10.3389/fmars.2019.00672.

Yao, H. M., M. R. McCutcheon, C. J. Staryk, and X. P. Hu. "Hydrologic controls on CO2 chemistry and flux in subtropical lagoonal estuaries of the northwestern Gulf of Mexico." *Limnology and Oceanography*:19. doi: 10.1002/lno.11394.

Zavala-Hidalgo, Jorge, Rosario Romero-Centeno, Adriana Mateos-Jasso, Steven L. Morey, and Benjamín Martínez-López. 2014. "The response of the Gulf of Mexico to wind and heat flux forcing: What has been learned in recent years?" *Atmósfera* 27 (3):317-334. doi: https://doi.org/10.1016/S0187-6236(14)71119-1.

Zeebe, R. E., A. Ridgwell, and J. C. Zachos. 2016. "Anthropogenic carbon release rate unprecedented during the past 66 million years." *Nature Geoscience* 9 (4):325-329. doi: 10.1038/ngeo2681.

Zeebe, R. E., and T. Tyrrell. 2019. "History of carbonate ion concentration over the last 100 million years II: Revised calculations and new data." *Geochimica Et Cosmochimica Acta* 257:373-392. doi: 10.1016/j.gca.2019.02.041.

Zingula, Dick. 2008a. "Title." Geology & Paleontology of Stetson Bank, Flower Garden Banks National Marine Sanctuary web page.

Zingula, Richard. 2008b. "Geology of Stetson Bank." National Oceanic and Atmospheric Administration. https://flowergarden.noaa.gov/document_library/aboutdocs/geopaleostetson.html.

APPENDIX A

FIGURES

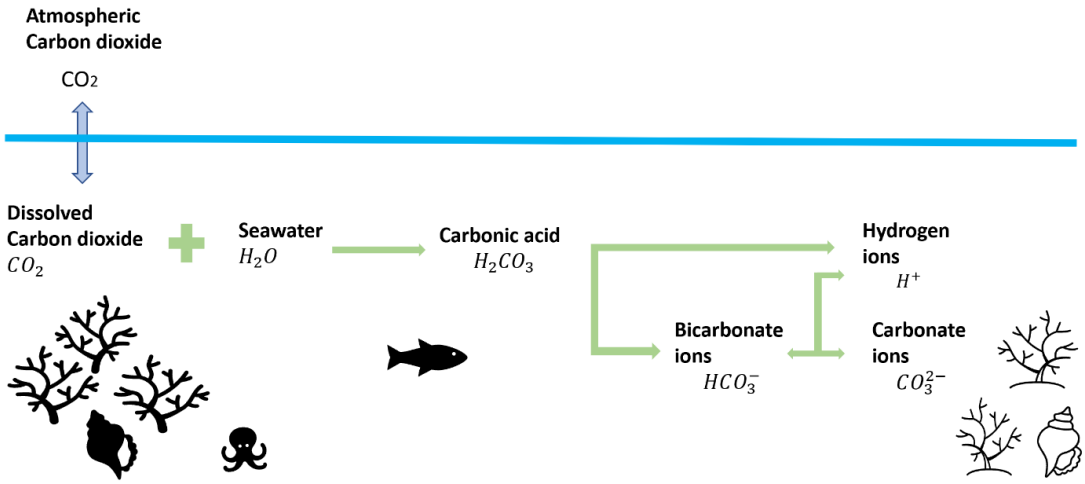

Fig 1. Diagram showing the flow of carbon in the process of ocean acidification

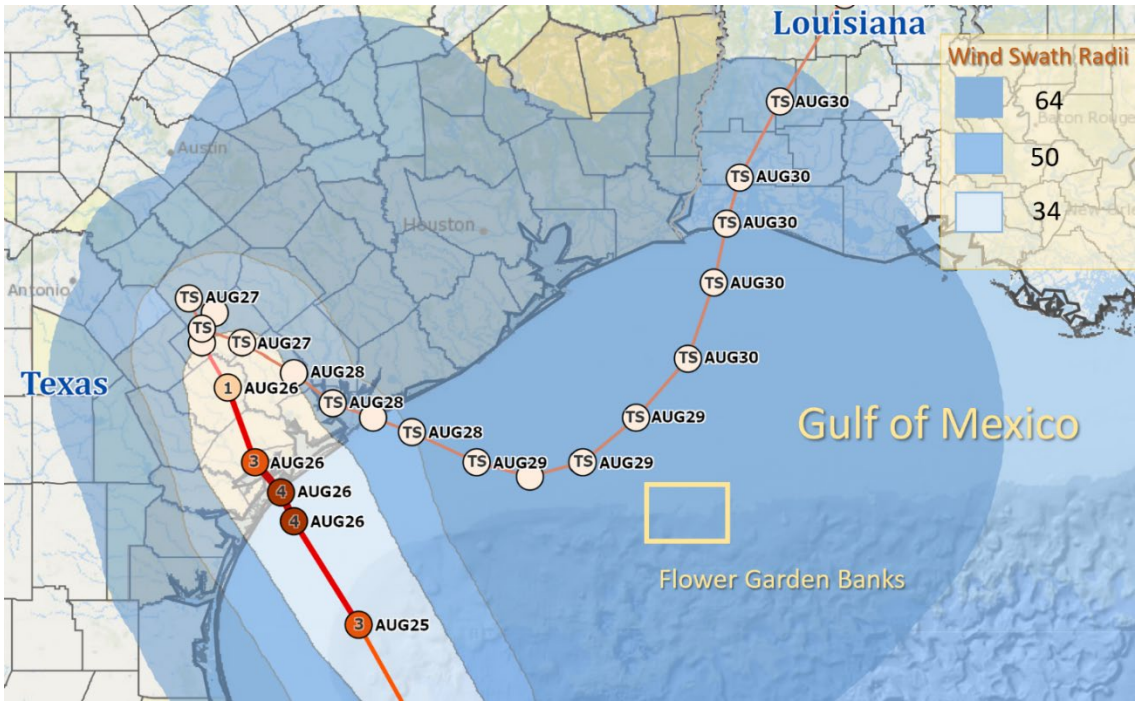

Fig 2*. Path and intensity of Hurricane Harvey (modified from cuahsi hurricane data project archive; NOAA NHC et al. 2018, https://doi.org/10.4211/hs.6168b9969c984b658952a896710b65ef)*
https://www.cuahsi.org/projects/hurricanes-2017-data-archive/

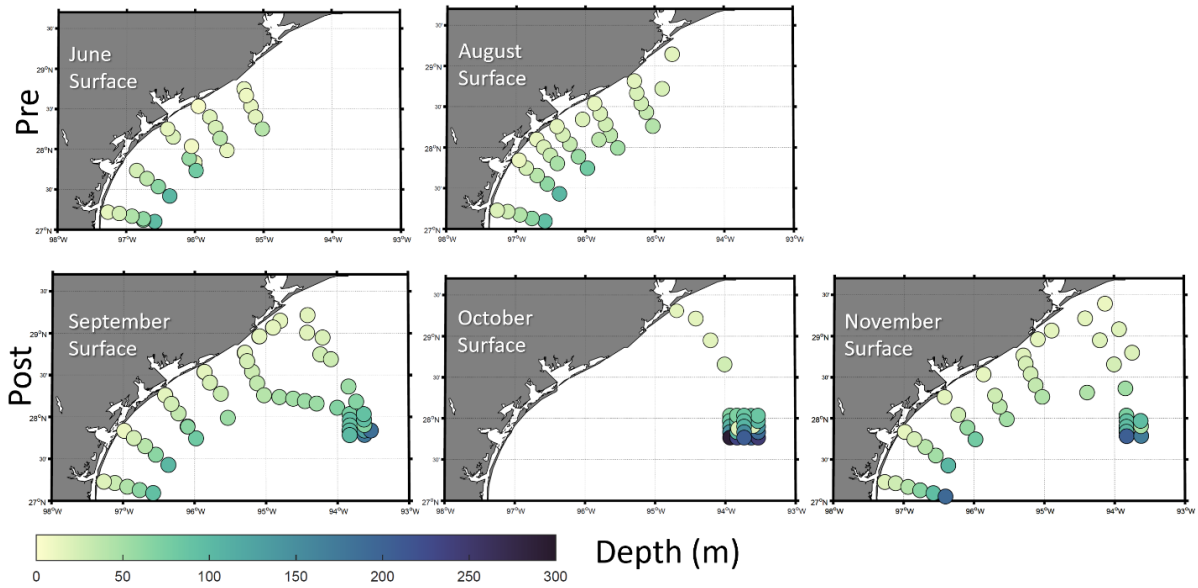

Fig 3. Depth maps indicating the deepest sample taken in each transect. *Collected in 2017 on research cruises from June 12-15, August 8-11, September 23 – October 1, October 20-24, and November 15-20. Data shown in the upper two panels were collected before Hurricane Harvey and in the lower three panels after Hurricane Harvey.*

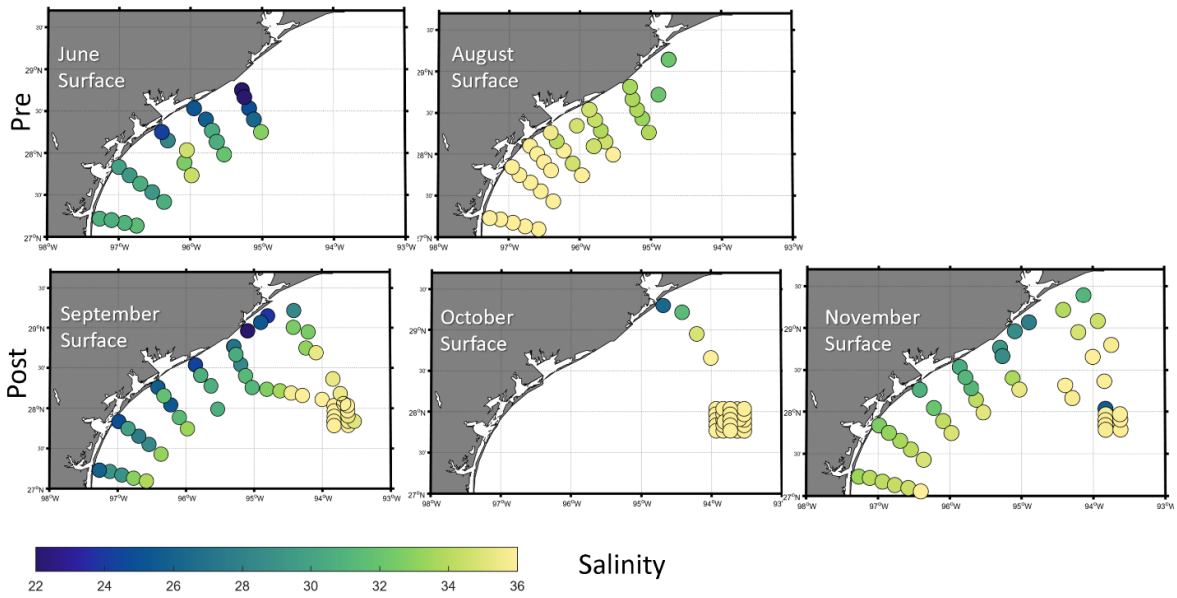

Fig 4. *Surface water salinity data collected in 2017 on research cruises from June 12-15, August 8-11, September 23 – October 1, October 20-24, and November 15-20. Data shown in the upper two panels were collected before Hurricane Harvey and in the lower three panels after Hurricane Harvey.*

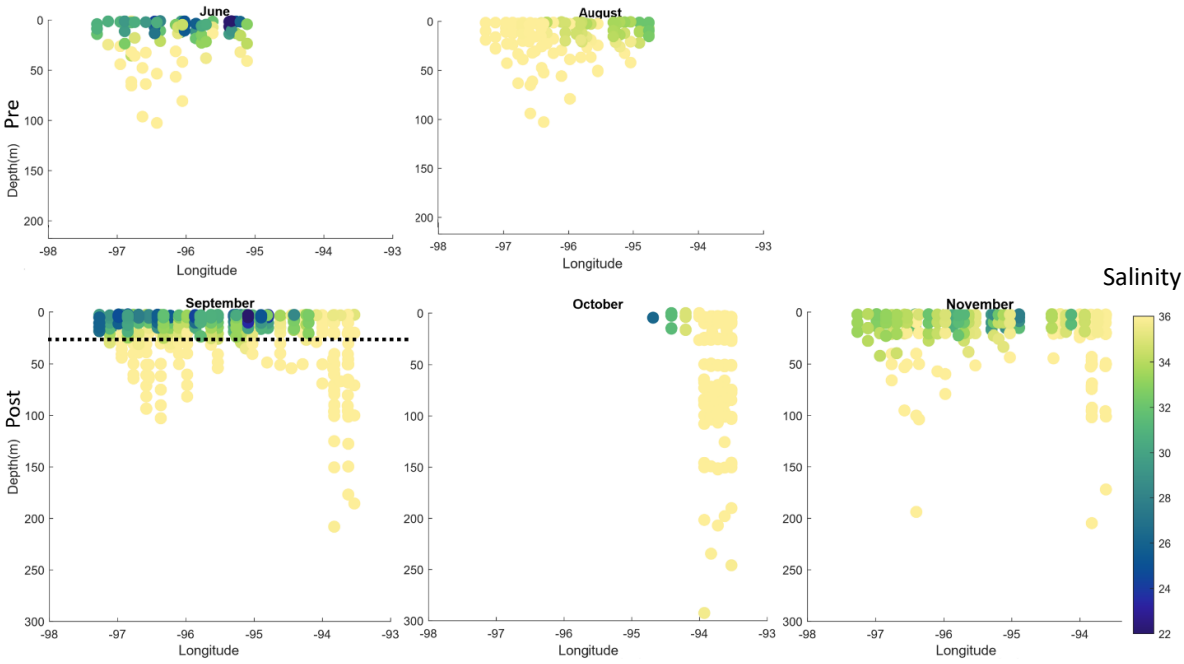

Fig 5*. Salinity data represented by colors and plotted versus depth and longitude. Data shown in the upper two panels were collected before Hurricane Harvey and in the lower three panels after Hurricane Harvey. In September, the black dashed line indicates the depth of the freshwater plume at about 25 m.*

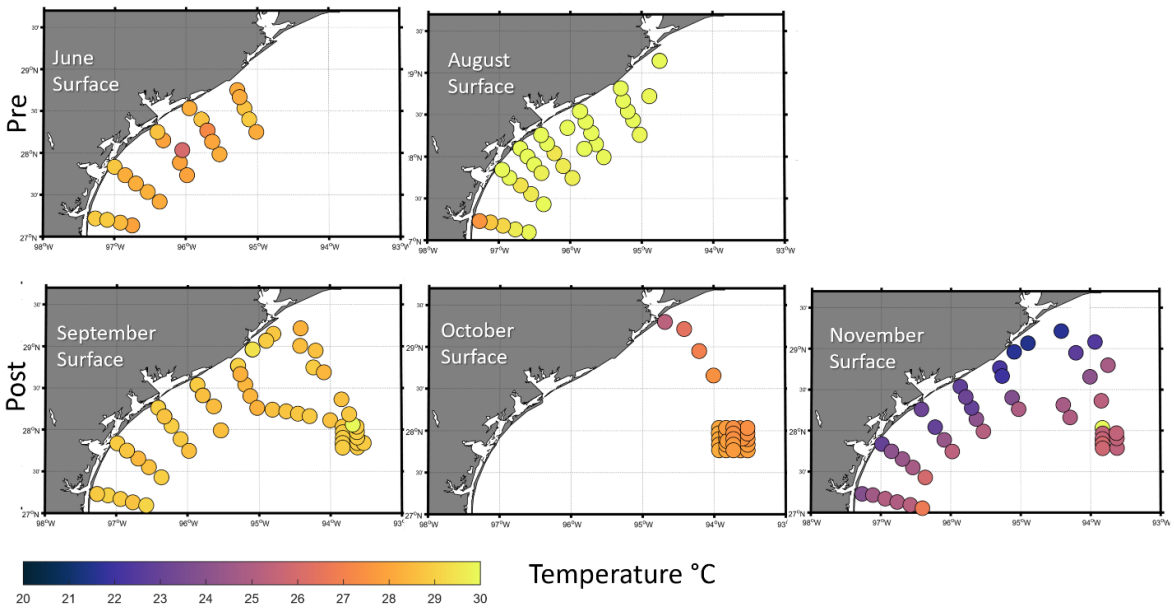

***Fig 6**. Surface water Temperature data collected in 2017 on research cruises from June 12-15, August 8-11, September 23 – October 1, October 20-24, and November 15-20. Data shown in the upper two panels were collected before Hurricane Harvey and in the lower three panels after Hurricane Harvey.*

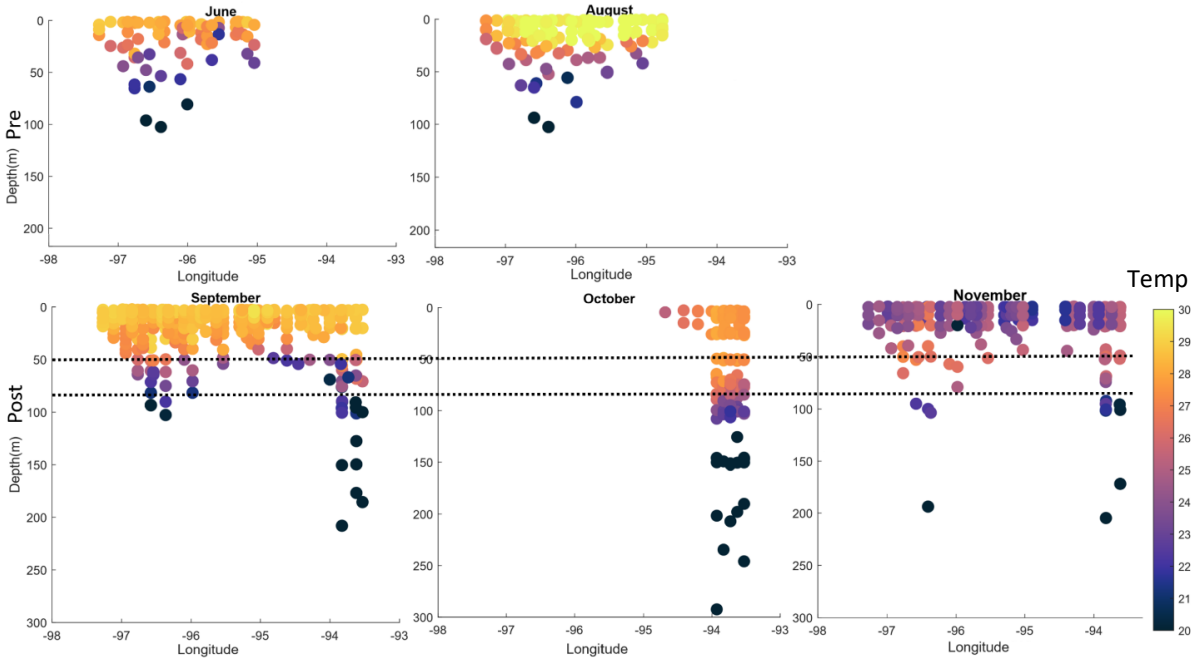

***Fig 7**. Temperature (Temp) data represented by colors and plotted versus depth and longitude. Data shown in the upper two panels were collected before Hurricane Harvey and in the lower three panels after Hurricane Harvey. In September, October, and November, the horizontal black dashed lines indicate depths from 50-75 m to highlight changes at depth induced by Hurricane Harvey*

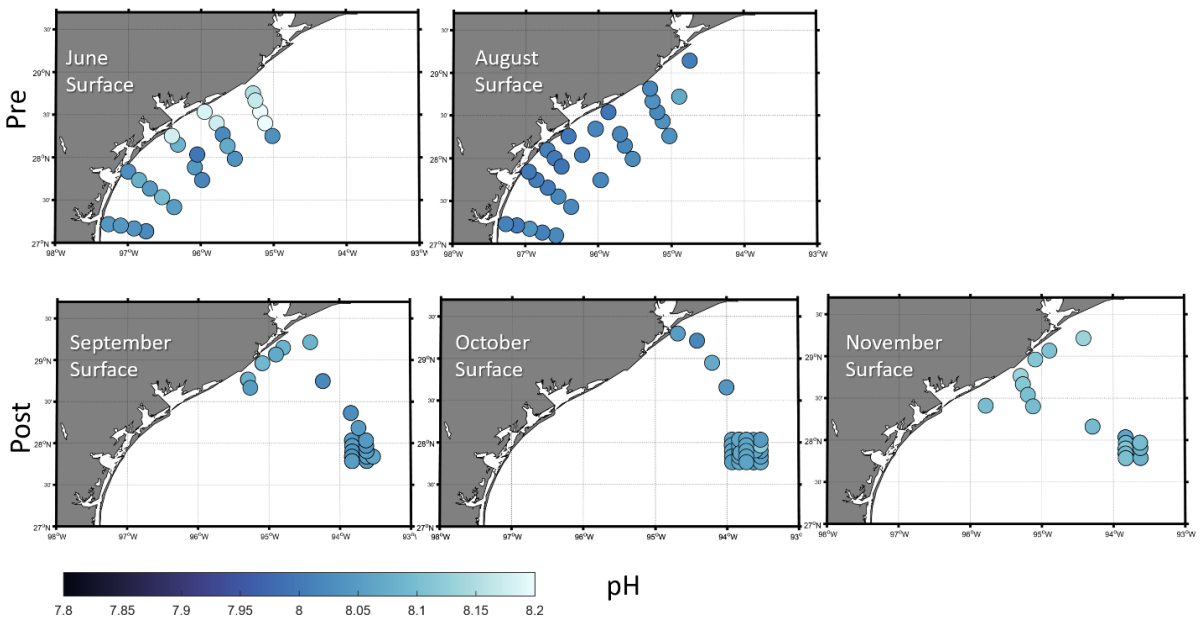

Fig 8*. Surface water pH data collected in 2017 on research cruises from June 12-15, August 8-11, September 23 – October 1, October 20-24, and November 15-20. Data shown in the upper two panels were collected before Hurricane Harvey and in the lower three panels after Hurricane Harvey.*

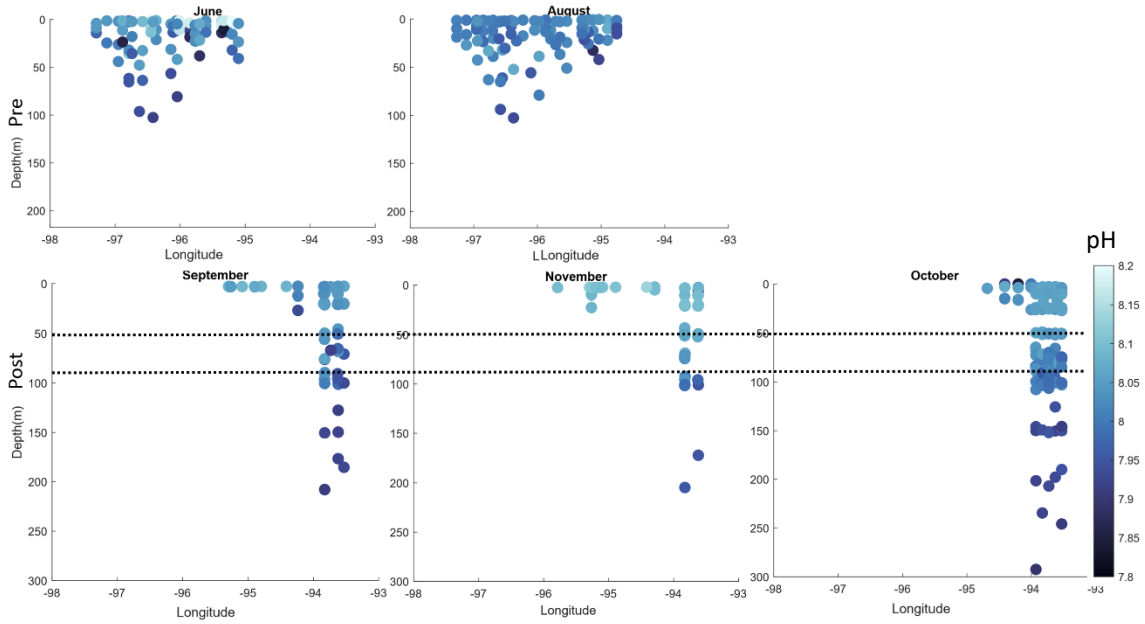

Fig 9. *pH data represented by colors and plotted versus depth and longitude. Data shown in the upper two panels were collected before Hurricane Harvey and in the lower three panels after Hurricane Harvey. In September, October, and November, the black dashed line indicates change due in pH due to upwelling induced by Hurricane Harvey*

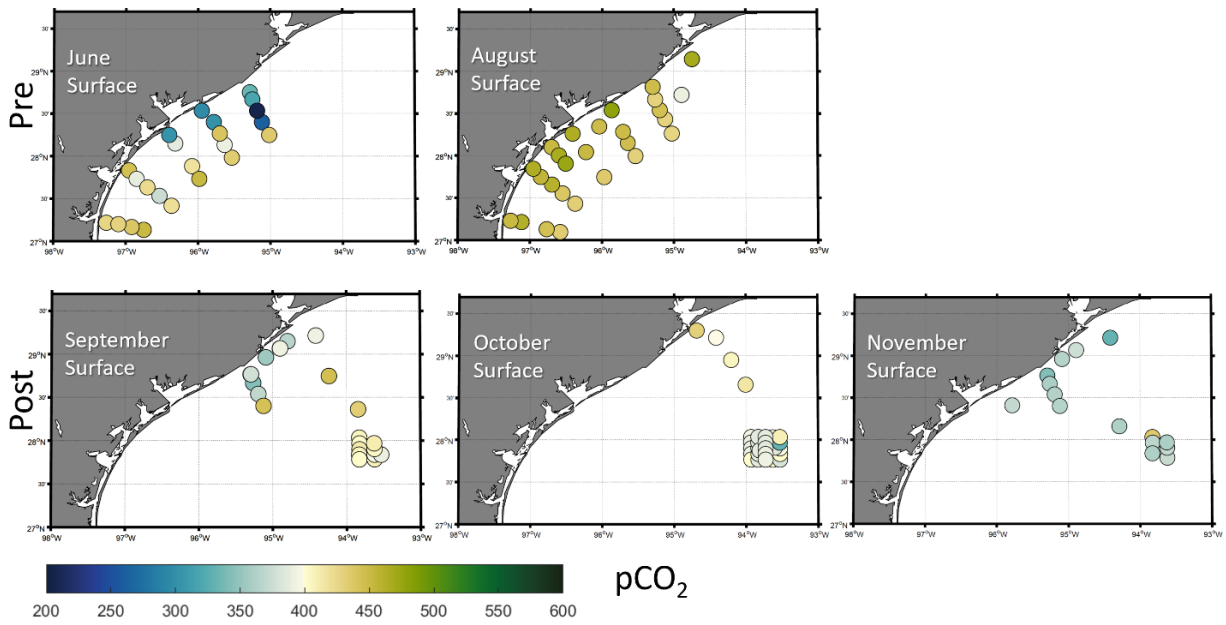

Fig 10. *Surface water partial pressure of carbon dioxide (pCO_2) data collected in 2017 on research cruises from June 12-15, August 8-11, September 23 – October 1, October 20-24, and November 15-20. Data shown in the upper two panels were collected before Hurricane Harvey and in the lower three panels after Hurricane Harvey.*

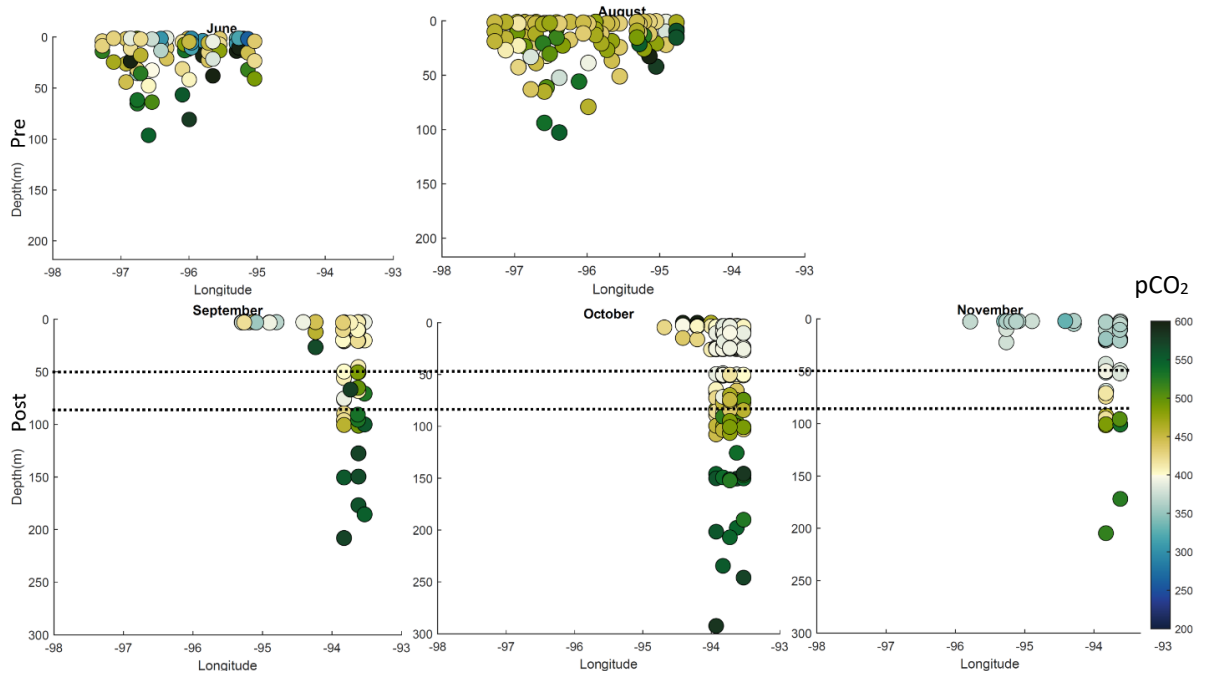

Fig 11. *pCO_2 data represented by colors and plotted versus depth and longitude. Data shown in the upper two panels collected before Hurricane Harvey and in the lower three panels after Hurricane Harvey. In September, October, and November, the black dashed line indicates change due in pCO_2 due to upwelling induced by Hurricane Harvey*

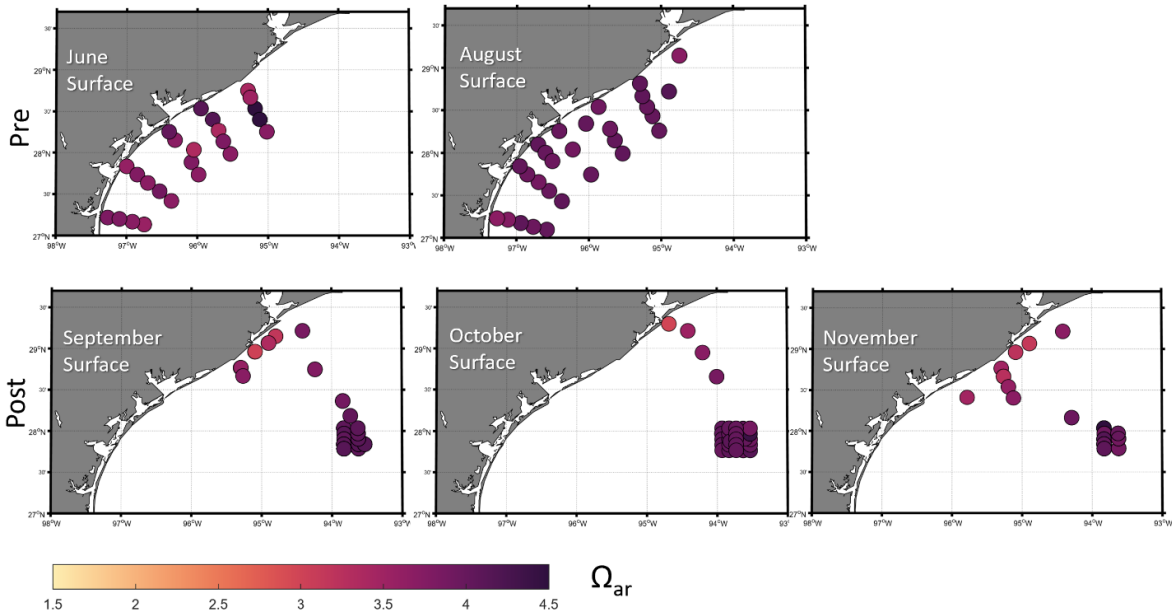

Fig 12. *Surface water aragonite saturation state (Ω_{ar}) data collected in 2017 on research cruises from June 12-15, August 8-11, September 23 – October 1, October 20-24, and November 15-20. Data shown in the upper two panels were collected before Hurricane Harvey and in the lower three panels after Hurricane Harvey.*

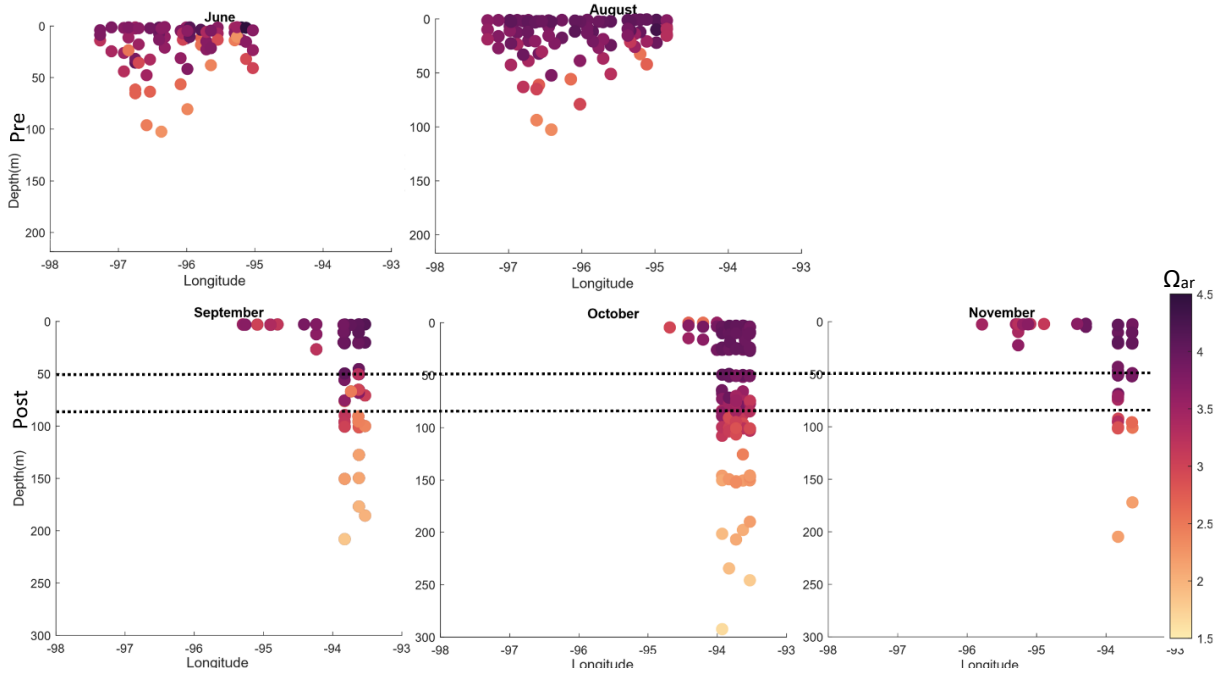

Fig 13. *Aragonite saturation state (Ω_{ar}) data represented by colors and plotted versus depth and longitude. Data shown in the upper two panels were collected before Hurricane Harvey and in the lower three panels after Hurricane Harvey. In September, October, and November, the black dashed line indicates change due in Ω_{ar} due to upwelling induced by Hurricane Harvey*

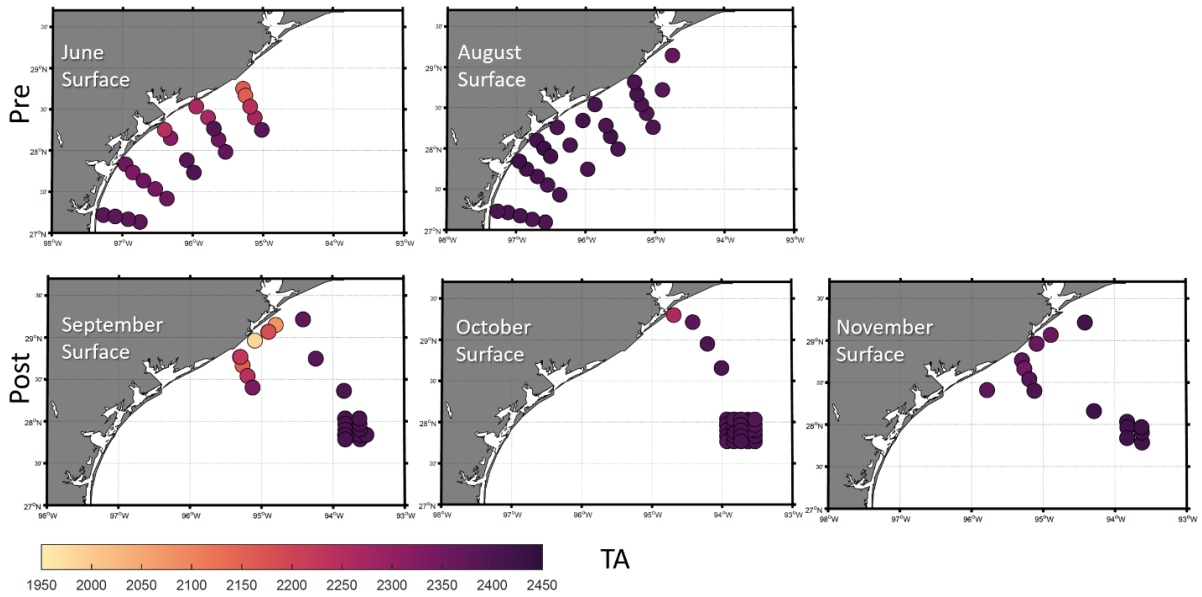

Fig 14. *Surface water total alkalinity (TA) data collected in 2017 on research cruises from June 12-15, August 8-11, September 23 – October 1, October 20-24, and November 15-20. Data shown in the upper two panels were collected before Hurricane Harvey and in the lower three panels after Hurricane Harvey*

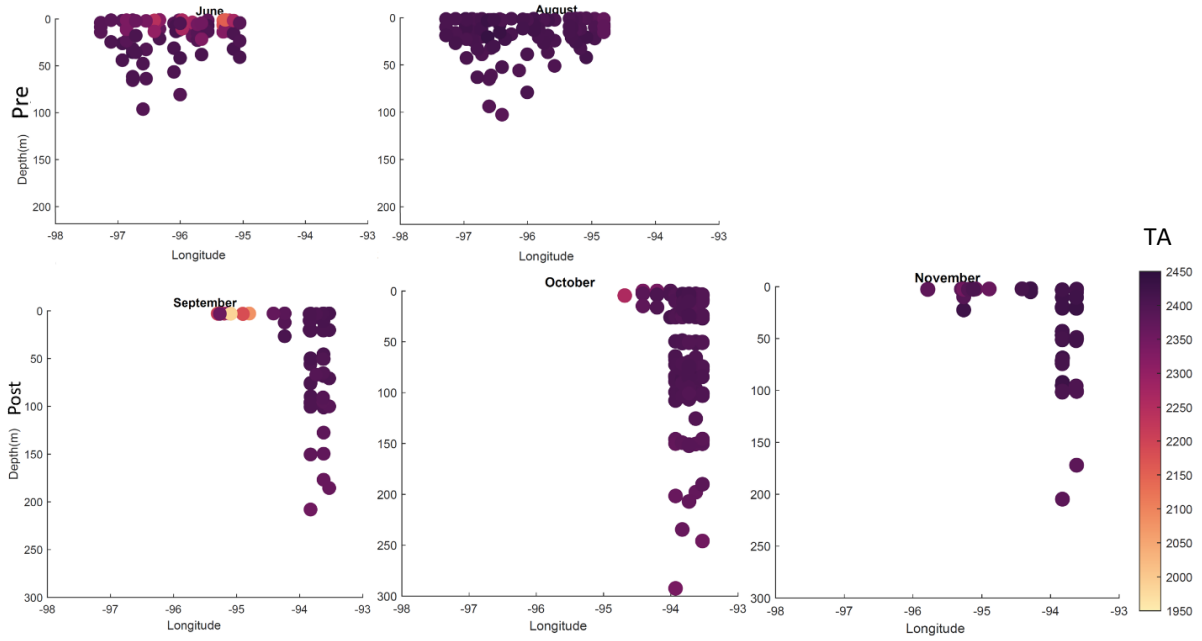

Fig 15. *TA data represented by colors and plotted versus depth and longitude. Data shown in the upper two panels were collected before Hurricane Harvey and in the lower three panels after Hurricane Harvey*

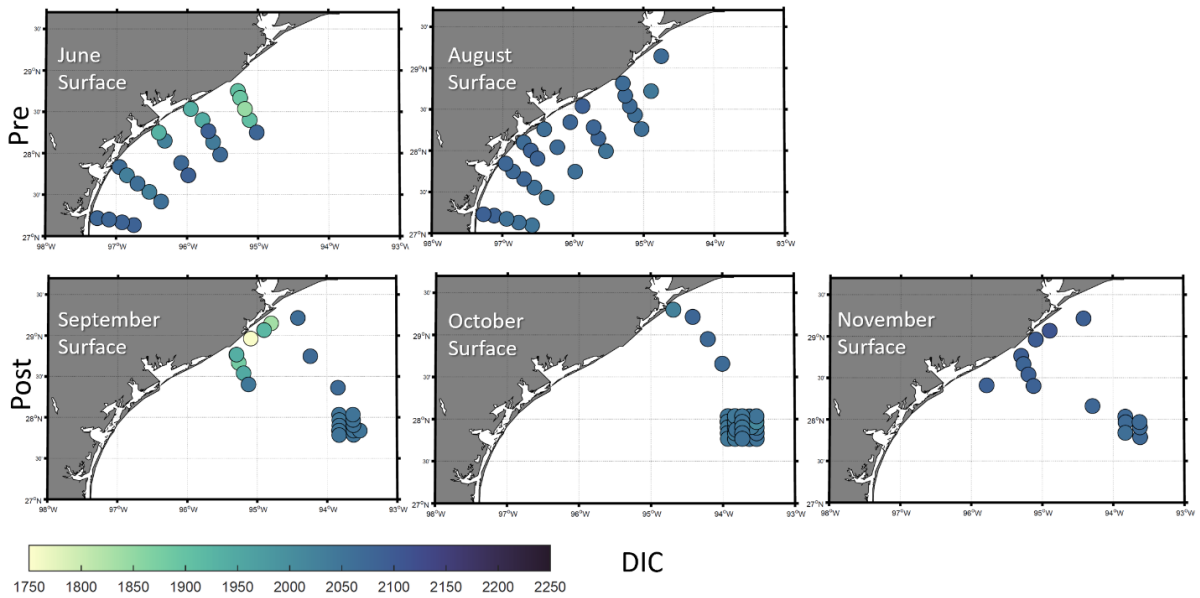

Fig 16. *Surface water dissolved inorganic carbon (DIC) data collected in 2017 on research cruises from June 12-15, August 8-11, September 23 – October 1, October 20-24, and November 15-20. Data shown in the upper two panels were collected before Hurricane Harvey and in the lower three panels*

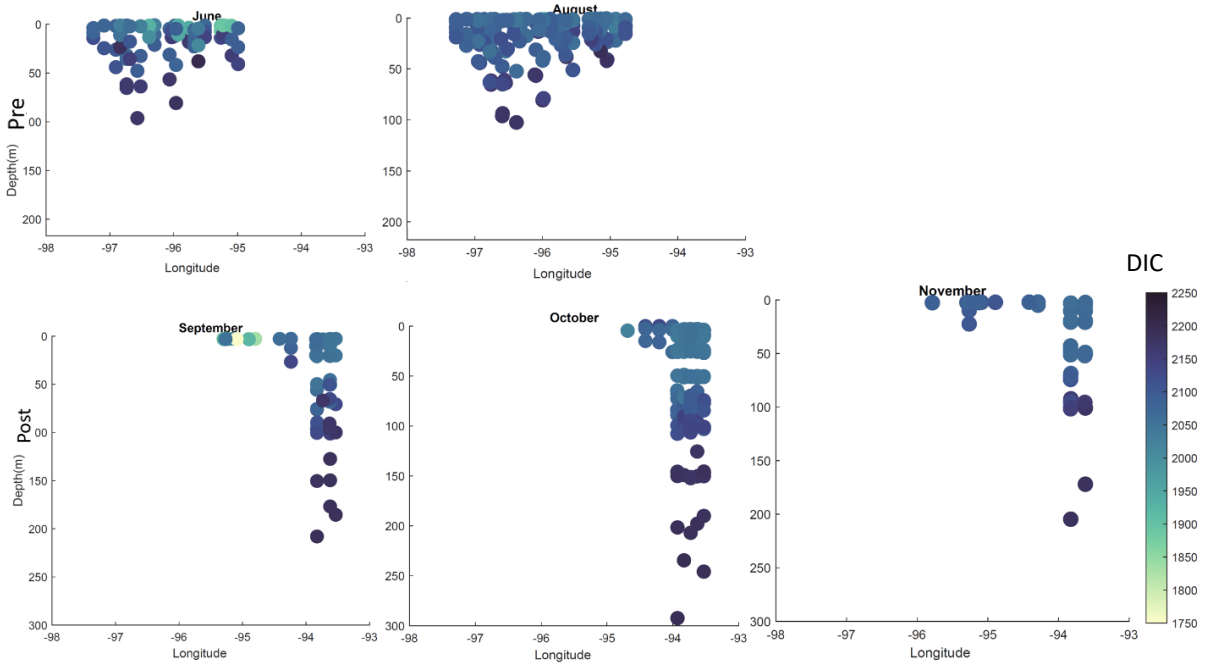

Fig 17. *Dissolved inorganic carbon (DIC) data represented by colors and plotted versus depth and longitude. Data shown in the upper two panels were collected before Hurricane Harvey and in the lower three panels after Hurricane*

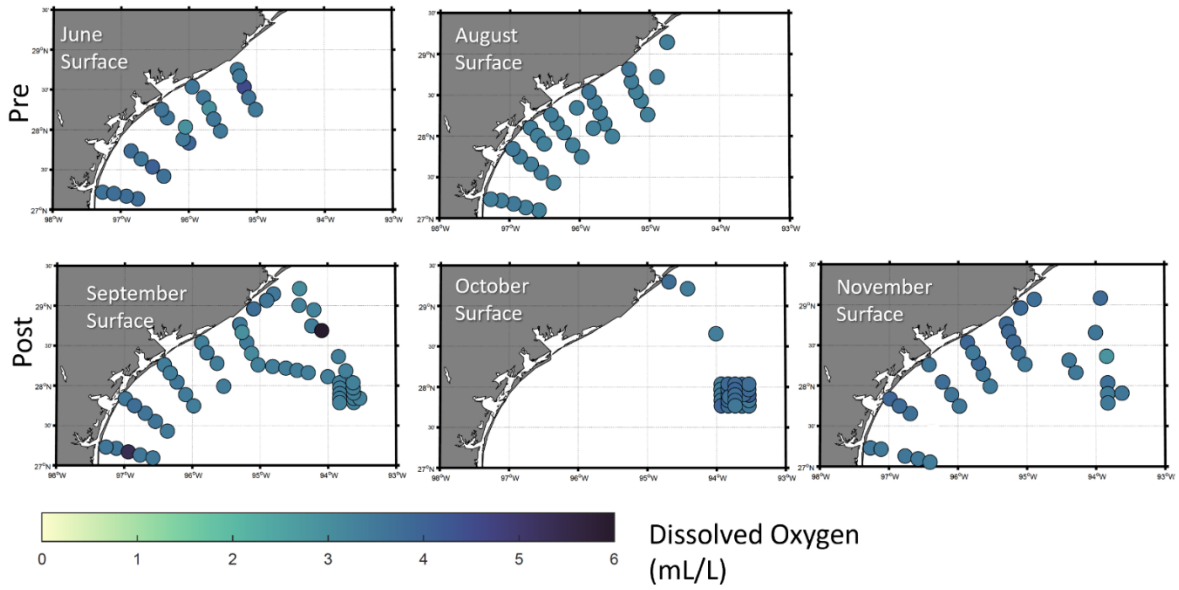

Fig 18. *Surface water dissolved oxygen (DO) data collected in 2017 on research cruises from June 12-15, August 8-11, September 23 – October 1, October 20-24, and November 15-20. Data shown in the upper two panels were collected before Hurricane Harvey and in the lower three panels after Hurricane Harvey*

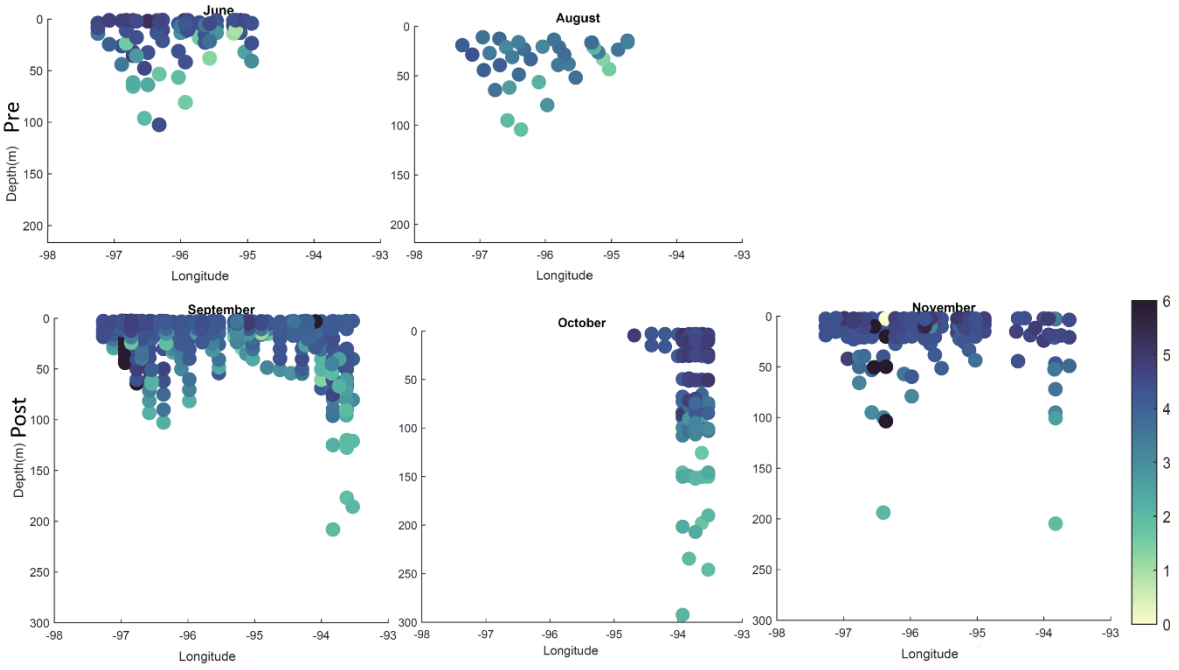

Fig 19. *Discrete dissolved oxygen (DO) samples plotted against depth reveal lower concentrations with deeper waters. The upper two plots are before Hurricane Harvey while the lower three plots are after Hurricane Harvey*

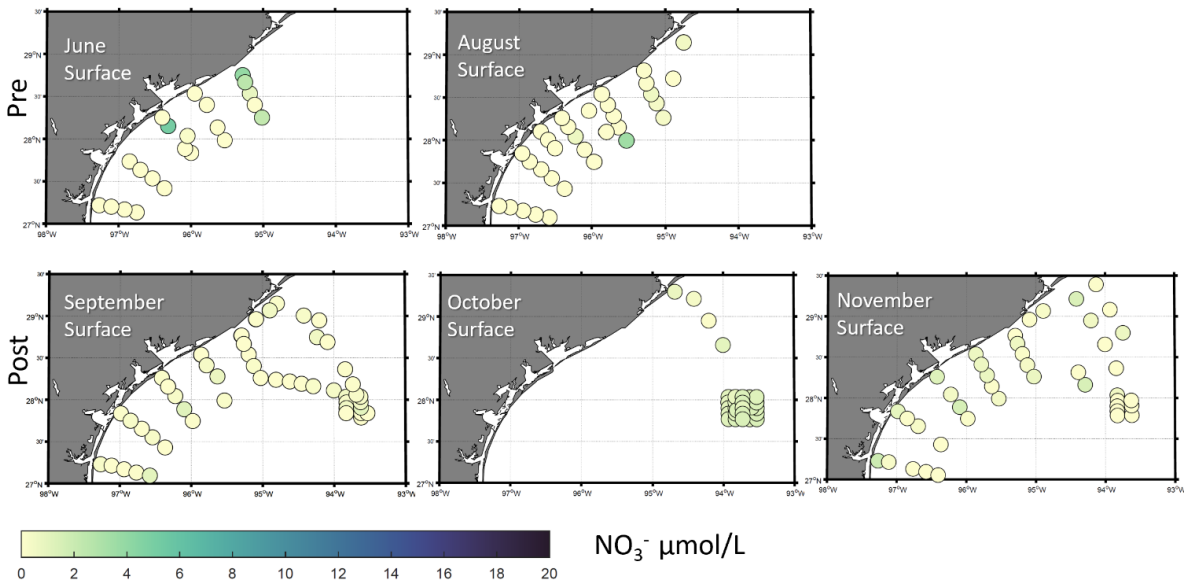

Fig 20. *Surface nitrate (NO^-_3) data collected in 2017 on research cruises from June 12-15, August 8-11, September 23 – October 1, October 20-24, and November 15-20. Data shown in the upper two panels were collected before Hurricane Harvey and in the lower three panels after Hurricane Harvey*

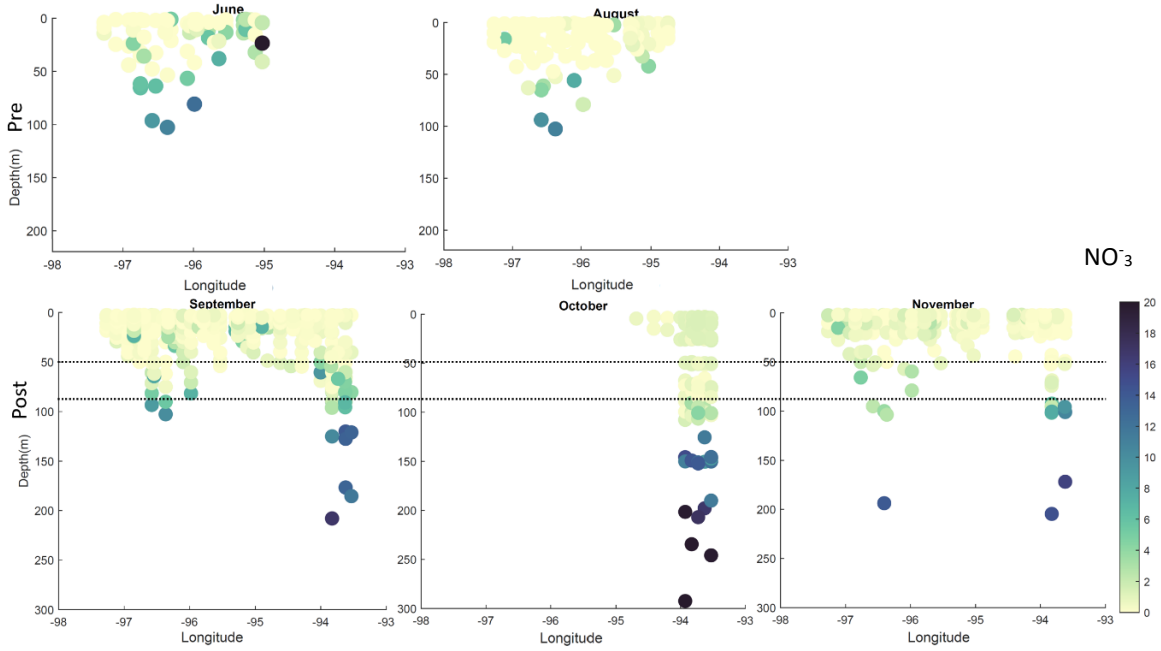

Fig 21. *Nitrate (NO^-_3) data represented by colors and plotted versus depth and longitude. Data shown in the upper two panels were collected before Hurricane Harvey and in the lower three panels after Hurricane Harvey. In September, October, and November, the black dashed line indicates change in Nitrate due to upwelling induced by Hurricane Harvey*

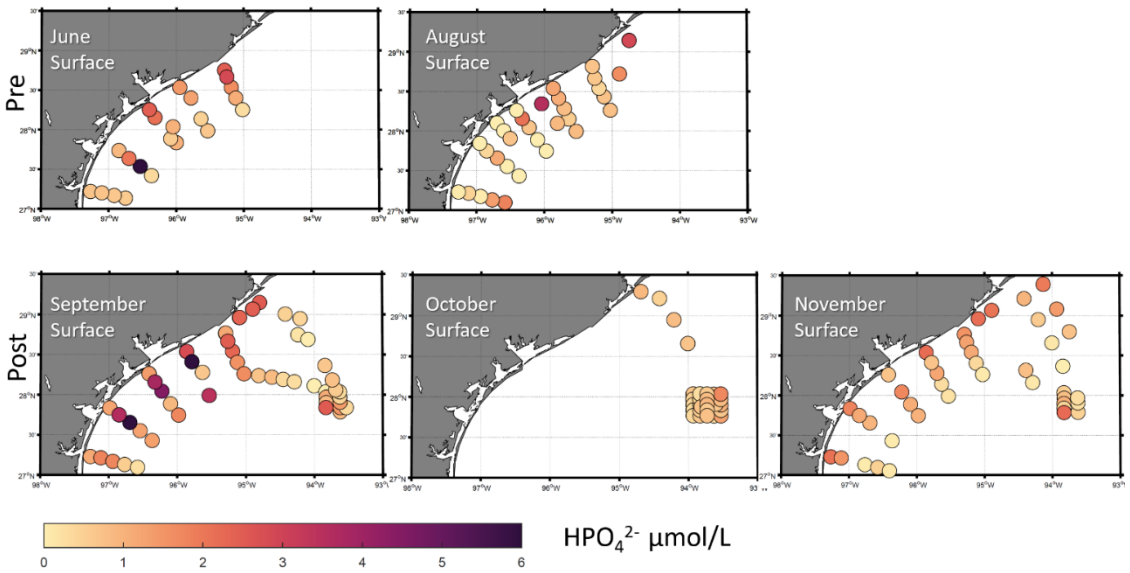

Fig 22. *Surface phosphate (HPO_4^{2-}) data collected in 2017 on research cruises from June 12-15, August 8-11, September 23 – October 1, October 20-24, and November 15-20. Data shown in the upper two panels were collected before Hurricane Harvey and in the lower three panels after Hurricane Harvey*

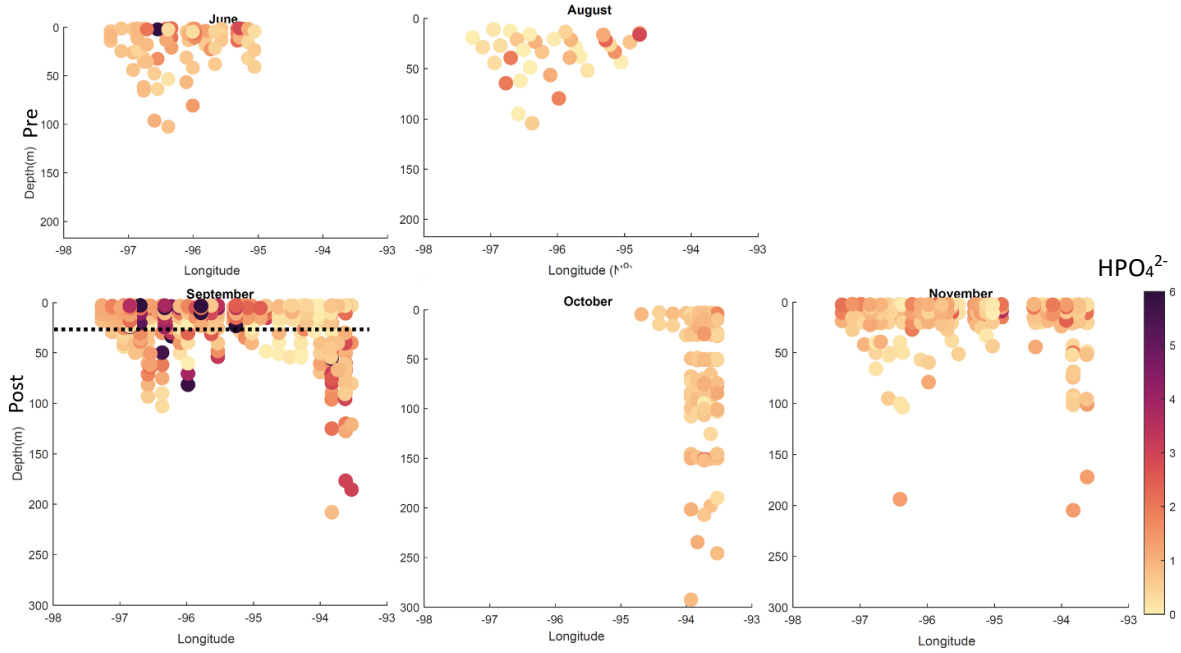

Fig 23. *Discrete Phosphate (HPO_4^{2-}) samples plotted against depth indicating there are lower levels with deeper waters. The upper two plots are before Hurricane Harvey while the lower three plots are after Hurricane Harvey. The black dashed line indicates change induced by Hurricane Harvey*

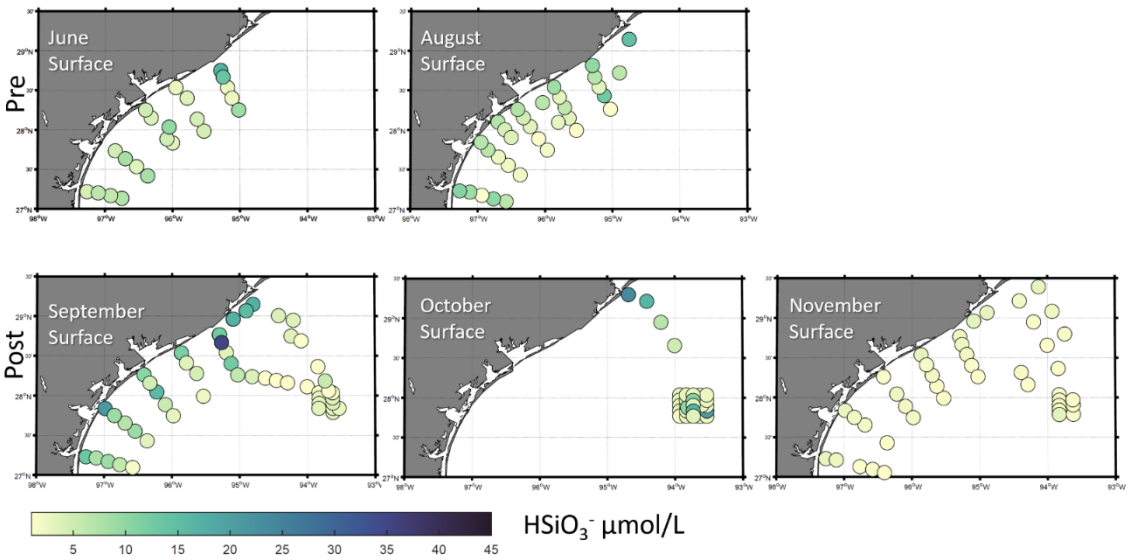

Fig 24. *Surface Silicate ($HSiO_3^-$) data collected in 2017 on research cruises from June 12-15, August 8-11, September 23 – October 1, October 20-24, and November 15-20. Data shown in the upper two panels were collected before Hurricane Harvey and in the lower three panels after Hurricane Harvey*

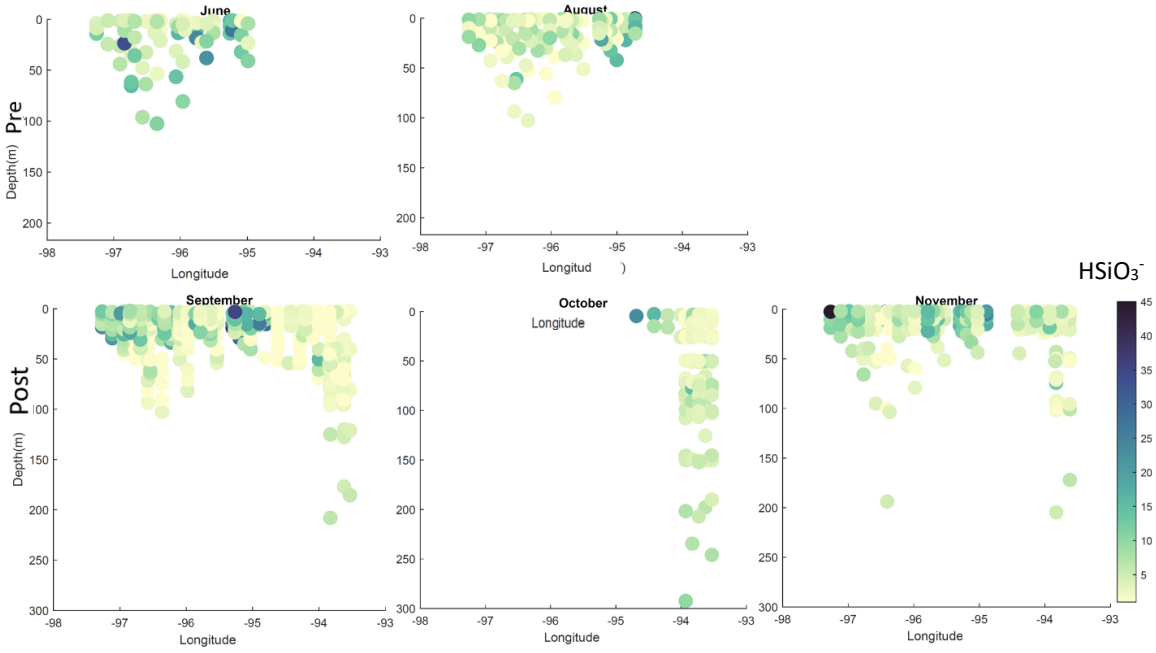

Fig 25. *Discrete Silicate ($HSiO_3^-$) samples plotted against depth reveal there are lower concentrations in deeper waters. The upper two plots are before Hurricane Harvey while the lower three plots are after Hurricane Harvey*

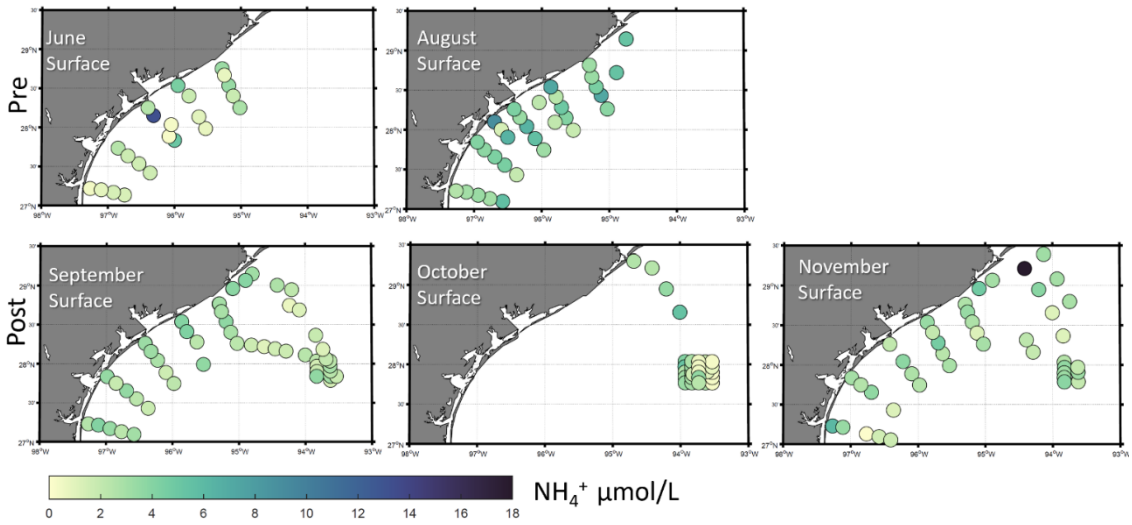

Fig 26. *Surface Ammonium (NH^{+}_{4}) data collected in 2017 on research cruises from June 12-15, August 8-11, September 23 – October 1, October 20-24, and November 15-20. Data shown in the upper two panels were collected before Hurricane Harvey and in the lower three panels after Hurricane Harvey*

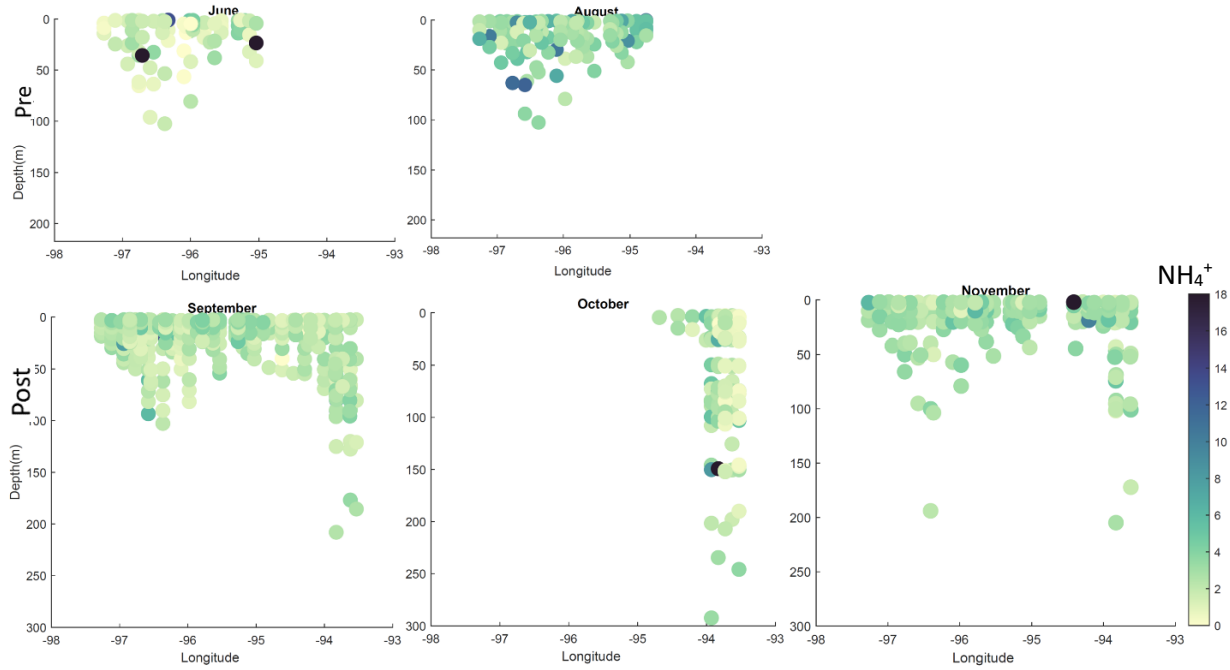

Fig 27. *Discrete Ammonium (NH^{+}_{4}) samples plotted against depth reveal lower levels in deeper waters. The upper two plots are before Hurricane Harvey while the lower three plots are after Hurricane Harvey*

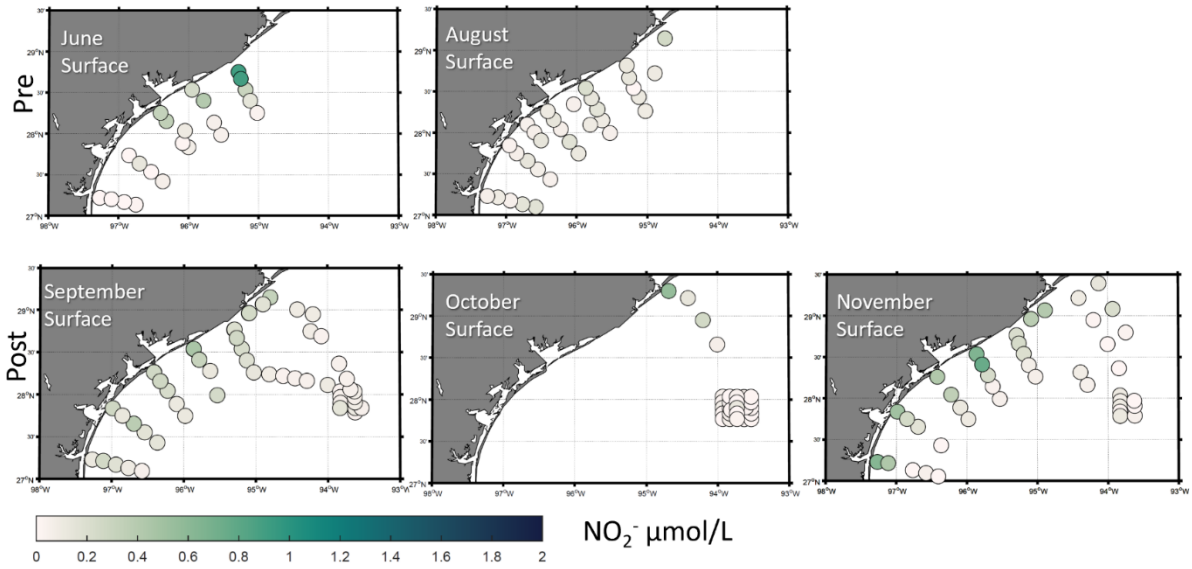

Fig 28. *Surface nitrite (NO^-_2) data collected in 2017 on research cruises from June 12-15, August 8-11, September 23 – October 1, October 20-24, and November 15-20. Data shown in the upper two panels were collected before Hurricane Harvey and in the lower three panels after Hurricane Harvey*

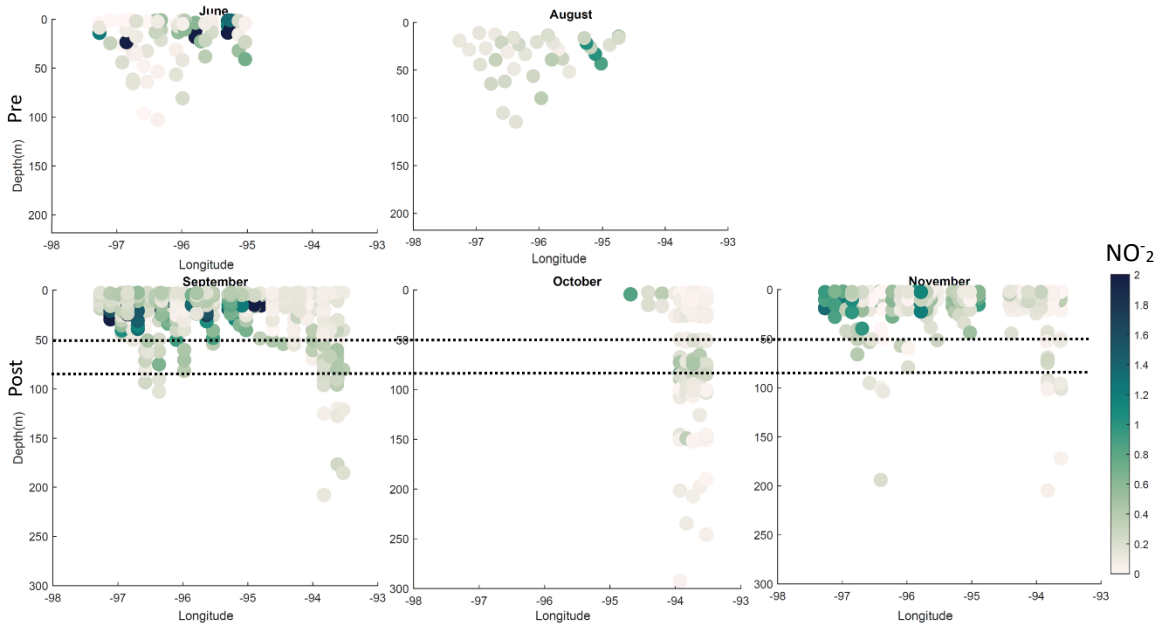

Fig 29. *Nitrite data represented by colors and plotted versus depth and longitude. Data shown in the upper two panels were collected before Hurricane Harvey and in the lower three panels after Hurricane Harvey. In September, October, and November, the black dashed line indicates change due in Nitrite due to upwelling induced by Hurricane Harvey*

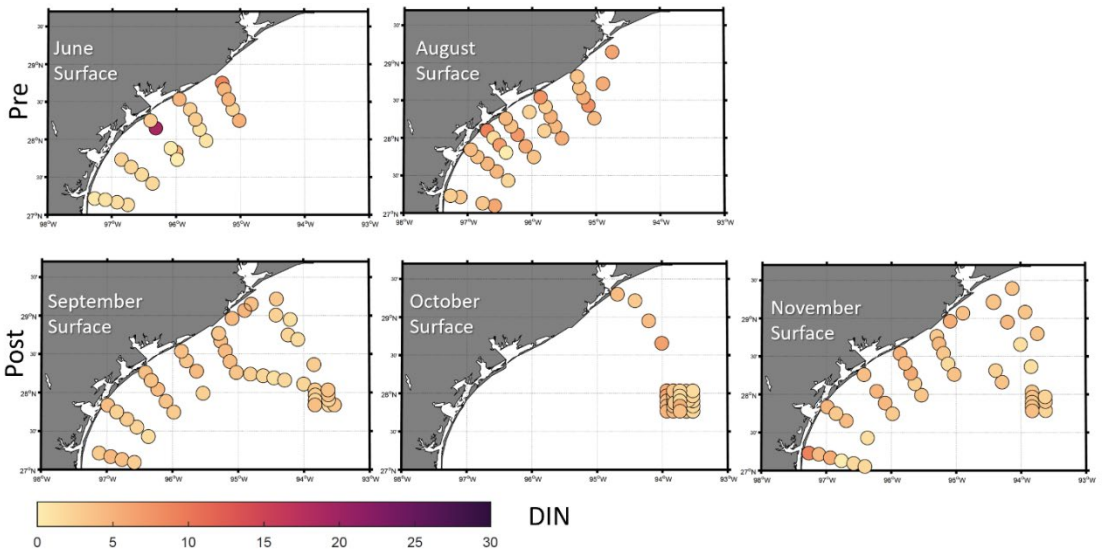

Fig 30. *Surface dissolved inorganic nutrients (DIN) data collected in 2017 on research cruises from June 12-15, August 8-11, September 23 – October 1, October 20-24, and November 15-20. Data shown in the upper two panels were collected before Hurricane Harvey and in the lower three panels after Hurricane Harvey*

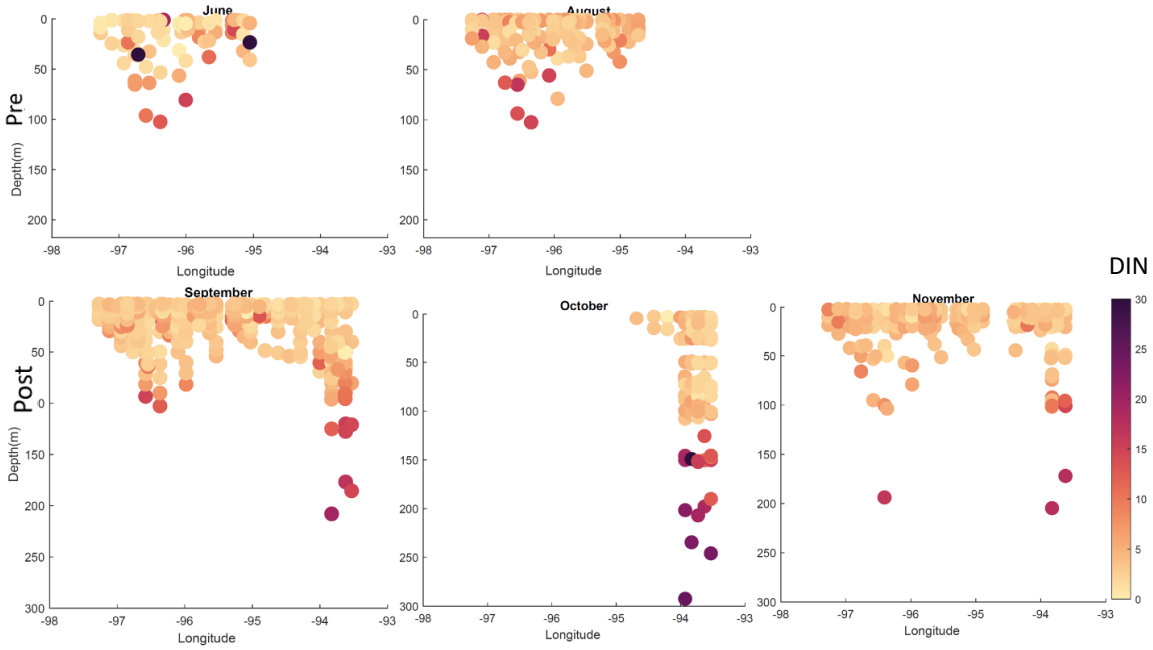

Fig 31. *Discrete DIN samples plotted against depth reveal there are lower concentrations with deeper waters. The upper two plots are before Hurricane Harvey while the lower three plots are after Hurricane Harvey*

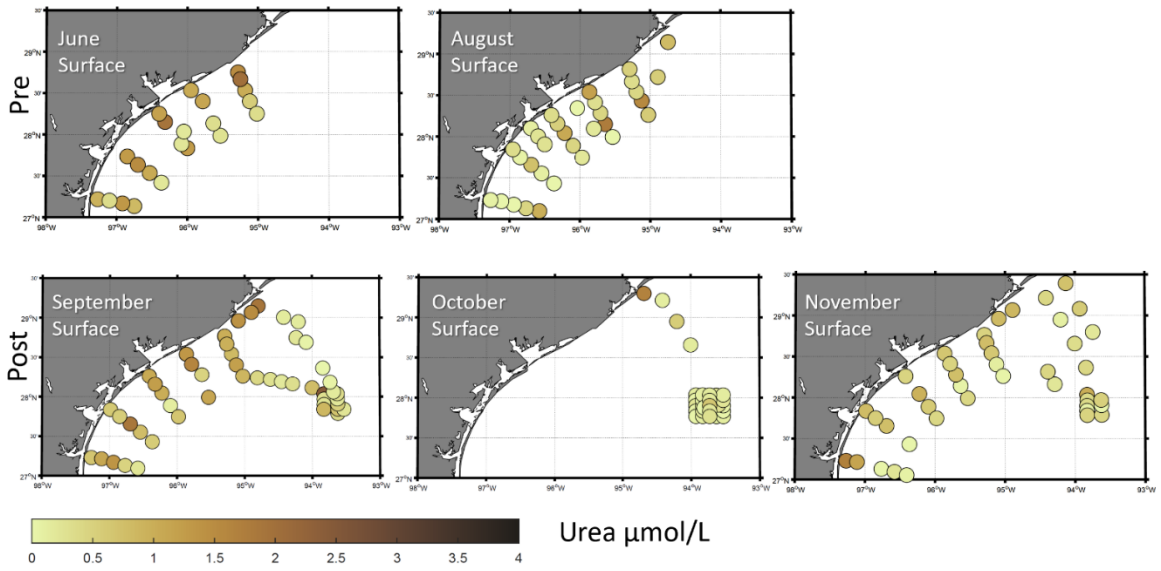

Fig 32. *Surface urea data collected in 2017 on research cruises from June 12-15, August 8-11, September 23 – October 1, October 20-24, and November 15-20. Data shown in the upper two panels were collected before Hurricane Harvey and in the lower three panels after Hurricane Harvey*

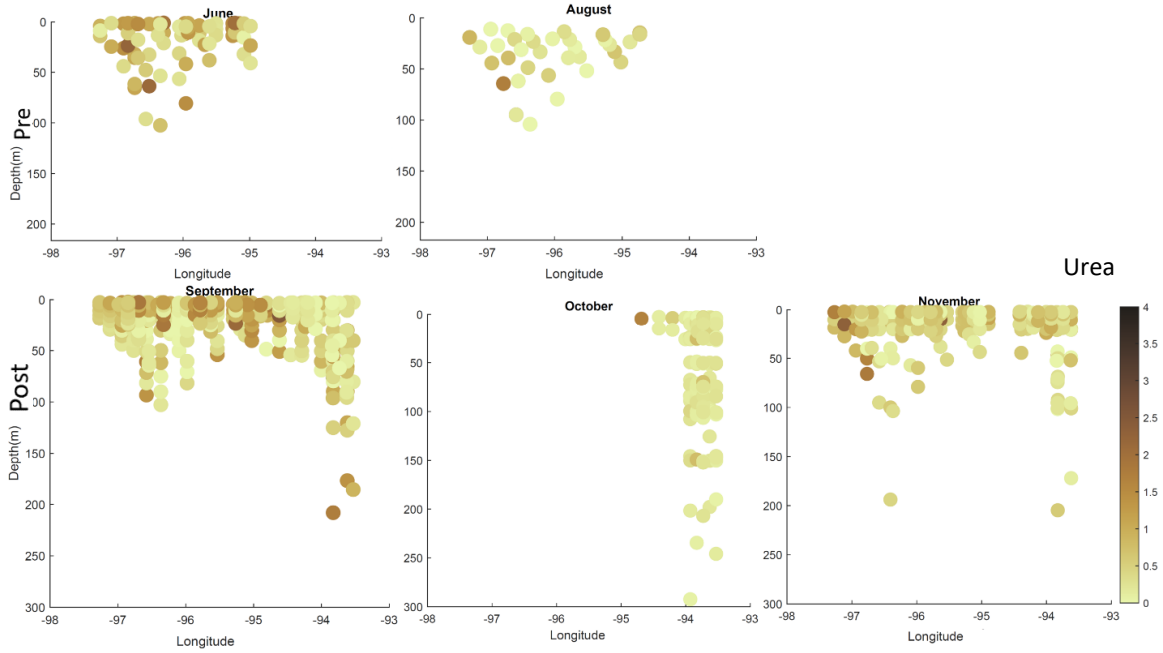

Fig 33. *Discrete urea samples plotted against depth reveal lower levels with deeper waters. The upper two plots are before Hurricane Harvey while the lower three plots are after Hurricane Harvey*

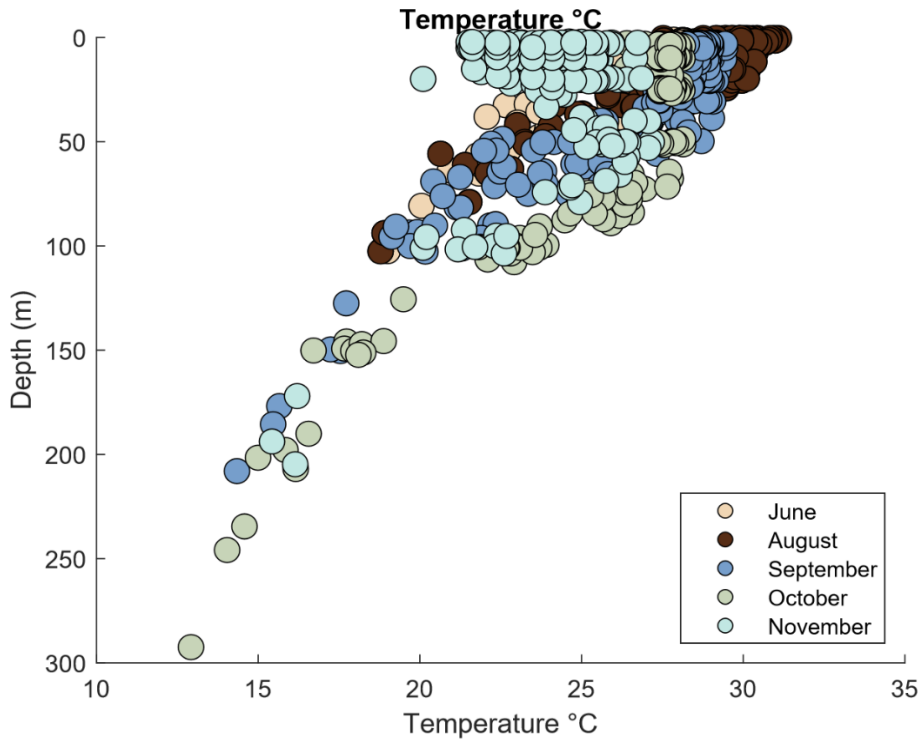

Fig 34*. Temperature versus depth. Data were collected in 2017 on research cruises from* June 12-15 *(tan), August* 8-11 *(brown), September* 23 – October 1 *(blue), October 20-24 (green), and November 15-20 (teal).*

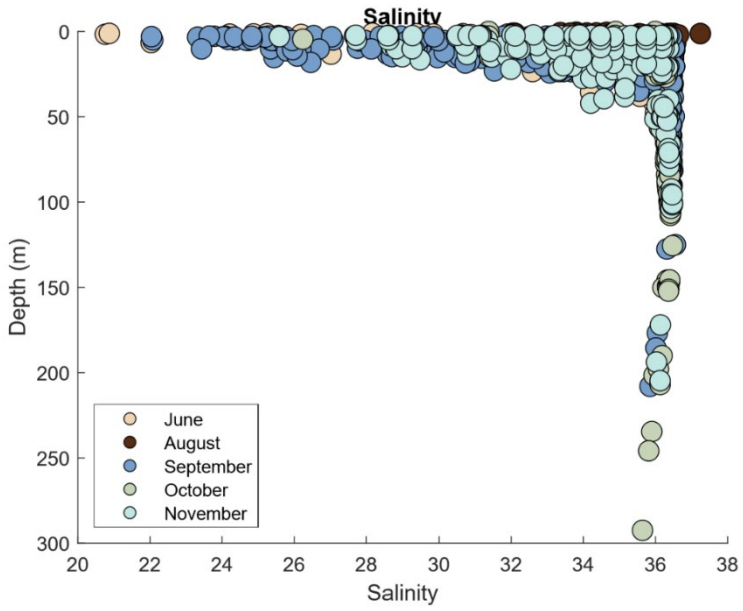

Fig 35. *Salinity versus depth. Data were collected in 2017 on research cruises from* June 12-15 *(tan), August* 8-11 *(brown), September* 23 – October 1 *(blue), October 20-24 (green), and November 15-20 (teal).*

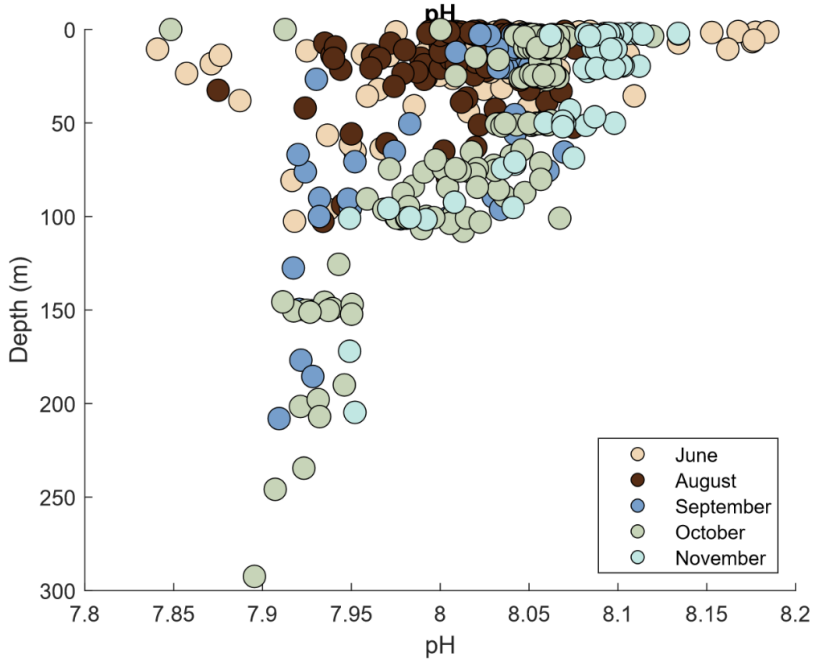

***Fig 36**. pH versus depth. Data were collected in 2017 on research cruises from* June 12-15 *(tan), August* 8-11 *(brown), September* 23 – October 1 *(blue), October 20-24 (green), and November 15-20 (teal).*

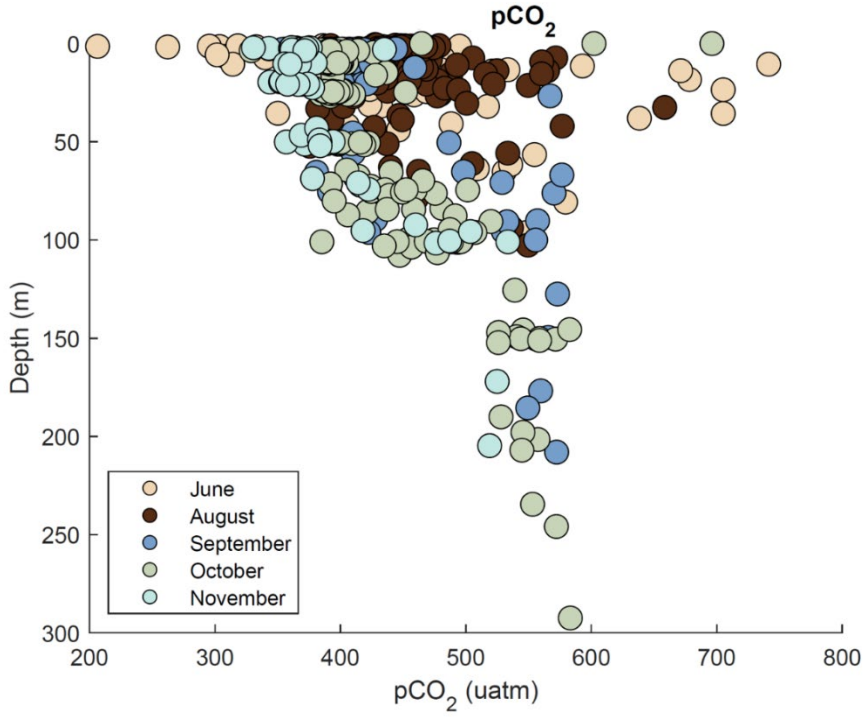

***Fig 37.** pCO_2 versus depth. Data were collected in 2017 on research cruises from* June 12-15 *(tan), August* 8-11 *(brown), September* 23 – October 1 *(blue), October 20-24 (green), and November 15-20 (teal).*

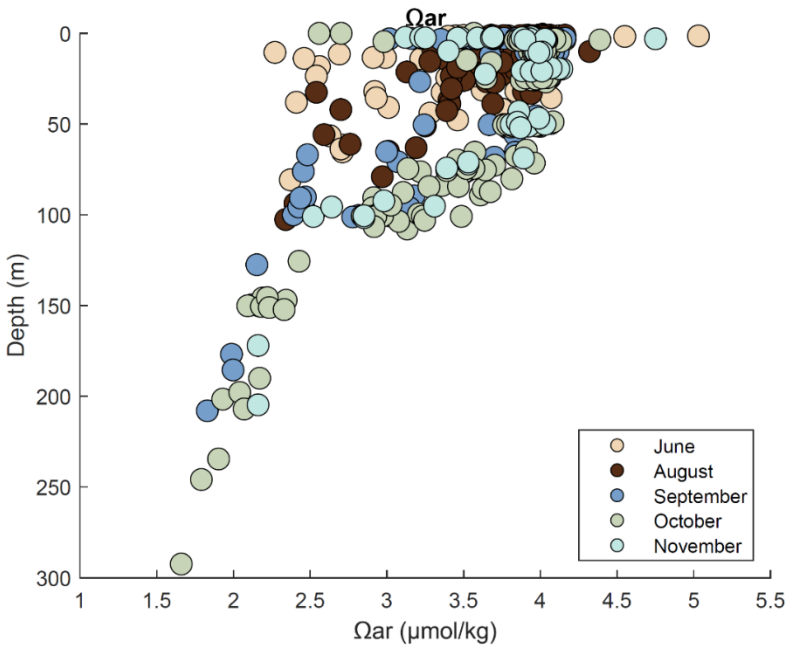

***Fig 38**. Ω_{ar} versus depth. Data were collected in 2017 on research cruises from* June 12-15 *(tan), August* 8-11 *(brown), September* 23 – October 1 *(blue), October 20-24 (green), and November 15-20 (teal).*

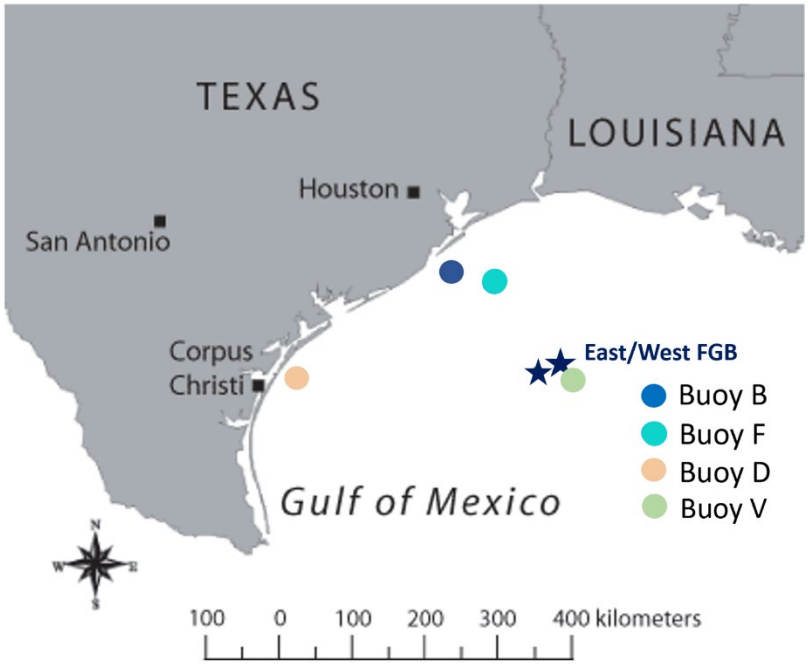

***Fig 39**. Some locations of the Texas Automated Buoy System (TABS), a coastal network of moored near real time observation buoys which are scattered around the continental shelf of Texas and take seawater measurements including salinity. The dark blue stars indicate the location of the East and West Flower Garden Banks (FGB) coral reefs.*

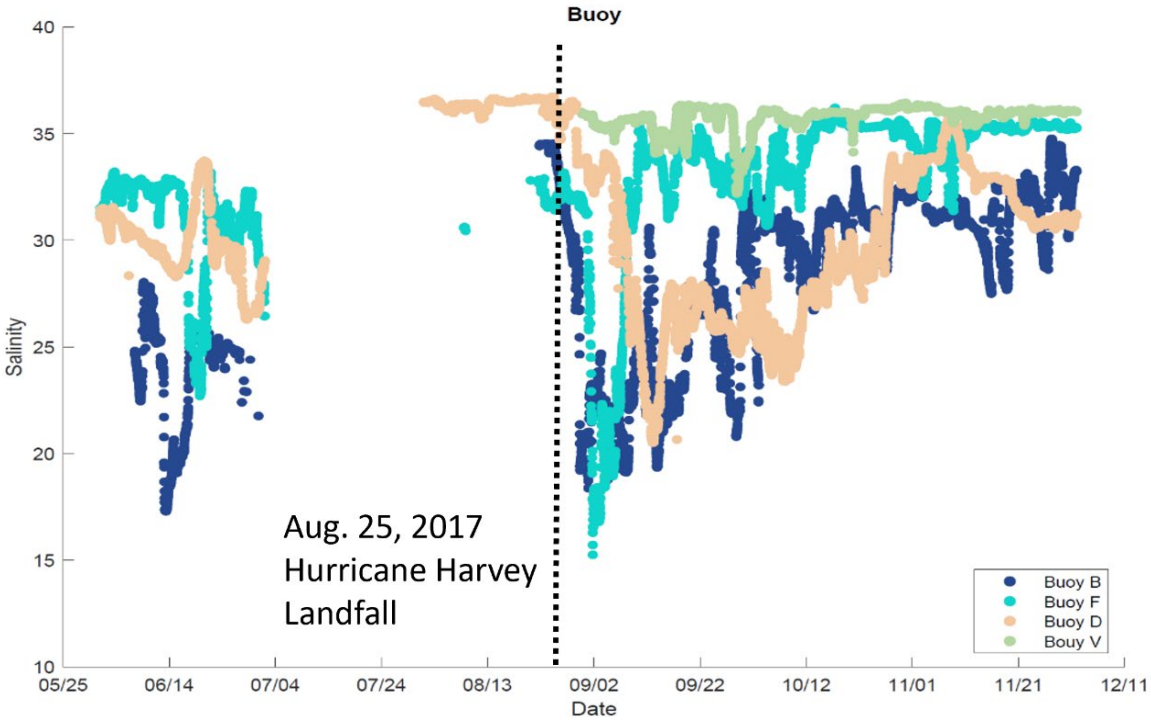

Fig 40*. The colors here correspond to the locations and buoys in Fig 41. Hurricane Harvey made landfall on August 25, 2017 and is approximately indicated by the horizontal black dashed line.*

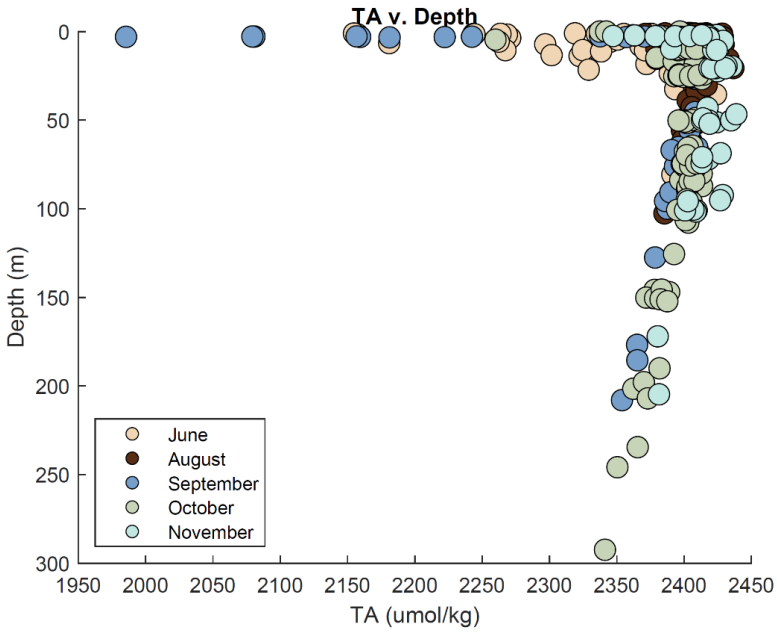

Fig 41. *TA versus depth. Data were collected in 2017 on research cruises from* June 12-15 *(tan), August* 8-11 *(brown), September* 23 – October 1 *(blue), October 20-24 (green), and November 15-20 (teal).*

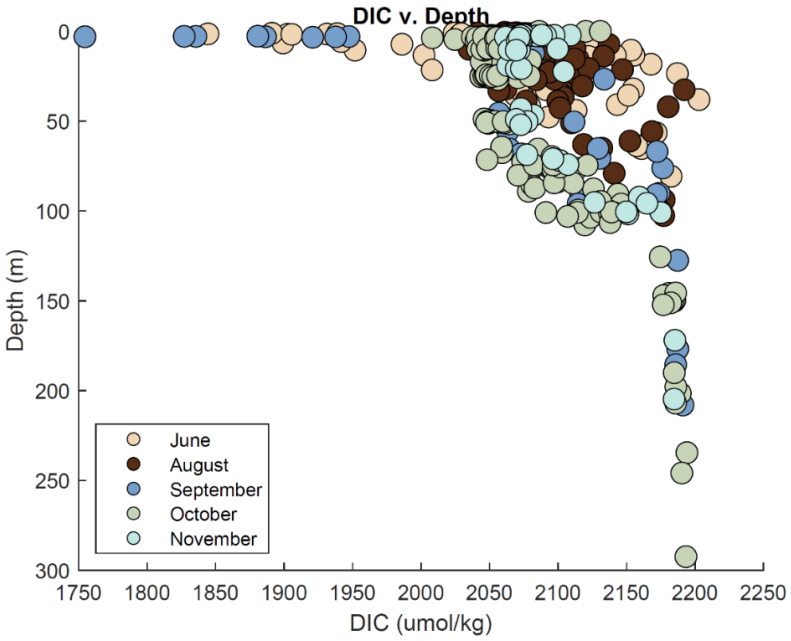

***Fig 42**. DIC versus depth. Data were collected in 2017 on research cruises from* June 12-15 *(tan), August* 8-11 *(brown), September* 23 – October 1 *(blue), October 20-24 (green), and November 15-20 (teal).*

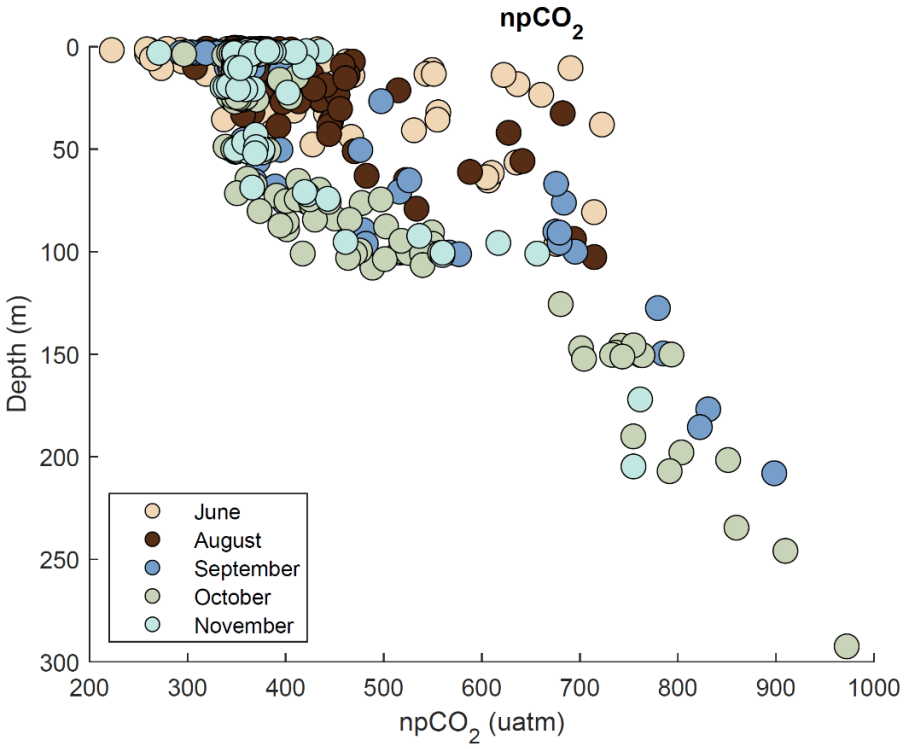

***Fig 43**. pCO_2 ($npCO_2$) normalized to a constant temperature of 25°C versus depth. Data were collected in 2017 on research cruises from* June 12-15 *(tan), August* 8-11 *(brown), September* 23 – October 1 *(blue), October 20-24 (green), and November 15-20 (teal).*

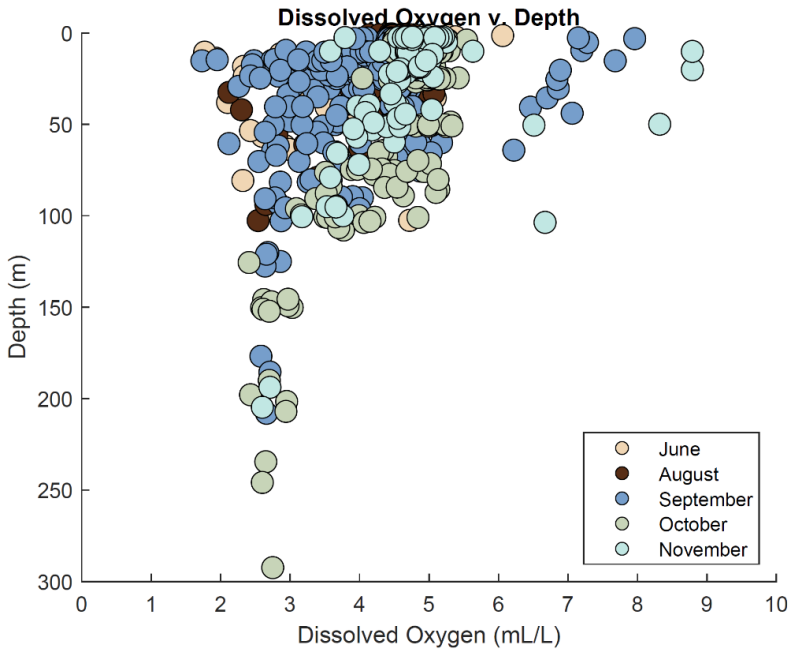

Fig 44*. Dissolved oxygen versus depth. Data were collected in 2017 on research cruises from* June 12-15 *(tan), August* 8-11 *(brown), September* 23 – October 1 *(blue), October 20-24 (green), and November 15-20 (teal).*

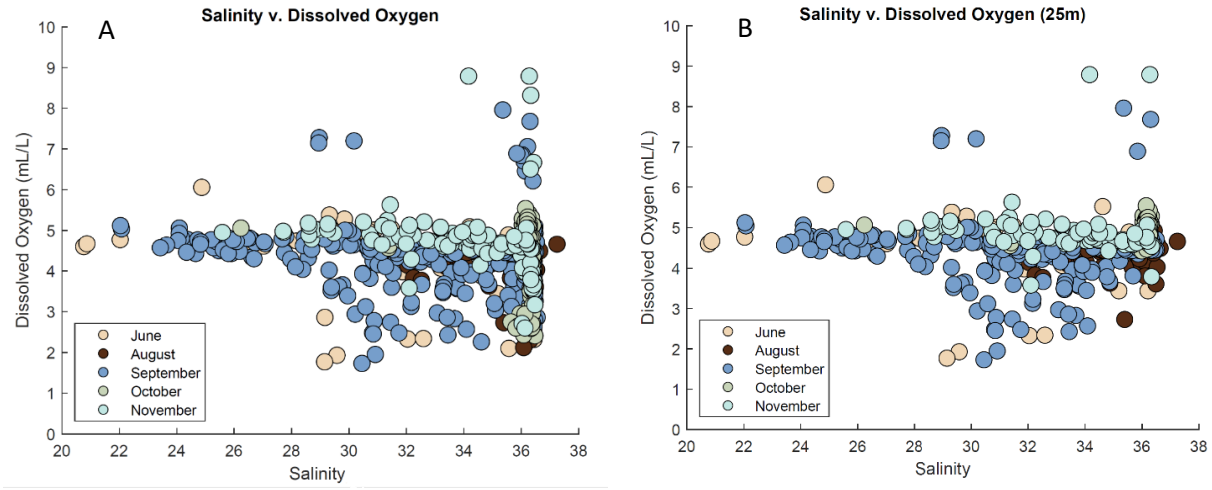

Fig 45. *Left: Dissolved oxygen versus Salinity for all available data. Right: Dissolved oxygen versus Salinity from 0 to 25 m depth. Data were collected in 2017 on research cruises from* June 12-15 *(tan), August* 8-11 *(brown), September* 23 – October 1 *(blue), October 20-24 (green), and November 15-20 (teal).*

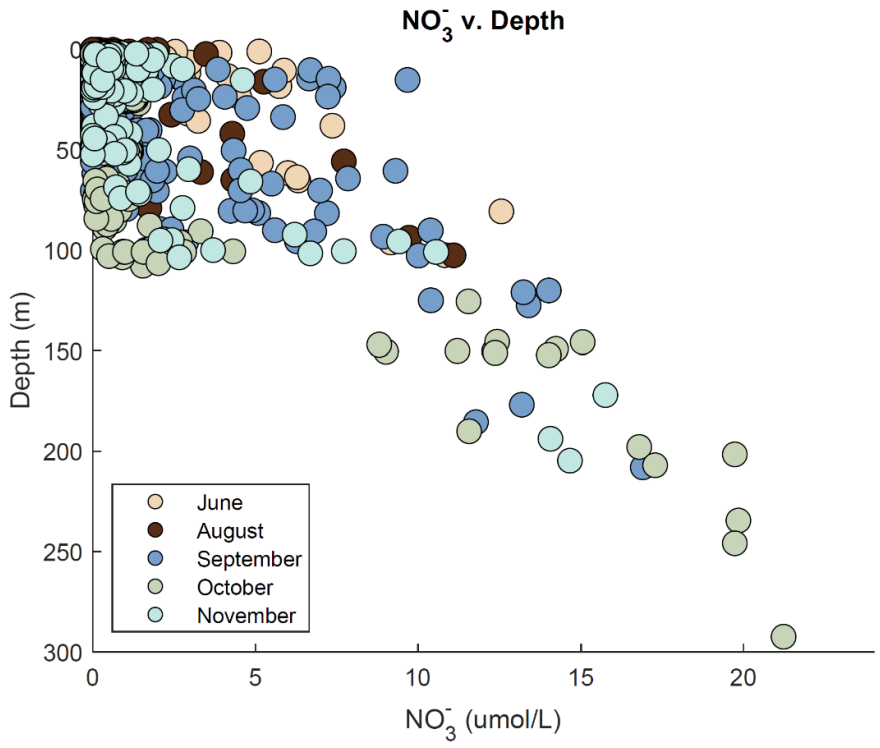

***Fig 46**. NO^-_3 versus depth. Data were collected in 2017 on research cruises from* June 12-15 *(tan), August* 8-11 *(brown), September* 23 – October 1 *(blue), October 20-24 (green), and November 15-20 (teal).*

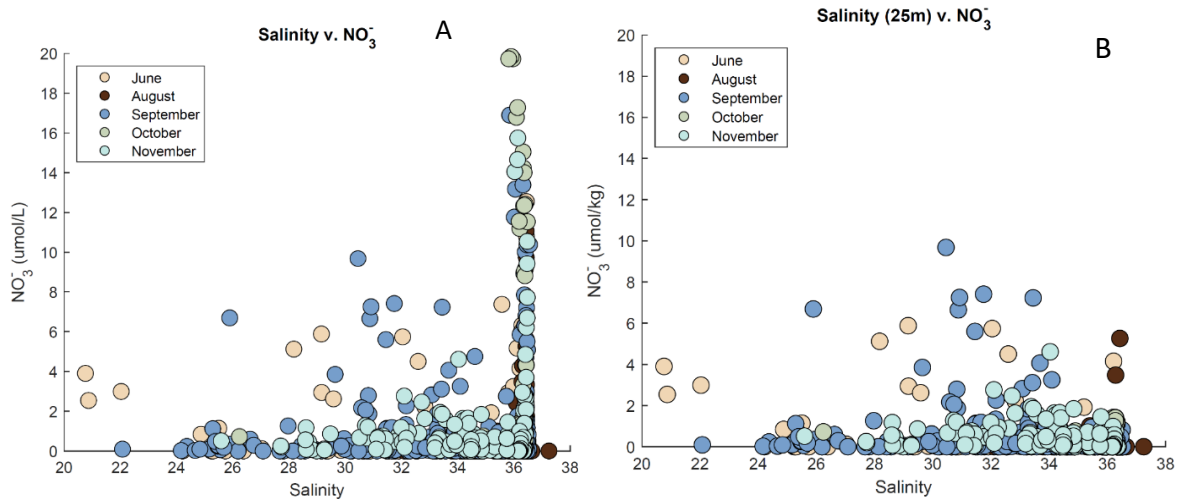

***Fig 47**. Left: NO^-_3 versus Salinity. Right: NO^-_3 versus Salinity to a depth of 25 m. Data were collected in 2017 on research cruises from* June 12-15 *(tan), August* 8-11 *(brown), September* 23 – October 1 *(blue), October 20-24 (green), and November 15-20 (teal).samples Right: B. Salinity against discrete NO^-_3 samples up until 25 m*

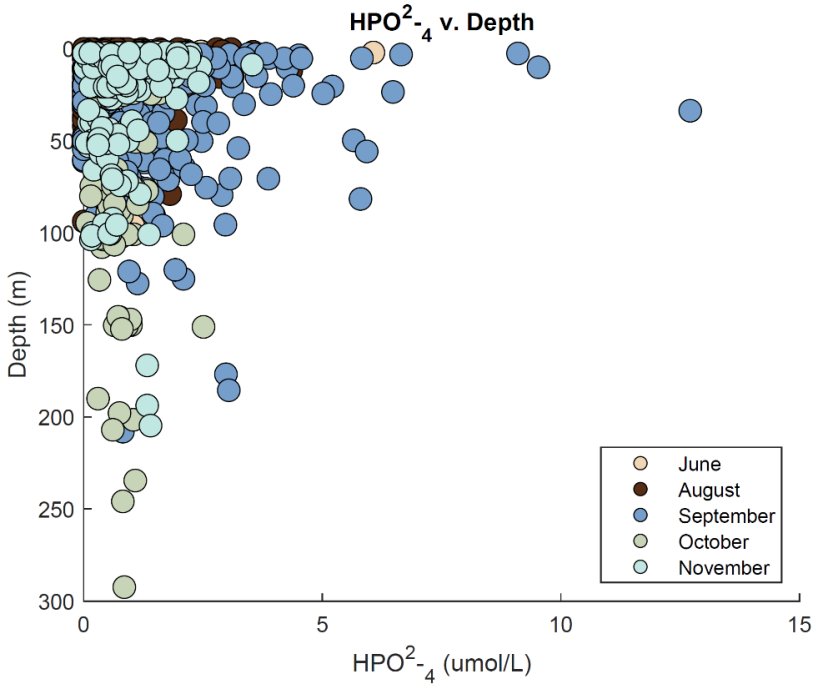

***Fig 48**. Discrete HPO^{2-}_4 versus depth. Data were collected in 2017 on research cruises from* June 12-15 *(tan), August* 8-11 *(brown), September* 23 – October 1 *(blue), October 20-24 (green), and November 15-20 (teal).*

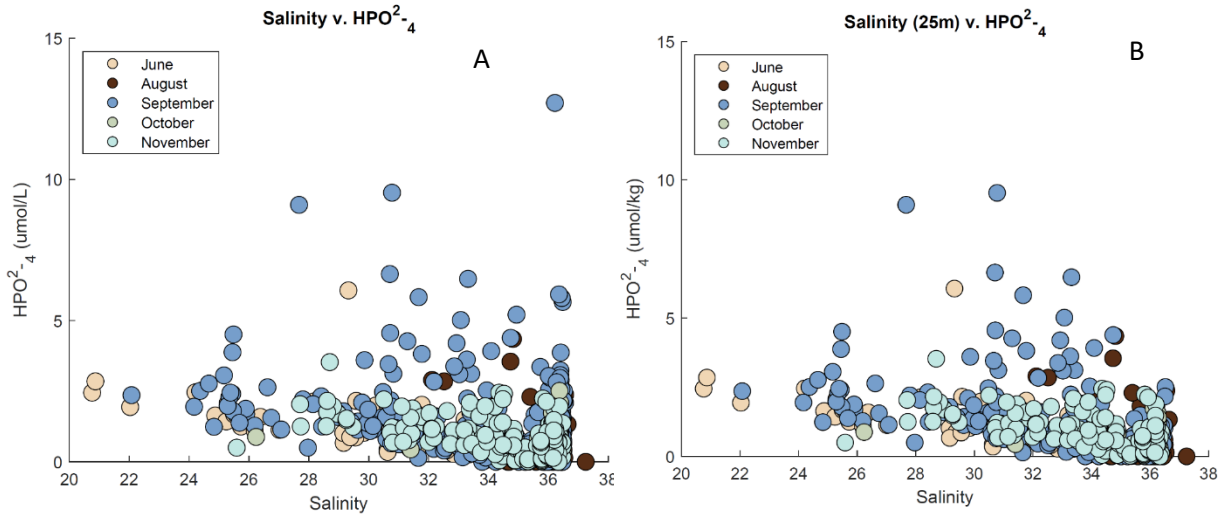

***Fig 49**. Left: A. HPO^{2-}_4 samples versus Salinity Right: HPO^{2-}_4 versus salinity to a depth of 25 m. Data were collected in 2017 on research cruises from* June 12-15 *(tan), August* 8-11 *(brown), September* 23 – October 1 *(blue), October 20-24 (green), and November 15-20 (teal).samples Right: B. Salinity against discrete NO^{-}_3 samples up until 25 m*

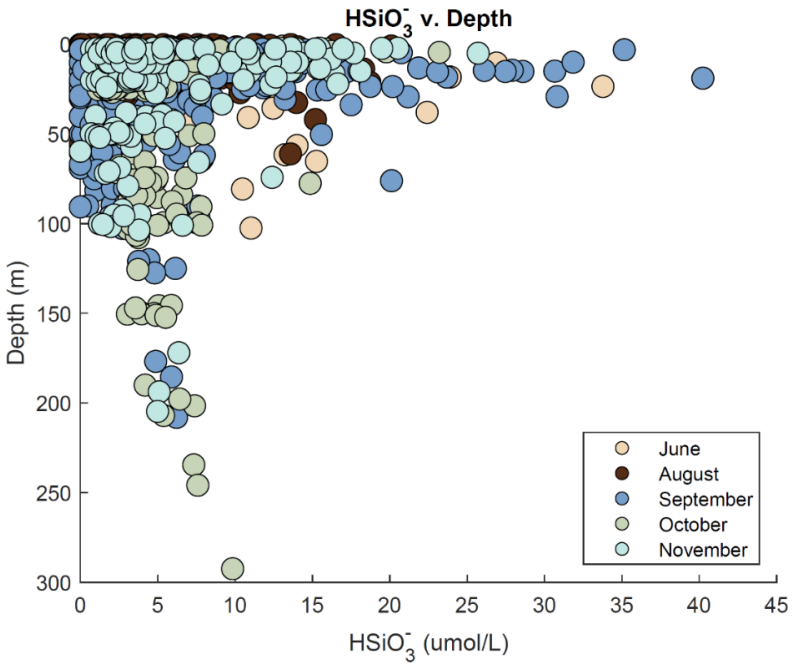

Fig 50*. HSiO$^{-}_{3}$ versus depth. Data were collected in 2017 on research cruises from* June 12-15 *(tan), August* 8-11 *(brown), September* 23 – October 1 *(blue), October 20-24 (green), and November 15-20 (teal).*

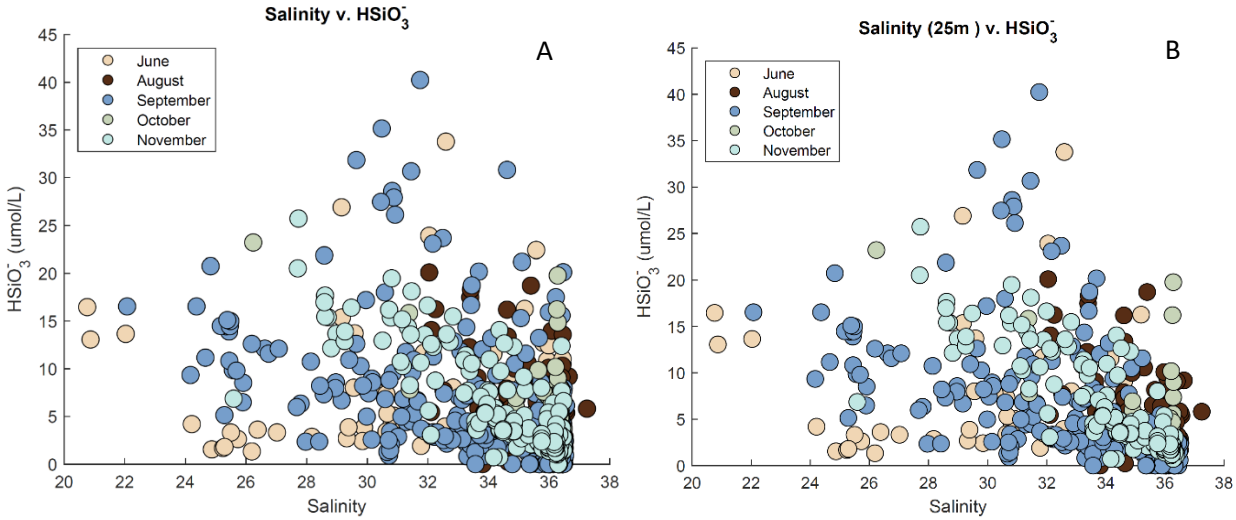

Fig 51. *Left: A. HSiO$^{-}_{3}$ versus Salinity. Right: HSiO$^{-}_{3}$ versus Salinity to a depth of 25 m. Data were collected in 2017 on research cruises from* June 12-15 *(tan), August* 8-11 *(brown), September* 23 – October 1 *(blue), October 20-24 (green), and November 15-20 (teal).samples Right: B. Salinity against discrete NO$^{-}_{3}$ samples up until 25 m*

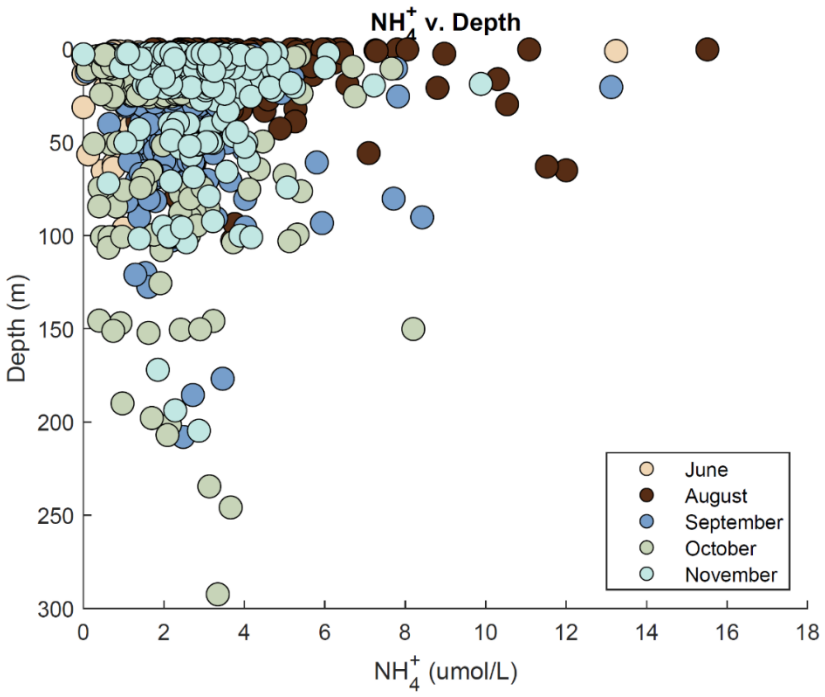

***Fig 52**. Discrete NH^{+}_{4} versus depth. Data were collected in 2017 on research cruises from* June 12-15 *(tan), August* 8-11 *(brown), September* 23 – October 1 *(blue), October 20-24 (green), and November 15-20 (teal).*

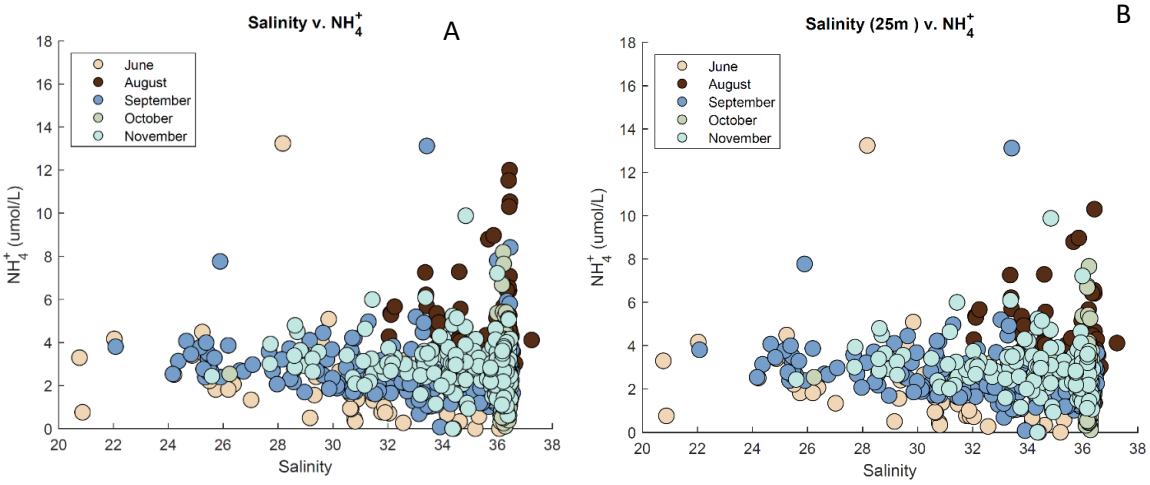

***Fig 53**. Left: A. NH^{+}_{4} Left: A. $HSiO^{-}_{3}$ versus Salinity. Right: NH^{+}_{4} versus Salinity to a depth of 25 m. Data were collected in 2017 on research cruises from* June 12-15 *(tan), August* 8-11 *(brown), September* 23 – October 1 *(blue), October 20-24 (green), and November 15-20 (teal).samples Right: B. Salinity against discrete NO^{-}_{3} samples up until 25 m*

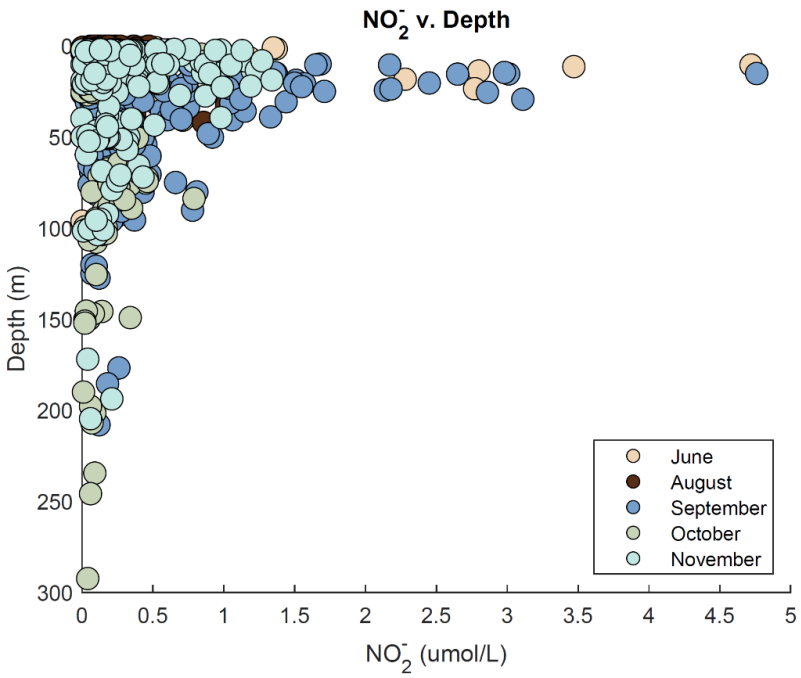

***Fig 54**. NO^-_2 versus depth. Data were collected in 2017 on research cruises from* June 12-15 *(tan), August* 8-11 *(brown), September* 23 – October 1 *(blue), October 20-24 (green), and November 15-20 (teal).*

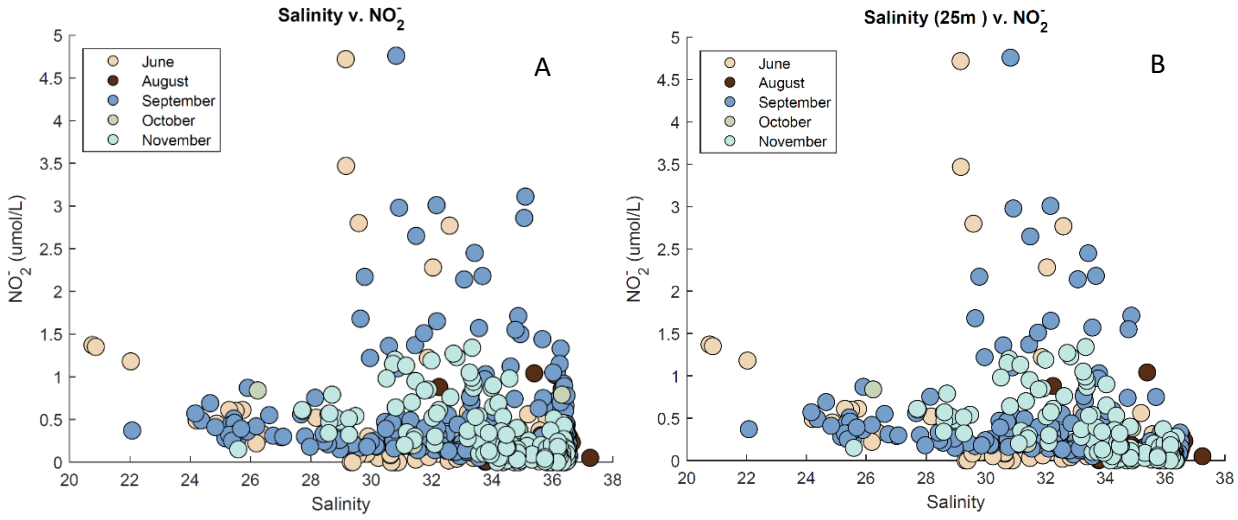

***Fig 55**. Left: A. NO^-_2 versus Salinity. Right: NO^-_2 versus Salinity to a depth of 25 m. Data were collected in 2017 on research cruises from* June 12-15 *(tan), August* 8-11 *(brown), September* 23 – October 1 *(blue), October 20-24 (green), and November 15-20 (teal).samples Right: B. Salinity against discrete NO^-_3 samples up until 25 m*

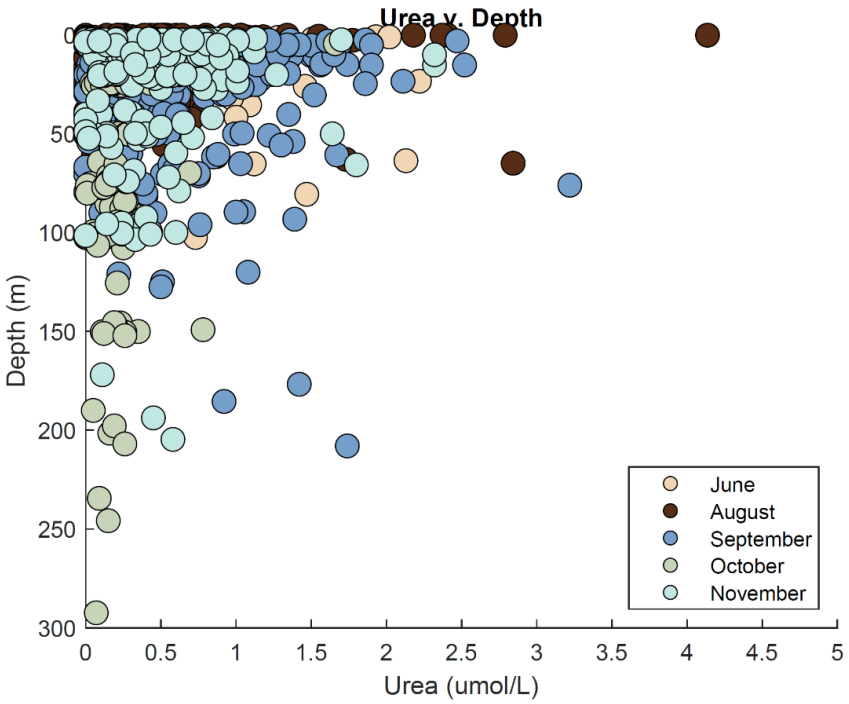

***Fig 56**. Urea versus depth. Data were collected in 2017 on research cruises from* June 12-15 *(tan), August* 8-11 *(brown), September* 23 – October 1 *(blue), October 20-24 (green), and November 15-20 (teal).*

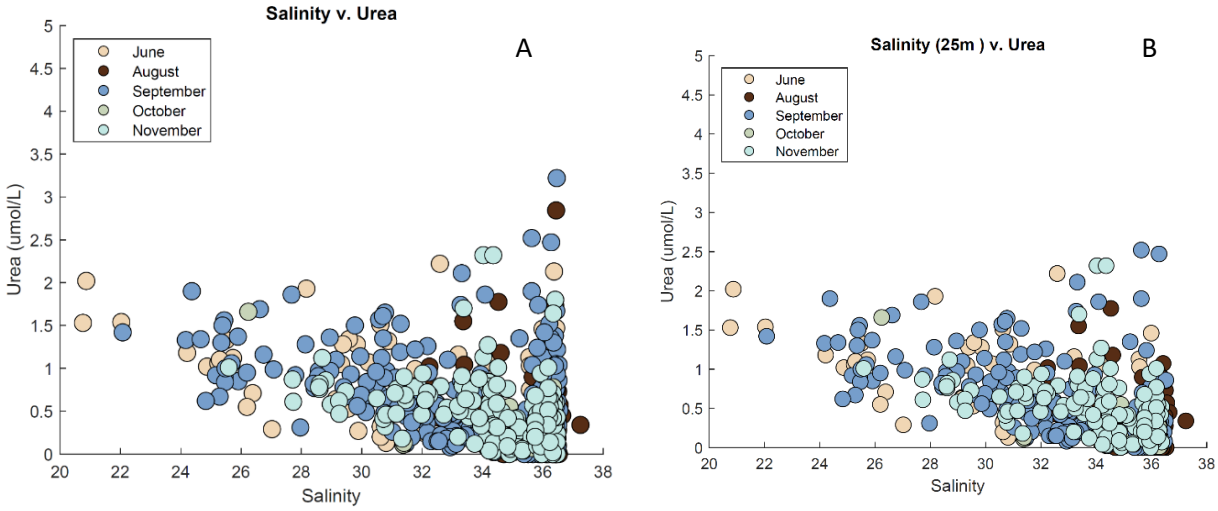

***Fig 57**. Left: A. Urea versus Salinity. Right: Urea versus Salinity to a depth of 25 m. Data were collected in 2017 on research cruises from* June 12-15 *(tan), August* 8-11 *(brown), September* 23 – October 1 *(blue), October 20-24 (green), and November 15-20 (teal).samples Right: B. Salinity against discrete NO^{-}_{3} samples up until 25 m*

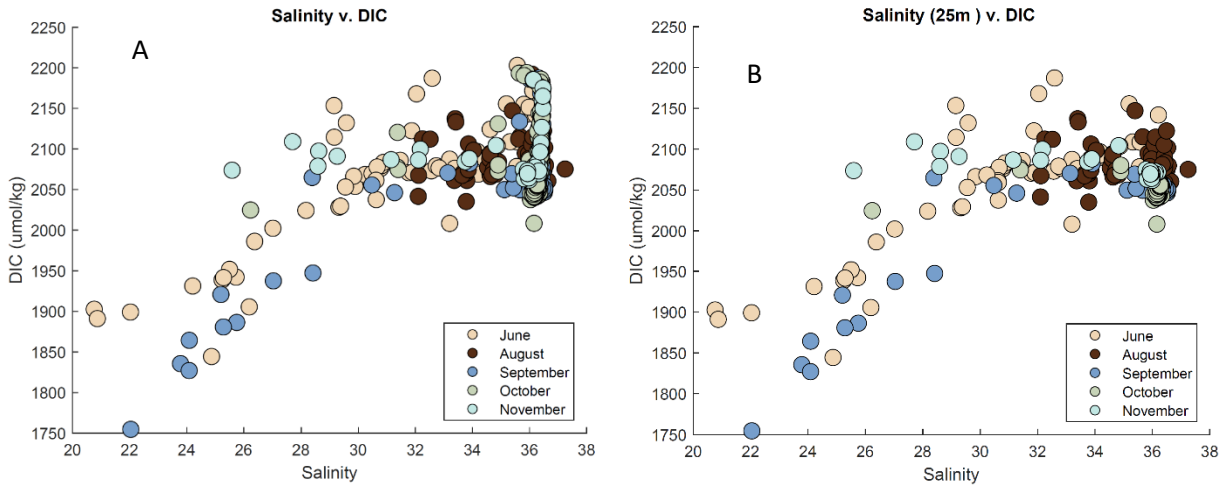

***Fig 58**. Left: DIC versus salinity. Right: DIC versus salinity up to 25 m. Data were collected in 2017 on research cruises from* June 12-15 *(tan), August* 8-11 *(brown), September* 23 – October 1 *(blue), October 20-24 (green), and November 15-20 (teal).*

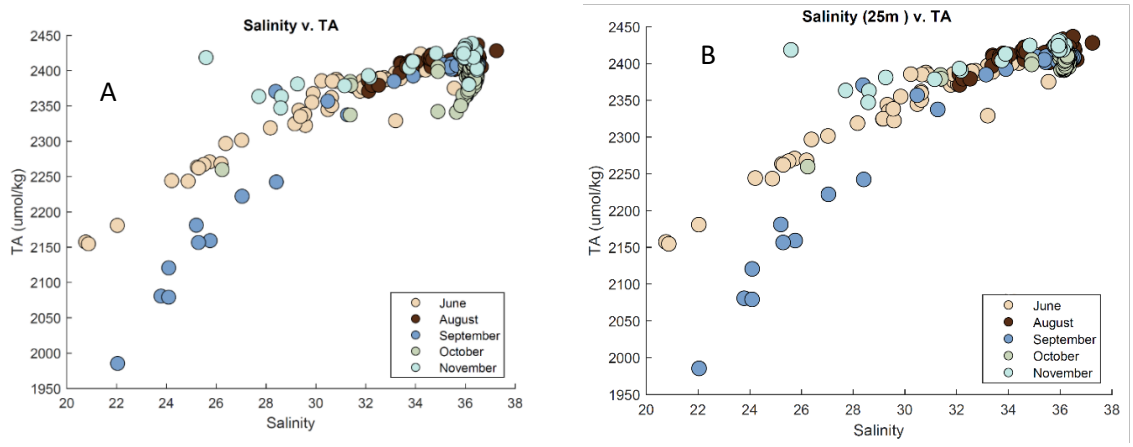

***Fig 59**. Right TA versus salinity. Left: TA versus salinity up to 25 m. Data were collected in 2017 on research cruises from* June 12-15 *(tan), August* 8-11 *(brown), September* 23 – October 1 *(blue), October 20-24 (green), and November 15-20 (teal).*

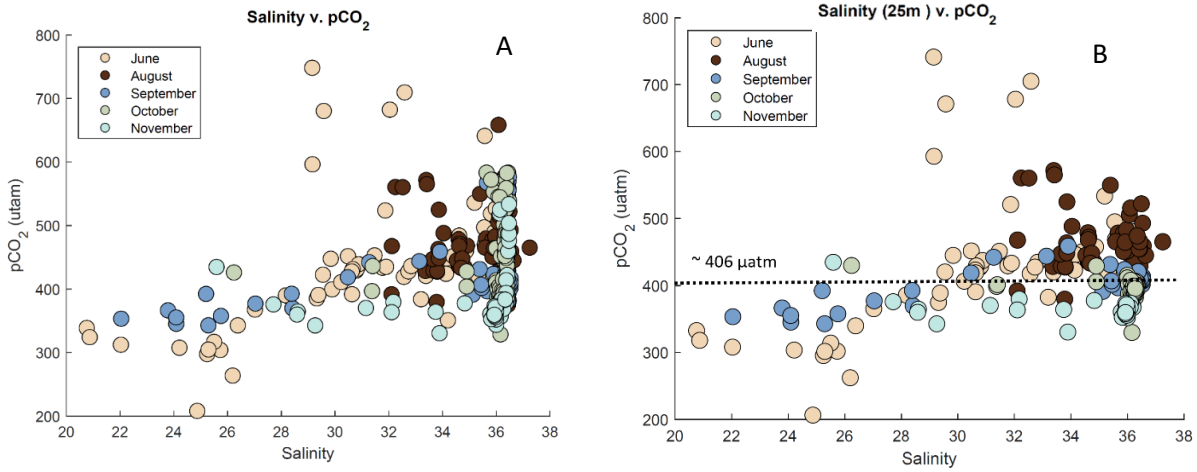

***Fig 60**. Right: pCO_2 versus salinity. Left: pCO_2 versus salinity. Data were collected in 2017 on research cruises from* June 12-15 *(tan), August* 8-11 *(brown), September* 23 – October 1 *(blue), October 20-24 (green), and November 15-20 (teal). The black dashed indicates the Monthly $CO_{2\ (atm)}$ data from NOAA. In August 2017, the monthly $CO_{2\ (atm)}$ was 405.7 µatm*

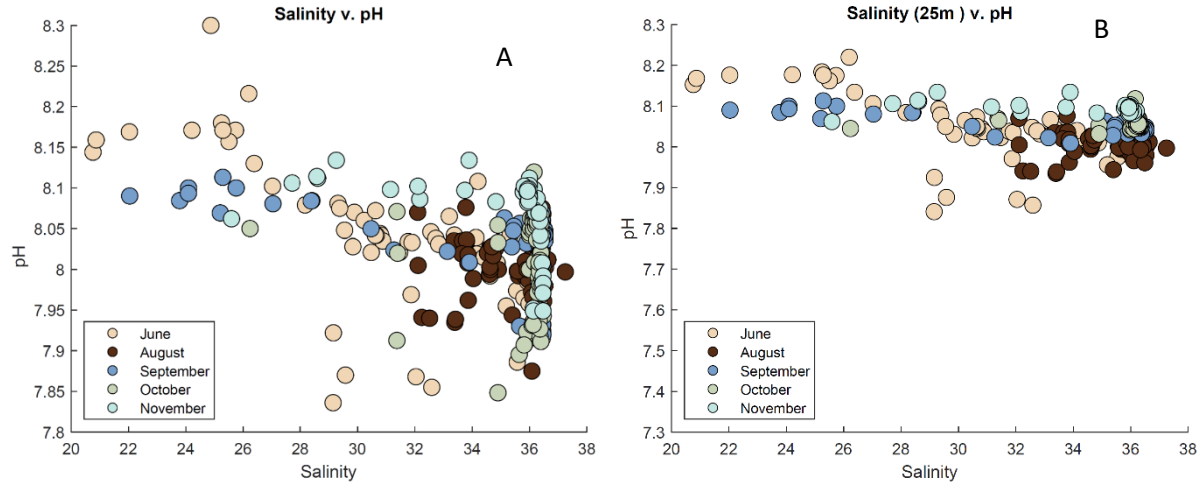

***Fig 61**. Left: pH versus salinity. Right: pH versus salinity up to 25 m. Data were collected in 2017 on research cruises from* June 12-15 *(tan), August* 8-11 *(brown), September* 23 – October 1 *(blue), October 20-24 (green), and November 15-20 (teal).*

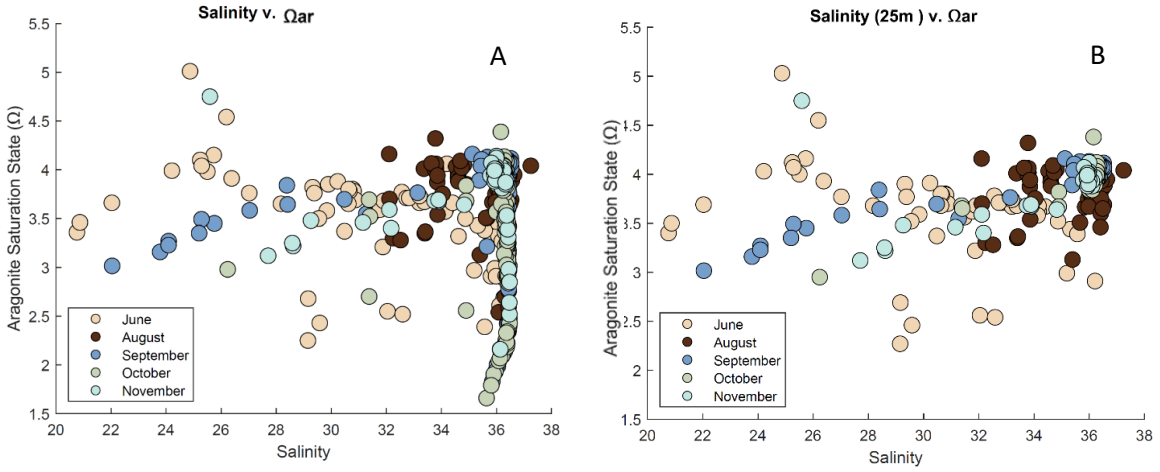

***Fig 62**. Right: Ω_{ar} versus salinity. Left: Ω_{ar} versus salinity up to 25 m. Data were collected in 2017 on research cruises from* June 12-15 *(tan), August* 8-11 *(brown), September* 23 – October 1 *(blue), October 20-24 (green), and November 15-20 (teal).*

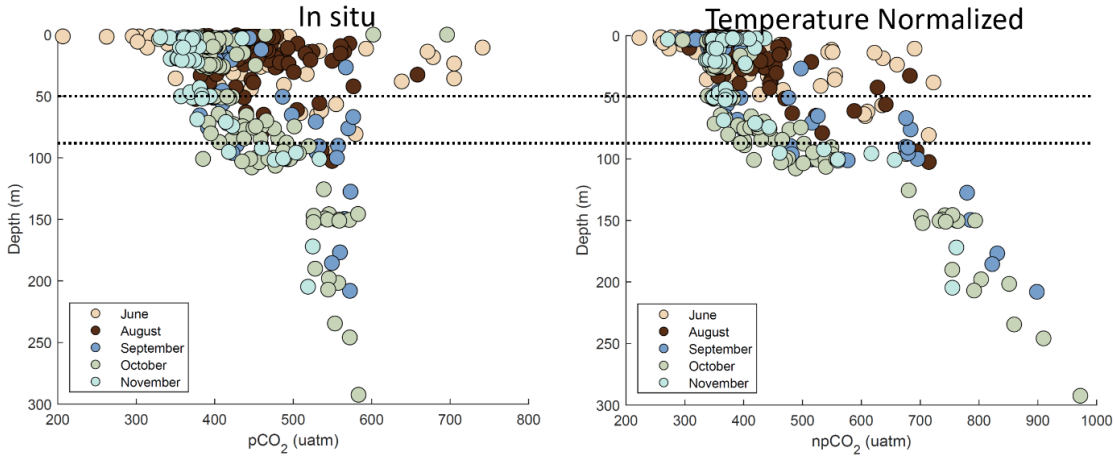

***Fig 63.** Left: pCO_2 samples against depth. A shift in September outside of normal seasonal changes are highlighted within the black dashed line. Right: Temperature normalized pCO_2 samples. The shift in $npCO_2$ in September outside of normal ranges suggest an upwelling*